

การเปรียบเทียบอุณหภูมิลิควิด์สของ E-GLASS โดยวิธีใช้อุณหภูมิสม่ำเสมอ  
และกล้องจุลทรรศน์อุณหภูมิสูง



นายอภิรัฐ ชีรภาพพิเศษพงษ์

สถาบันวิทยบริการ

จุฬาลงกรณ์มหาวิทยาลัย

วิทยานิพนธ์นี้เป็นส่วนหนึ่งของการศึกษาตามหลักสูตรปริญญาวิทยาศาสตรมหาบัณฑิต

สาขาวิชาเทคโนโลยีเซรามิก ภาควิชาวัสดุศาสตร์


คณะวิทยาศาสตร์ จุฬาลงกรณ์มหาวิทยาลัย

ปีการศึกษา 2548

ISBN 974-14-3309-3

ลิขสิทธิ์ของจุฬาลงกรณ์มหาวิทยาลัย

COMPARISON OF LIQUIDUS TEMPERATURE OF E-GLASS BY UNIFORM  
TEMPERATURE METHOD AND HEATING STAGE MICROSCOPE



Mr Apirat Theerapapvisetpong

สถาบันวิทยบริการ  
จุฬาลงกรณ์มหาวิทยาลัย

A Thesis Submitted in Partial Fulfillment of the Requirements  
for the Degree of Master of Science Program in Ceramic Technology

Department of Materials Science

Faculty of Science

Chulalongkorn University

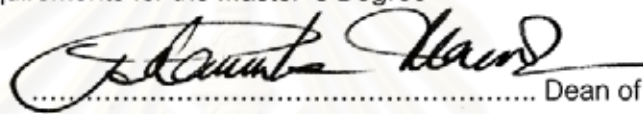
Academic Year 2005

ISBN 974-14-3309-3


Thesis Title Comparison of Liquidus Temperature of E-glass by Uniform  
Temperature Method and Heating Stage Microscope  
By Mr Apirat Theerapapvisetpong  
Field of study Ceramic Technology  
Thesis Advisor Assistant Professor Sirithan Jiemsirilers, Ph.D.  
Thesis Co-advisor Lada Punsukumtana, Ph.D.

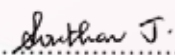
---


Accepted by the Faculty of Science, Chulalongkorn University in Partial  
Fulfillment of the Requirements for the Master 's Degree


  
..... Dean of the Faculty of Science  
(Professor Piamsak Menasveta, Ph.D.)

THESIS COMMITTEE

  
..... Chairman  
(Associate Professor Saowaroj Chuayjuljit)

  
..... Thesis Advisor  
(Assistant Professor Sirithan Jiemsirilers, Ph.D.)

  
..... Thesis Co-advisor  
(Lada Punsukumtana, Ph.D.)

  
..... Member  
(Associate Professor Supatra Jinawath, Ph.D.)

อภิรัฐ ทิรภาพพิเศษพงษ์ : การเปรียบเทียบอุณหภูมิวิกฤตของ E-GLASS โดยวิธีใช้อุณหภูมิ  
สม่ำเสมอและกล้องจุลทรรศน์อุณหภูมิสูง (COMPARISON OF LIQUIDUS TEMPERATURE OF  
E-GLASS BY UNIFORM TEMPERATURE METHOD AND HEATING STAGE MICROSCOPE)  
อ.ที่ปรึกษา : ผศ.ดร.ศิริธันว์ เจียมศิริเลิศ, อ.ที่ปรึกษาร่วม : ดร.ลดา พันธุ์สุภมรนา, 115 หน้า.  
ISBN 974-14-3309-3.

อุณหภูมิวิกฤตเป็นสมบัติที่ยากแก่การตรวจสอบ โดยเฉพาะแก้วที่ผลิตจากโรงงานอุตสาหกรรม  
ทั่วไปเป็นแก้วที่มีองค์ประกอบเคมีหลายชนิดรวมกัน การหาอุณหภูมิวิกฤตจากไบนารีเฟสไดอะแกรม  
และเทอร์นารีเฟสไดอะแกรมไม่เพียงพอที่จะหาอุณหภูมิที่แม่นยำได้ การใช้ข้อมูลอุณหภูมิวิกฤตด้วย  
การประมาณค่าที่สูงเกินไปสำหรับการควบคุมอุณหภูมิเตาทำให้เสียพลังงานไปโดยไม่จำเป็น งานวิจัยนี้  
จึงได้ทำการศึกษาอุณหภูมิวิกฤตของแก้วในระบบของ E-glass และ ECR-glass โดยเตรียมจาก  
สารประกอบออกไซด์เกรดเคมี สูตรแก้วแต่ละสูตรทำการแปรค่าส่วนผสมของอัลคาไลออกไซด์ ได้แก่  
โซเดียมออกไซด์ และโพแทสเซียมออกไซด์ อย่างละ 1 และ 3 เปอร์เซ็นต์ ตามลำดับ เพื่อหาผลกระทบ  
ของปริมาณอัลคาไลออกไซด์ต่ออุณหภูมิวิกฤต การวัดอุณหภูมิวิกฤตใช้วิธีอุณหภูมิสม่ำเสมอ และ  
กล้องจุลทรรศน์อุณหภูมิสูง โดยสอบเทียบด้วยการวัดอุณหภูมิวิกฤต และจุดหลอมเหลวของตัวอย่าง  
แก้วและโลหะอะลูมิเนียมมาตรฐาน จากการเปรียบเทียบผลการวัดอุณหภูมิวิกฤตของแก้วชนิดเดียวกัน  
ด้วยวิธีทั้งสอง พบว่าอุณหภูมิวิกฤตที่วัดได้จากการวัดด้วยกล้องจุลทรรศน์อุณหภูมิสูงมีค่าสูงกว่า  
ประมาณ 115 องศาเซลเซียส และยังได้ทำการสร้างสมการทำนายอุณหภูมิวิกฤตโดยใช้ความสัมพันธ์  
ระหว่างองค์ประกอบเคมีของแก้วกับอุณหภูมิวิกฤต เป็นฟังก์ชันพอลิโนเมียลกำลังหนึ่ง ผลึกปฐมภูมิ  
ของแก้วทั้งสองชนิดนี้คือ โวลลาสโทไนต์ และอะนอร์ไทต์ ซึ่งทำการตรวจสอบด้วยกล้องจุลทรรศน์  
แสง เอกซ์เรย์ดิฟแฟรกโทมิเตอร์ และกล้องจุลทรรศน์อิเล็กตรอน /อีเนอร์จิสเพอร์ซิฟ เอกซ์เรย์ไมโคร  
แอนาไลซิส การศึกษาผลของอัลคาไลออกไซด์พบว่าโพแทสเซียมออกไซด์มีอิทธิพลต่ออุณหภูมิวิกฤต  
มากกว่าโซเดียมออกไซด์ และพบว่าปริมาณอัลคาไลออกไซด์เพิ่มส่งผลให้มีการตกผลึกของโวลลาสโท  
ไนต์มากขึ้น กรณีศึกษาตัวอย่างแก้วที่ผลิตจากโรงงาน ผลการวัดอุณหภูมิวิกฤตด้วยวิธีอุณหภูมิ  
สม่ำเสมอของตัวอย่างแก้วที่ได้จากโรงงาน คือ 1080 องศาเซลเซียส ซึ่งต่ำกว่าแก้วที่เตรียมด้วยสารเคมี  
ในส่วนผสมใกล้เคียงกัน การเติมเหล็กออกไซด์ 0 - 1.3 เปอร์เซ็นต์ มีผลทำให้อุณหภูมิวิกฤตลดลง  
เล็กน้อยตามปริมาณการเพิ่มของเหล็กออกไซด์

ภาควิชา.....วัสดุศาสตร์..... ลายมือชื่อนิสิต..... *Apit T.*  
สาขาวิชา.....เทคโนโลยีเซรามิก..... ลายมือชื่ออาจารย์ที่ปรึกษา..... *Siithan J.*  
ปีการศึกษา ..2548..... ลายมือชื่ออาจารย์ที่ปรึกษาร่วม..... *Lada Panankunana*

## 4672493223 : MAJOR CERAMIC TECHNOLOGY

KEY WORD: E-GLASS / ECR-GLASS / LIQUIDUS TEMPERATURE / HEATING STAGE / WOLLASTONITE

APIRAT THEERAPAPVISETPONG : COMPARISON OF LIQUIDUS TEMPERATURE OF E-GLASS BY UNIFORM TEMPERATURE METHOD AND HEATING STAGE MICROSCOPE.

THESIS ADVISOR : ASST.PROF. SIRITHAN JIEMSIRILERS, Ph.D., THESIS COADVISOR : LADA PUNSUKUMTANA, Ph.D. 115 pp. ISBN 974-14-3309-3.

Liquidus temperature ( $T_L$ ) is a glass property that is difficult to determine or calculate.  $T_L$  of binary and ternary systems can be found in phase diagram but not available for multi-component systems such an industrial glass. The furnace temperature control basing on an excess of  $T_L$  data from approximation will increase unnecessary energy used. In this work, series of glass in system of E-Glass and ECR-Glass were fabricated from chemical grade oxides. The effects of addition of alkali oxides (1 and 3 wt% of  $\text{Na}_2\text{O}$  and  $\text{K}_2\text{O}$ ) on  $T_L$  were study.  $T_L$  was measured using two different methods which were a uniform temperature method and heating stage microscope. The reference standard glass and standard aluminum were used to assess the accuracy of the furnace and the heating stage used respectively. It was found that  $T_L$  measured by the uniform temperature method was higher than that measured by heating stage about  $115^\circ\text{C}$ . In addition, first order polynomial function was used to model an equation for predicting  $T_L$  relate to component concentrations. The major primary crystalline phases detected by optical microscope, XRD and SEM/EDX were wollastonite and anorthite. The study of effect of alkali oxides on  $T_L$  was noticed that  $\text{K}_2\text{O}$  containing glasses tended to have higher  $T_L$  compared to  $\text{Na}_2\text{O}$  containing glasses. Addition of alkali oxides led to crystallization of wollastonite crystals.  $T_L$  of industrial glass composition was  $1085^\circ\text{C}$  while the simulated glasses showed higher  $T_L$ . The variation 0-1.3 wt% of iron oxide in these glass compositions showed that  $T_L$  tended to decrease slightly with increasing of concentration of iron oxide.

Department.....Materials Science.....Student's signature.....*Apirat T.*  
 Field of study....Ceramic Technology.....Advisor's signature.....*Sirithan J.*  
 Academic year..2005.....Co-advisor's signature.....*Lada Punsukumtana*

## ACKNOWLEDGEMENTS

I would like to thank Asst.Prof.Dr. Sirithan Jiemsirilers, my thesis advisor, for her help and valuable suggestions. My thanks are also to Dr. Lada Punsukumtana, my co-advisor for her suggestions and inviting me to visit the glassfiber production plants which gave me a clear understanding of the production process. I would like to thank Microfiber Industries Ltd. and Saint-Gobain Vetrotex (Thailand) Ltd. for their permission to visit their glassfiber production plants and collect glass samples. I would like to acknowledge Prof.Dr. Reinhard Conradt for his kindness and help in repairing heating stage, and thanks for his uncopyright 'Uniglass' software. I would like to thank the Department of Science Service for the research fund.

To my colleage, Khun Yupayong Tulyanon, I would like to thank for her help and good suggestions many times.

To my friends, Mink and Noi who did everything that I had requested. I will not forget it. To buss, Koi, Nun and Ae, my old friends from CMU, thank you for your guidance concerning how to study in this program and how to spend my life in Chula. To all of my friends and my teachers in Materials Science Department. It was a great time to get a long with all of you in this warm house.

Finally, I am very grateful to my family for all supports; fund, love, encouragement and understanding.

สถาบันวิทยบริการ  
จุฬาลงกรณ์มหาวิทยาลัย

# CONTENTS

|  | Page |
|--|------|
| Abstract (Thai).....   | iv   |
| Abstract (English) .....   | v    |
| Acknowledgments.....   | vi   |
| Contents.....  | vii  |
| List of tables .....   | xi   |
| List of figures .....  | xii  |
| Chapter I Introduction .....   | 1    |
| Chapter II Literature reviews .....  | 3    |
| 2.1 Structure of glass .....   | 3    |
| 2.2 Phase transformation.....  | 4    |
| 2.3 Crystallization .....  | 5    |
| 2.3.1. Homogeneous nucleation .....  | 5    |
| 2.3.2. Heterogeneous nucleation .....  | 9    |
| 2.4 Liquidus temperature .....   | 11   |
| 2.4.1. Definition of liquidus temperature .....  | 11   |
| 2.4.2. Liquidus temperature measurements of glass .....                                    | 12   |
| 2.5 Liquidus prediction using statistical modeling .....                                   | 14   |
| 2.6 E-glass and ECR-glass .....  | 17   |
| 2.6.1. Definition of glass fibers.....   | 17   |
| 2.6.2. Glass melting and fiber forming .....   | 19   |
| 2.7 Effect of compositions on melt properties and liquidus temperature<br>of E-glass ..... | 21   |

|   |           |
|---|-----------|
| <b>Chapter III Experimental procedures</b> .....  | <b>24</b> |
| 3.1 Glass formula selection .....   | 24        |
| 3.2 Glass preparation.....  | 27        |
| 3.3 Homogeneity examination of as-fabricated glasses .....                                | 27        |
| 3.4 Determination of glass transition temperature and crystallization<br>temperature..... | 27        |
| 3.5 Liquidus temperature determination using uniform temperature<br>method .....          | 29        |
| 3.6 Primary phase identification .....  | 30        |
| 3.7 Liquidus temperature determination using heating stage<br>microscope.....             | 33        |
| 3.8 Case study on liquidus temperature of industrial glass.....                           | 35        |
| <b>Chapter IV Results and discussions</b> .....   | <b>36</b> |
| 4.1 Observation of as-fabricated glasses .....  | 36        |
| 4.2 Determination of glass transformation and crystallization<br>temperatures .....       | 37        |
| 4.3 Liquidus temperature measurement using an uniform temperature<br>method .....         | 40        |
| 4.3.1. Liquidus temperature determination .....   | 40        |
| 4.3.2. Crystalline phases identification.....   | 46        |
| 4.3.2.1. Visual observation and energy dispersive x-ray<br>microanalysis .....            | 46        |
| 4.3.2.2. X-ray diffraction.....   | 49        |
| 4.4 Effect of glass compositions on liquidus temperature.....                             | 52        |



|                                    |  |           |
|------------------------------------|--|-----------|
| 4.5                                | Composition-properties prediction model .....                                | 54        |
| 4.5.1.                             | Composition-properties modeling using Scheffe' Polynomial .....              | 54        |
| 4.5.2.                             | Prediction $T_L$ from relation between $T_g$ and $T_L$ .....                 | 57        |
| 4.6                                | Liquidus temperature measurement using heating stage microscope .....        | 61        |
| 4.7                                | Case study on liquidus temperature of industrial glass .....                 | 65        |
| 4.7.1.                             | Observation of as-receive industrial glass and as-fabricated glasses .....   | 65        |
| 4.7.2.                             | Chemical analysis results .....  | 66        |
| 4.7.3.                             | Measurement of liquidus temperature using a uniform temperature method ..... | 67        |
| 4.7.4.                             | Primary phase identification .....   | 70        |
| <b>Chapter V Conclusions</b> ..... |  | <b>71</b> |
| 5.1                                | Conclusions .....  | 71        |
| 5.2                                | Future works .....   | 72        |
| <b>References</b> .....            |  | <b>73</b> |
| <b>Appendices</b> .....            |  | <b>79</b> |
| Appendix A .....                   |  | 80        |
| Appendix B .....                   |  | 81        |
| Appendix C .....                   |  | 84        |
| Appendix D .....                   |  | 87        |
| Appendix E .....                   |  | 88        |
| Appendix F .....                   |  | 89        |
| Appendix G .....                   |  | 102       |

|                 |     |
|-----------------|-----|
| Appendix H..... | 107 |
| Appendix I..... | 112 |
| Biography.....  | 115 |



สถาบันวิทยบริการ  
จุฬาลงกรณ์มหาวิทยาลัย

## LIST OF TABLES

|   | Page |
|---|------|
| Table 2.1 Definitions of glass fiber followed ASTM.....   | 17   |
| Table 2.2 E-glass compositions classified by application used .....                                     | 18   |
| Table 2.3 Chemical composition of ECR-glass .....   | 19   |
| Table 3.1 Chemical compositions of E-glass and ECR-glass (wt %) .....                                   | 24   |
| Table 3.2 Chemical compositions of 25 selected glass samples .....                                      | 25   |
| Table 3.3 Predicted normative mineral contents calculated by “Uniglass” .....                           | 26   |
| Table 3.4 Comparison of Measured and Targetted chemical compositions (wt%) .....                        | 35   |
| Table 4.1 Thermal analysis results using DTA.....   | 39   |
| Table 4.2 $T_L$ and visual observation of heat-treated glasses .....                                    | 42   |
| Table 4.3 Summation of heat-treatment results for E1 and E2 group .....                                 | 44   |
| Table 4.4 Summation of heat-treatment results of E3 and E4group.....                                    | 45   |
| Table 4.5 Summation of heat-treatment results of E5 group.....  | 46   |
| Table 4.6 Component coefficients for fist order liquidus temperature models .....                       | 55   |
| Table 4.7 Measured $T_L$ and calculated $T_L$ of glasses E2, E3, E4 and E5 group .....                  | 56   |
| Table 4.8 $T_g$ , $T_L$ and ratio of transformation temperature $T_g$ : Liquidus temperature $T_L$ .... | 59   |
| Table 4.9 Comparison measured $T_L$ and calculated $T_L$ by $T_g/T_L$ ratio .....                       | 60   |
| Table 4.10 Measured $T_L$ using heating stage microscope .....  | 65   |
| Table 4.11 Comparing between measured and target compositions (wt%).....                                | 67   |
| Table 4.12 $T_L$ and visual observation of heat-treated glasses .....                                   | 68   |
| Table 4.13 Summation of heat-treatment results of industrial glass and EF group.....                    | 68   |

## LIST OF FIGURES

|  | Page |
|--|------|
| Fig. 2.1 Schematic 2-D representation of the structure of (a) Crystal and<br>(b) Glassy or vitreous form ..... | 4    |
| Fig. 2.2 Types of phase transformation .....   | 4    |
| Fig. 2.3 Change in free energy of a spherical nucleus as a function of radius .....                            | 7    |
| Fig. 2.4 Variation with temperature of homogeneous nucleation rate and growth<br>rate of the second phase..... | 8    |
| Fig. 2.5 Time-temperature-transformation curve .....   | 9    |
| Fig. 2.6 Formation of a crystal cluster on a solid substrate .....   | 10   |
| Fig. 2.7 Binary phase diagram .....  | 12   |
| Fig. 2.8 Platinum tray and gradient furnace used in ASTM-C829 .....  | 13   |
| Fig. 2.9 Viscosity of boron-free and boron-containing E-glass.....   | 20   |
| Fig. 2.10 Furnace for glass melting .....  | 21   |
| Fig. 2.11 Effect of Na <sub>2</sub> O and Li <sub>2</sub> O concentration .....                                | 23   |
| Fig. 3.1 Glass transition region measured temperatures.....  | 28   |
| Fig. 3.2 T <sub>g</sub> and T <sub>c</sub> determined using computer software .....                            | 28   |
| Fig. 3.3 Sketch of bottom load furnace .....   | 30   |
| Fig. 3.4 Flow chart of experimental procedure.....   | 31   |
| Fig. 3.5 Flow chart of uniform temperature method.....   | 32   |
| Fig. 3.6 Heating stage microscope .....  | 34   |
| Fig. 4.1 As-fabricated glasses obtained by melting at 1450°C .....   | 36   |
| Fig. 4.2 XRD pattern of as-fabricated glasses (E1 group).....  | 37   |
| Fig. 4.3 T <sub>g</sub> , T <sub>c</sub> and T <sub>c</sub> peak in DTA curve of E1R Glass.....                | 38   |

|           |  |    |
|-----------|--|----|
| Fig. 4.4  | Example of visual observations of heat-treated glass for $T_L$ determination .....                                   | 41 |
| Fig. 4.5  | The summarized crystalline phases detected in heat-treated glass<br>at near $T_L$ .....                              | 47 |
| Fig. 4.6  | EDX semi-quantitative analysis aid identifying crystalline phases .....  | 48 |
| Fig. 4.7  | XRD pattern of glass samples in E1 group heat-treated at 1130°C for 24 h....   | 49 |
| Fig. 4.8  | XRD pattern of glass samples in E2 group heat-treated at 1090°C for 24 h....   | 50 |
| Fig. 4.9  | XRD pattern of glass samples in E3 group heat-treated at 1090°C for 24 h....   | 51 |
| Fig. 4.10 | XRD pattern of glass samples in E4 group heat-treated at 1150°C for 24 h....   | 51 |
| Fig. 4.11 | XRD pattern of glass samples in E5 group heat-treated at 1150°C for 24 h....   | 52 |
| Fig. 4.12 | Isothermal section of system $\text{Na}_2\text{O}-\text{CaO}-\text{Al}_2\text{O}_3-\text{SiO}_2$ phase diagram ..... | 53 |
| Fig. 4.13 | Ternary phase diagram of system $\text{SiO}_2 - \text{CaO} - \text{Al}_2\text{O}_3$ .....                            | 54 |
| Fig. 4.14 | Plot of calculated $T_L$ vs. measured $T_L$ .....  | 57 |
| Fig. 4.15 | Ratio of transformation temperature $T_g$ : melt or liquidus temperature $T_m$ .....                                 | 58 |
| Fig. 4.16 | Plot of measured $T_L$ vs. predicted $T_L$ (using $T_g/T_L = 0.60$ or $3/5$ ) .....                                  | 61 |
| Fig. 4.17 | Melting point measurement of aluminum standard material using .....  | 63 |
| Fig. 4.18 | Step to observed and determined liquidus temperature of E2K3 using<br>heating stage microscope.....                  | 64 |
| Fig. 4.19 | Industrial E-glass (EFR) and as-fabricated glasses after melted at 1450°C ....                                       | 66 |
| Fig. 4.20 | Visual observations of heat-treated glass for $T_L$ determination.....   | 69 |
| Fig. 4.21 | XRD Pattern of glass samples heat-treated at 1140°C/24 h for EF0, EF03<br>and EF13, and 1000°C/24 h for EFR.....     | 70 |

## CHAPTER I

### INTRODUCTION

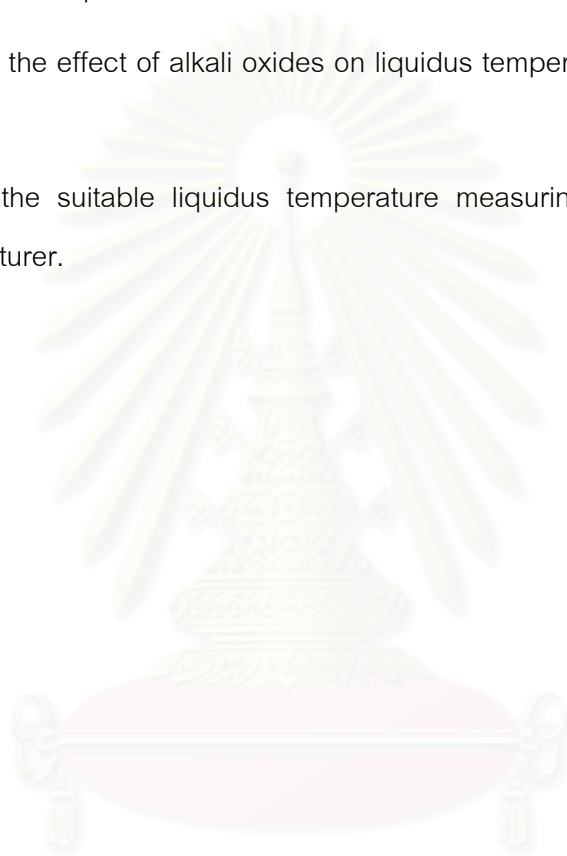
In recent years, There are more than 120 glass production plants in Thailand, composed of a large, medium, and small size, with total production volume more than one billion baht per year and continue increase a production capacity every year [1]. Many large plants are cooperated with oversea companies and imported modern and high technologies to apply into their production lines, while the smaller plants are facing with problems in production line cause by insufficient technology and skill for solving problems. The importance to identify and solve a production problem is the powerful laboratory which is not existed in those small plants. Some manufacturers send out a sample to an analytical service company or government offices which have a service laboratory with very expensive analytical instruments to measure properties or solve problems. They must be spent a lot of time waiting for the results; sometime it was too late for 24 hours running plant.

Liquidus temperature ( $T_L$ ) of glass, the temperature above that crystal can not exist in equilibrium system. It is one of necessary properties to consider in glass production. If crystals occur in glass production, it is considered a defect. In continuous fiber forming, when the molten glass include crystals is drawn to form thin continuous glass fiber, the fiber will be broken at crystal existed point. In case of changing raw materials  $T_L$  will be changed, therefore the change of its  $T_L$  must be known. The  $T_L$  can be measured by ASTM C829 which is used a gradient furnace. This method will be serviced by powerful laboratory only. This work has researched the possibility of using the easy and low cost methods to measure  $T_L$  of E-glass and ECR-glass which are fiber glass using a uniform temperature method and a heating stage microscope. Both methods were compared their accuracy using a standard material for  $T_L$  measurement. Moreover, they were used to determine  $T_L$  of fabricated glasses of varied compositions covering E-glass and ECR-glass compositions in order to concern the effect of alkali on  $T_L$ . Primary crystalline phase analysis, crystal morphology and thermal properties were

examined. Furthermore, energy conservation was considered. In order to decrease melting temperature and save energy, the  $T_L$  of glass compositions must be known.

The objectives of this study are described as follows;

- To compare liquidus temperature of prepared glasses in E-glass and ECR-glass compositions ranges measured by uniform temperature method and a heating stage microscope.
- To study the effect of alkali oxides on liquidus temperature of E-glass and ECR-glass.
- To find the suitable liquidus temperature measuring method for Thai glass manufacturer.



สถาบันวิทยบริการ  
จุฬาลงกรณ์มหาวิทยาลัย

## CHAPTER II

### LITERATURE REVIEWS

#### 2.1 Structure of glass

Glass is an amorphous solid formed by the solidification of a melt or other techniques without crystallization. Compared with crystals, the structure of glass is lack of regular arrangement of atom in a periodic lattice. This basic difference between the structure of glass and crystalline substance is well clearly showed on  $\text{SiO}_2$ , which is known both in vitreous and crystalline states as demonstrate in Fig. 2.1. Zacharaisen [2] suggested a theory that, as in crystals, the atom in glass must form extended three-dimensional networks. But the diffusion of the X-ray diffraction patterns shows that the network in glass is not symmetrical and periodic as in crystals. In the case of  $\text{SiO}_2$  the only difference between the crystalline and glassy forms is that in vitreous silica the relative orientation of adjacent silicon-oxygen tetrahedral is variable whereas in the crystalline form it is constant throughout the structure. Zachariasen proposed a set of rules which an oxide must satisfy if it is to be a glass-former.

1. No oxygen atom may be linked to more than two atoms of cations.
2. The number of oxygen atoms surrounding cation atom must be small (probably 3 or 4).
3. The oxygen polyhedra share corners with each other, not edges or faces.
4. At least three corners of each polyhedron must be shared.

Various properties of glass such as liquidus temperature, viscosity, thermal expansion, and durability can be explained based on the nature of the glass network's polyhedra and the way in which polyhedra are linked together.



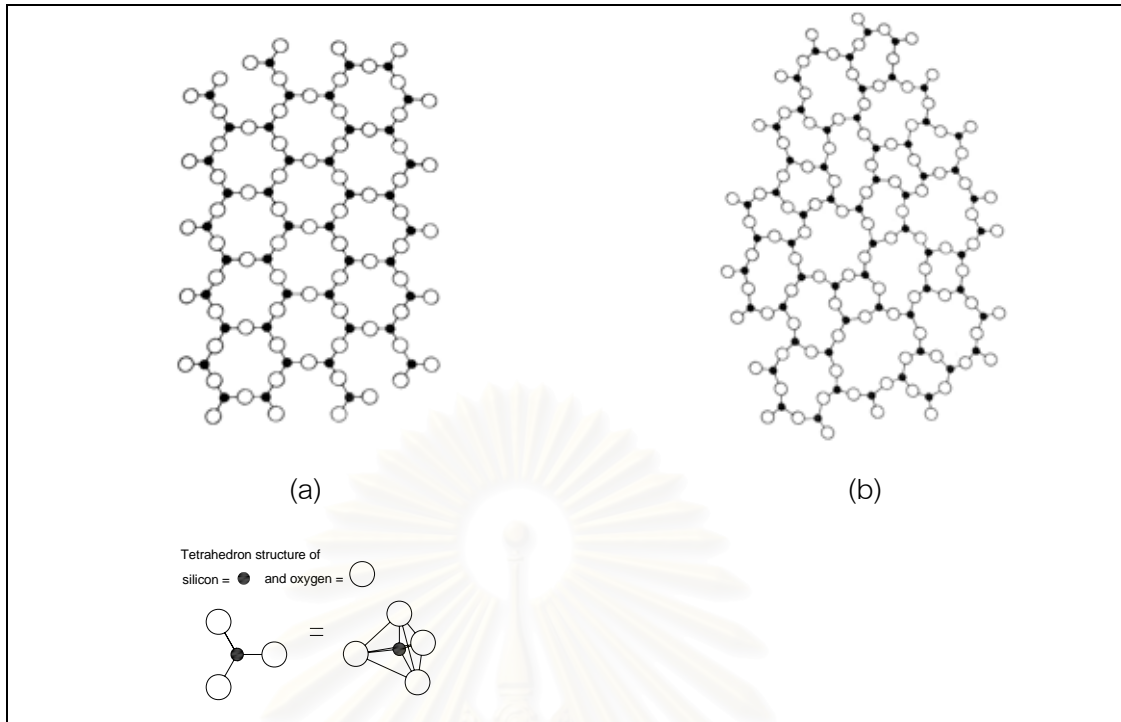


Fig. 2.1 Schematic 2-D representation of the structure of (a) Crystal and (b) Glassy or vitreous form [3].

## 2.2 Phase transformation

Phase transformation are usually observed in glass as showing types in Fig. 2.2

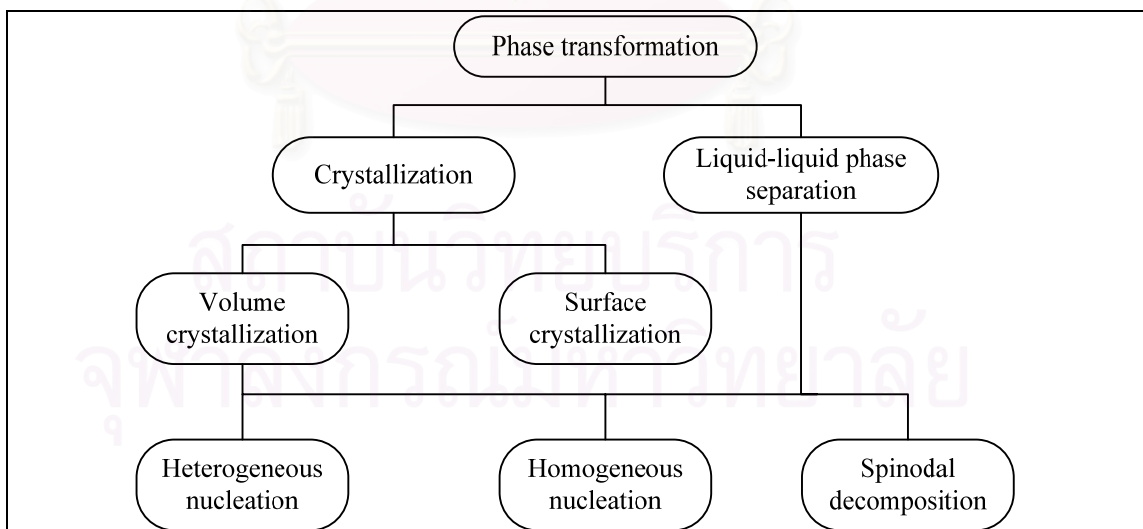


Fig. 2.2 Types of phase transformation [4]

Crystallization is the growth of a crystalline phase which may or may not have the same composition as the original liquid. Surface crystallization is the even that crystal growth begins from the glass atmosphere interface, and usually grows perpendicular to this interface. Volume crystallization will happen when crystal growth begins from “nucleation site” within the body of the material. The initial site for crystallization may be a substance foreign to the bulk of the material, when it is called *heterogeneous nucleation*, but if the nucleus is the same as the bulk material, it is called *homogeneous nucleation*. Liquid-liquid phase separation will occurs when the growth of non-crystalline phase which will have a different composition from the original phase. Spinodal decomposition is described that within a region which separates into two liquid phase there will be a region where there is no energy barrier to nucleation and phase separation is, therefore, limited by diffusion only. (surface crystallization)

## 2.3 Crystallization

### 2.3.1. Homogeneous nucleation

When a liquid is cooled down to its freezing point, crystallization occurs by the growth of crystals at a finite rate from a finite number of nuclei. Glass formation may be attributed to a low rate of crystal growth, a low rate of nuclei formation or a combination of both. The crystallization is referred to as a combination of nucleation and crystal growth, which occur simultaneously at some temperature range as shown in Fig. 2.4.

The stability of a particle of the new phase in homogeneous nucleation depends on two contributions: one from a difference in free energy between the two phases and the other from the interfacial energy. At the melting point the free energy of a given quantity of a material is the same in the crystalline and in the liquid forms. At lower temperatures the crystalline form will have the lower free energy and the liquid will crystallize if nuclei are available. If the increase in free energy per unit volume for the crystal-liquid transformation is  $\Delta G_v$ , the volume of the nucleus (crystal) is  $\frac{4}{3}\pi r^3$  (where  $r$  is the radius), the surface tension (or interfacial energy) is  $\gamma$ , the surface area  $4\pi r^2$ , then the free energy change for the nucleation  $\Delta G^*$  is given by

$$\Delta G = -\frac{4}{3}\pi r^3 \Delta G_v + 4\pi r^2 \gamma \quad (2.1)$$

At small value of  $r$  the surface term will dominate and  $\Delta G$  will be positive. However, as  $r$  increases the volume term will dominate and  $\Delta G$  will become negative. In Fig. 2.3 the two terms in equation (2.1) are plotted as functions of  $r$ , with the summation shown as a solid line. The critical radius,  $r^*$ , can be estimated by setting the derivative of  $\Delta G$  with respect to  $r$  equal to zero and solving for  $r$ :

$$r^* = -\frac{2\gamma}{\Delta G_v} \quad (2.2)$$

Particles of radius smaller than  $r^*$  are called embryos and are unstable, owing to the decrease in free energy which accompanies their reduction in size. Particles of radius greater than  $r^*$  are called nuclei and are stable, since growth is accompanied by a decrease in free energy.

The free energy barrier,  $\Delta G^*$ , associated with the formation of the critical-sized embryo is obtained by putting the value of  $r^*$  into equation 2.1.

$$\Delta G^* = \frac{16\pi\gamma^3}{3(\Delta G_v)^2}$$

สถาบันวิทยบริการ  
จุฬาลงกรณ์มหาวิทยาลัย

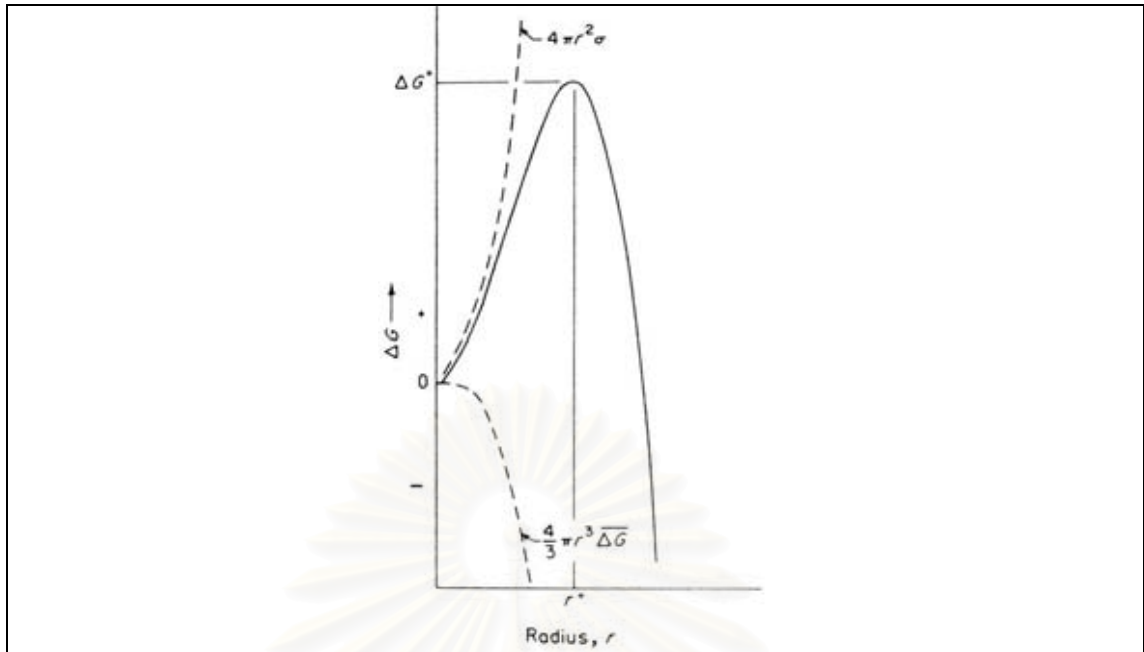


Fig. 2.3 Change in free energy of a spherical nucleus as a function of radius [4]

The overall nucleation process to form a nucleus with critical size  $r$  can be described by

$$I = A \exp \left[ - \frac{(\Delta G_{r^*} + \Delta G_D)}{kT} \right] \quad (2.3)$$

Where,  $I$  is a nucleation rate,  $A$  is a constant,  $\Delta G_{r^*}$  and  $\Delta G_D$  are the thermodynamic and kinetic free energy barriers to nucleation (in this case,  $\Delta G_{r^*}$  is the work required to form a nucleus of critical size that will grow instead of redissolve into the melt),  $k$  is the Boltzmann constant, and  $T$  is the absolute temperature (K).

For single glass the nucleation rate and growth rate depend strongly on temperature, as illustrated by Fig. 2.4. At liquidus temperature, they are both equal to zero, increase up to a maximum with decreasing temperature and then decrease asymptotically towards the temperature ordinate. The maximum in nucleation rate usually occurs at a lower temperature than the maximum in growth rate. This characteristic aids ready undercooling to glassy state while during heating up, the tendency to crystallization would be greater since nuclei first arise which are then capable of further growth. The diagram also represents the hatched area below the

liquidus point in which nucleation is quite difficult, because slight undercooling is hardly capable of overcoming the potential barrier related to the formation of the new melt-crystal phase boundary. However, when the nuclei are already present, crystals are capable of a comparatively rapid growth even in this region.

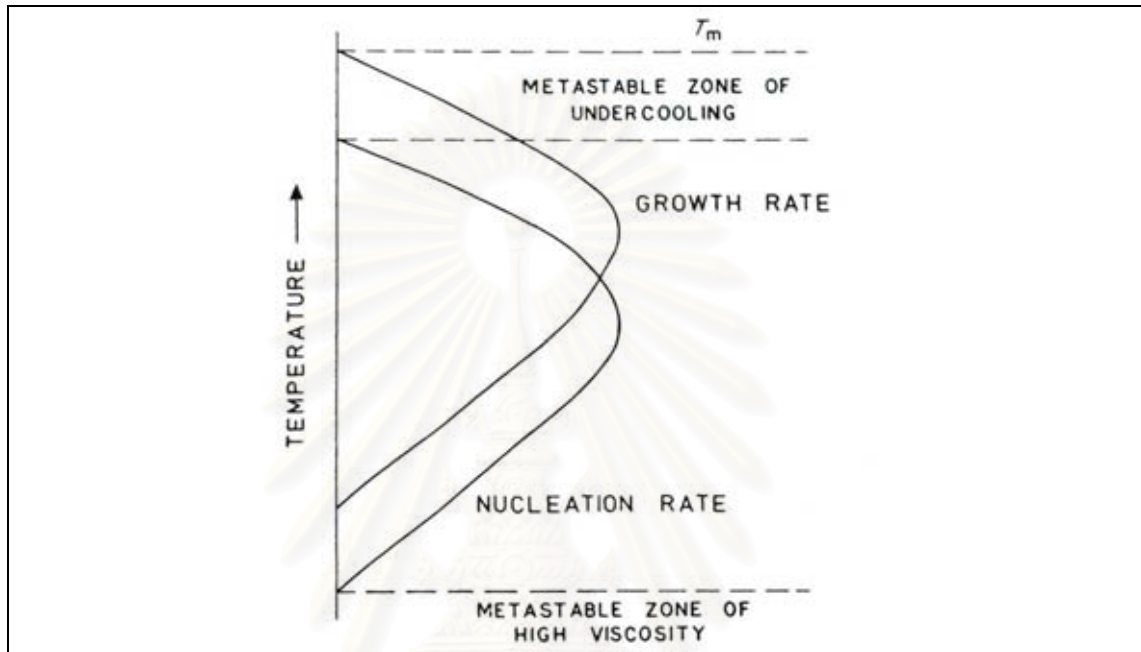


Fig. 2.4 Variation with temperature of homogeneous nucleation rate and growth rate of the second phase [4].

The volume fraction of crystals can be described by the equation with nucleation rate ( $I$ ) per unit volume ( $I_v$ ) and linear crystal growth rate ( $U$ ) terms. During cooling, both  $I_v$  and  $U$  will be time dependence due to their temperature dependence. For an isothermal condition, this curve is expressed by the following equation.

$$\frac{V_x}{V} = 1 - \exp\left(-\frac{\pi}{3} I_v U^3 t^4\right) \quad (2.4)$$

Where  $V_x$  = the volume of crystals and  $V$  = the sample volume

Fig. 2.5 shows the general shape of a TTT (Time-Temperature-Transformation) curve. A TTT curve is the result of the competition between thermodynamic and kinetic factors for both nucleation and growth rates.

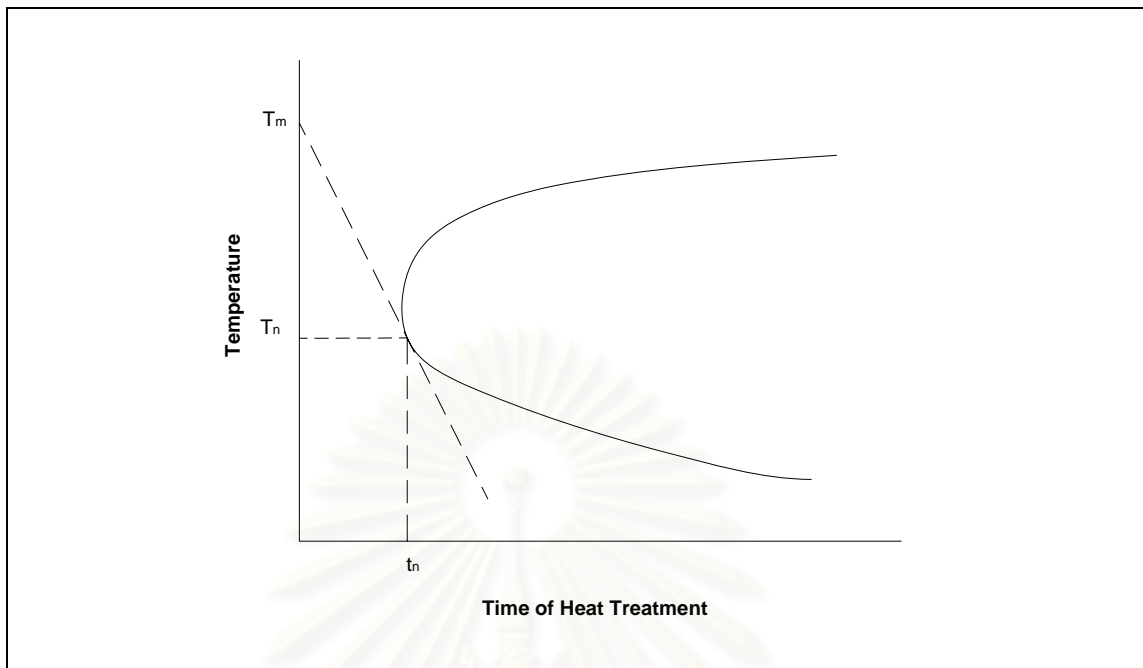


Fig. 2.5 Time-Temperature-Transformation curve

From Fig. 2.4, the temperature approaches  $T_m$  (melting temperature) both nucleation ( $I_v$ ) and growth rate ( $U$ ) approach zero, and the time required to form the specified volume fraction of crystals will approach infinity. At lower temperature,  $I_v$  and  $U$  also approach zero due to the very high viscosity of the melt, and the time to reach the specified value of  $\frac{V_x}{V}$  also approaches infinity. The nose of the TTT diagram,  $T_n$ , is the least favorable condition for glass forming where the time to reach the curve  $t_n$  is the least.

Crystallization is not only a function of temperature but also with time. Combination of heat treatment times and temperatures to the left of this curve will yield glass without a specified volume fraction of crystals, whereas any combinations to the right of this TTT curve will yield crystals.

### 2.3.2. Heterogeneous nucleation

In heterogeneous nucleation, the nucleus develops on the surface of a foreign solid or substrate. This may be the container wall or it may be a solid particle dispersed

throughout the liquid. Fig. 2.6 illustrates a crystal cluster which has formed on a solid surface with contact angle  $\theta$ . Equation 2.5 shows the free energy change,  $\Delta G$  involved in forming a crystal cluster now becomes

$$\Delta G = \frac{V_c}{V_m} \cdot \Delta G_V + S_{lc} \cdot \gamma_{lc} + S_{cs} (\gamma_{cs} - \gamma_{ls}) \quad (2.5)$$

Where  $\Delta G_V$  is free energy per unit volume for the crystal-liquid transformation.  $V_c$  is the volume of the crystal cluster,  $V_m$  is the molar volume of the crystalline phase,  $S_{lc}$ ,  $S_{cs}$  are the surface areas of the liquid-crystal and the crystal-substrate interface respectively, and  $\gamma_{lc}$ ,  $\gamma_{cs}$  and  $\gamma_{ls}$  are the interfacial energies between liquid-crystal, crystal-substrate, and liquid-substrate respectively.

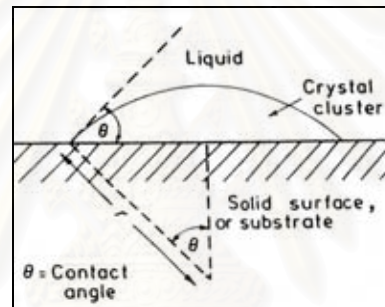


Fig. 2.6 Formation of a crystal cluster on a solid substrate

The crystal cluster is assumed a spherical cap of radius, and in condition of static equilibrium between the three phases, and also that substrate is plane, the following equations can be derived:

$$\gamma_{ls} = \gamma_{cs} + \gamma_{lc} \cos \theta$$

$$V_c = \frac{4}{3} \pi r^3 \left( \frac{2 - 3 \cos \theta + \cos^3 \theta}{4} \right)$$

$$S_{lc} = 2 \pi r^2 (1 - \cos \theta)$$

$$S_{cs} = \pi r^2 \sin^2 \theta$$

Substituting these value in equation 2.5 and differentiating with respect to  $r$ ,  $W_{het}^*$  is found to be

$$\Delta G_{\text{het}}^* = \frac{16\pi\gamma_{\text{lc}}^3 V_m^2}{3(\Delta G_V)^2} \cdot \left( \frac{2 - 3\cos\theta + \cos^3\theta}{4} \right)$$

or  $\Delta G_{\text{het}}^* = \Delta G^* \cdot f(\theta)$

$$f(\theta) = \left( \frac{2 - 3\cos\theta + \cos^3\theta}{4} \right)$$

and  $r^* = -\frac{2\gamma_{\text{lc}} V_m}{\Delta G_V}$

Hence the critical radius for the cap is the same as the critical radius for a sphere formed in homogeneous nucleation  $\left( r^* = -\frac{2\gamma}{\Delta G_V} \right)$ . However, the free energy  $\Delta G_{\text{het}}^*$  involved in forming the cap is less, since  $f(\theta) \leq 1$  for  $0 \leq \theta \leq \pi$ .

Thus the presence of the substrate causes a lowering in the thermodynamic barrier to nucleation. A low value of  $\Delta G_{\text{het}}^*$  is obtained if there is a high degree of 'wetting' between the crystal phase and the substrate.

From the previous discussion it is clear that, if suitable substrate is introduced into an undercooling liquid, the energy barrier to nucleation is capably reduced.

## 2.4 Liquidus temperature

### 2.4.1. Definition of liquidus temperature

Fundamentally, a crystallization which hinders glass formation can occur only below the melting temperature  $T_m$ . Only single-component systems, however, have a sharp melting point, while glasses in normal commercial usage consist almost entirely of several components. The liquidus temperature,  $T_L$ , then, is decisive for the possibility of crystallization. The  $T_L$  is the temperature below which a single liquid phase is no longer thermodynamically stable [5]. Consequently,  $T_L$  is defined as the highest temperature at which crystals can exist in equilibrium within the melt [186]. During the glass melting process, if the temperature of the melt was held above the liquidus temperature it should be free from crystallization.



Fig. 2.7 shows an example of  $T_L$  for binary phase diagram at a specific composition. When the temperature was decreased slowly from the X-position to reach the 1-position, the crystallization of this composition started at this point, which is  $T_L$ .

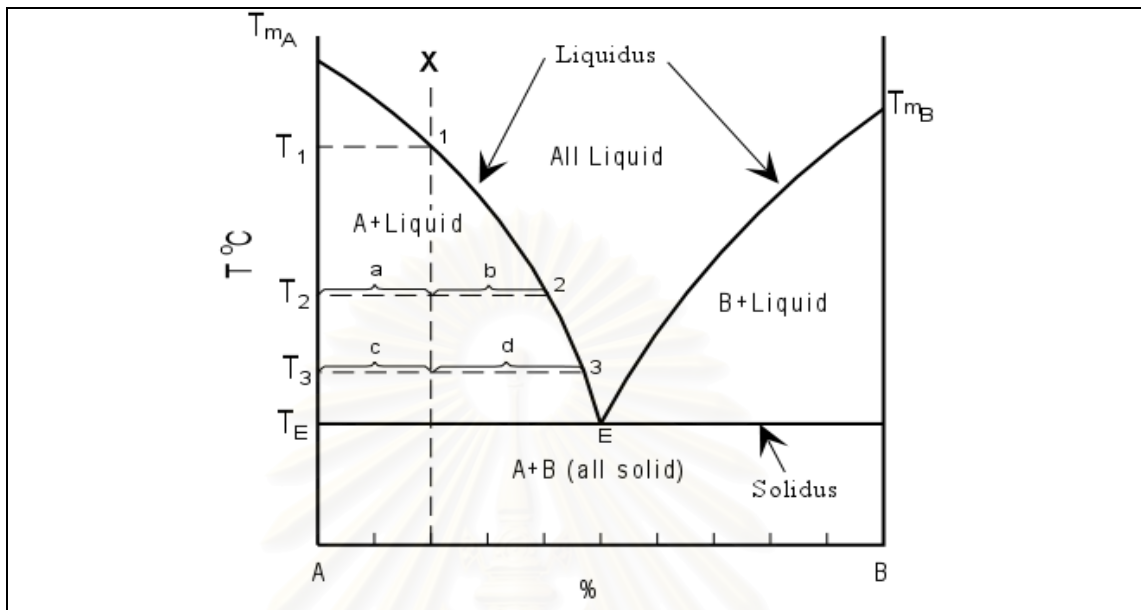


Fig. 2.7 Binary phase diagram

#### 2.4.2. Liquidus temperature measurements of glass

There are various methods to measure  $T_L$ ; however, just only one method is arranged as a measurement standard, which is ASTM-C829 [7] standard practices for measurement of liquidus temperature of glass by a gradient furnace. The other one method that is usually found in references is uniform temperature method of some work called isothermal process [8]. Using of heating stage microscope is alternative method to measure  $T_L$ . In this work the author concentrated on the results of liquidus temperature measurement using uniform temperature method and heating stage microscope to compared result and studies the possibility of using a faster method for  $T_L$  measurement.

The uniform temperature method is assumed to give higher degree of accuracy, but take time, while the heating stage microscope is hypothesized that it can be used to examine the crystallization temperature or liquidus temperature on glass with faster and shorter time consumed.

Following ASTM C829, the glass is placed in a platinum tray (Fig. 2.8) and heat-treated in a gradient furnace for 24 h. The time requirement is a function of the glass composition. Twenty four hours are sufficient for most glasses, but some glasses may take days to reach equilibrium. Then, the heat-treated glass is examined the  $T_L$  position by optical microscope. The  $T_L$  is examined at the position that the last crystal is detected. J.V. Crum [9] studied the liquidus of High-Level Waste Glasses, proposed that the temperature used for melting glass composition should be  $100^\circ\text{C}$  higher than their  $T_L$  to avoid the crystallization.

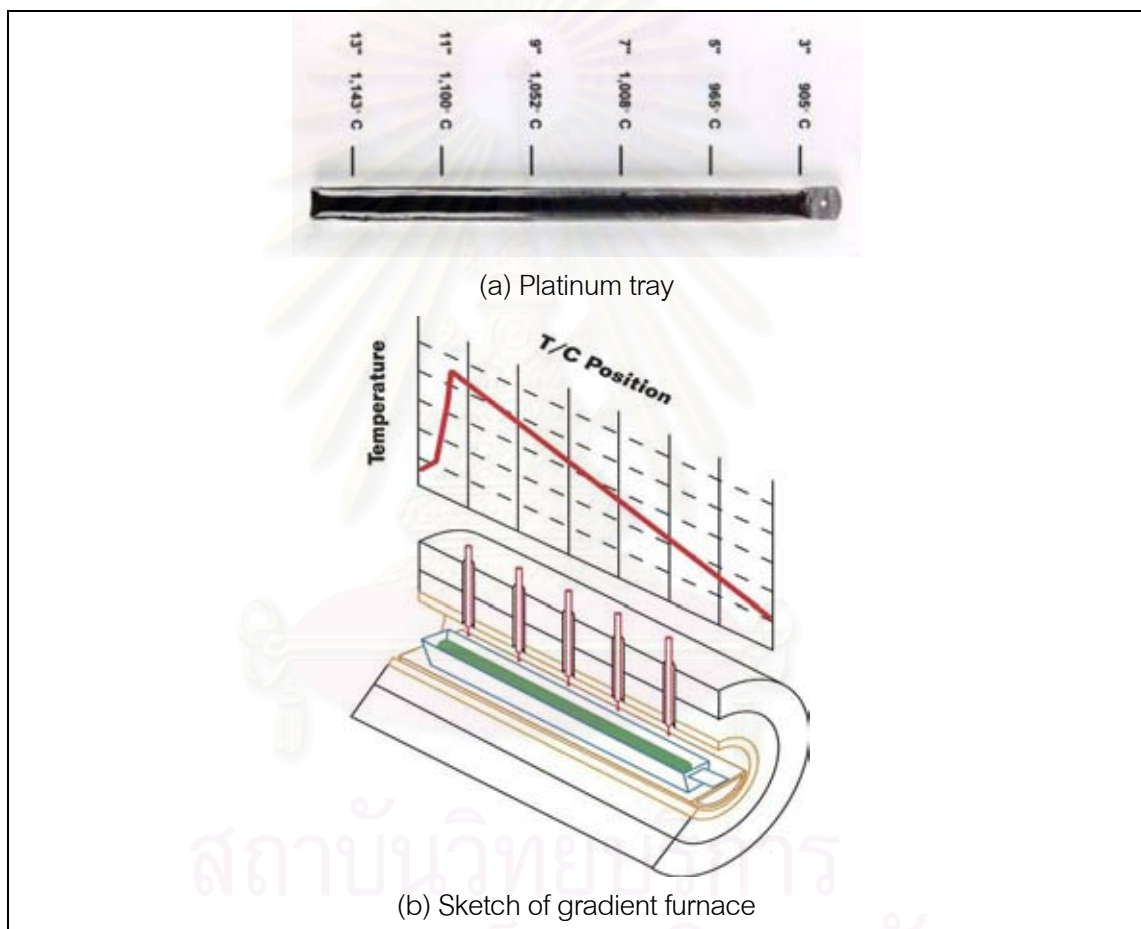


Fig. 2.8 Platinum tray and gradient furnace used in ASTM-C829 [10]

The uniform temperature method is similar to a methods used for phase diagram determination. In this method, glass samples are subjected to temperatures for a fixed period of time.  $T_L$  is given by the temperature range between the highest temperature at which a heat-treated sample contains crystals and the lowest temperature without crystals in the sample. This method is labor intensive and thus time

consuming. However, it has the potential for a more precise measurement (on the order of  $\pm 5^\circ\text{C}$ ) and is capable of measuring  $T_L$  values as high as important parameter for glass processing its determination is one of the principle goals for this study.

The idea of using the heating stage microscope to determine chemical and physical properties of compounds happened in the 19<sup>th</sup> century. The earliest mixed fusion experiments using a heating stage microscope, or the "Crystallization Microscope", as he called, to elucidate cocrystal formation were carried out in 1877 by Lehmann [11]. After that the heating stage microscope were developed and applied to various fields such as pharmaceutical, chemical, biological, materials science, geology, forensic, optical microscope crystal and many others. This equipment is a combination of heating stage and light microscope. The heating stage is capable to control heating rate and cooling rate and simultaneously observe the change of microstructure of the sample through the optical microscope. The high temperature heating stage is used to study in field of ceramics, metallurgy, materials, geology and high temperature polymers at both high and low heating and cooling rates. The crystallization is also observed by this equipment. In this work the heating stage was used to examine the temperature that crystals in the glass transform to be molten glass, which was assumed to be at the liquidus temperature.

## 2.5 Liquidus prediction using statistical modeling

In general, industrial glasses are blends of oxides, in which the total number of different oxides can be high. The composition of these blends is a key factor for many physical properties of glass. Many oxide glass properties vary smoothly with composition across a wide range of concentration; therefore, data obtained from a large amount of experimental work, extending over years, can be used for inferring many physical properties of glasses from their compositions [12]. Even simple additive equations are proposed to be quite successful for several important properties, such as thermal expansion, density at room temperature, refractive index [13]. And several approximation procedure have been proposed for viscosity [14, 15]. The liquidus temperature is the glass property that is the most difficult to predict [13]. Thermodynamic

modeling was found to be quite successful, but another study concluded that empirical models derived from series of glasses and statistical analysis still remain the most useful approach, because thermodynamic modeling might require the estimation of thermodynamic parameters that are not known accurately [16, 17]. Methodical studies of glass properties were initiated in the 19<sup>th</sup> century by E. Abbe, O. Schott and A. Winkelmann. Winkelmann and Schott published the first model that allowed the prediction of glass properties based on the chemical composition, using the multiple regression with linear functions. This principle is based on the assumption that the relation between the glass composition and a specific property is linear to all component concentrations, and all component influences can be summed.

$$\text{Property} = b_0 + \sum_{j=1}^n b_j \cdot C_j \quad (2.5)$$

$b_0$  in equation 2.5 is the model intercept (for main glass component silica ( $\text{SiO}_2$ ) this case  $b_0 = 0$ ).  $n$  is the total number of significant glass components excluding the main component (usually silica), the  $j$  value are the individual numbers of the significant glass components,  $b_j$  are the component-specific coefficients, and  $C_j$  are the concentrations of the glass components (also called model factors). This principle does allow very precise and accurate predictions within limited concentration ranges [18, 19, 20, 21, 22, 23]. Equation 2.5 is widely used for glass property modeling because of the simplicity of the technique, the ease of interpretation, and good prediction results within specified limits. However it cannot be applied for modeling glass properties over wide concentration range due to component interactions.

Although the liquidus temperature depends only on the composition of the blend, liquidus curves exhibit sharp minimum as well as inflexions and maximum across sections of most systems, so that multiple linear regression analysis cannot be expected to be successful. As the liquidus temperature exhibits a very strong non-linear behavior, it is difficult to account for it in a large range of composition, even by high order polynomial approximations. In order to eliminate the problems that arise near the boundaries, it was suggested to divide the data into different regions. As long as the composition was kept within the same primary phase field of the phase diagram,

polynomial relations between the composition and the liquidus temperature could be found in several papers in order to predict the liquidus temperature in usual industrial glass with up to 10 different oxides [17]. Equation 2.6 is second order polynomial functions.  $b_0$ - $b_3$  are the coefficients, with  $b_0$  being the intercept,  $b_1$  the single-component coefficients,  $b_2$  the coefficients of equared influences, and  $b_3$  the coefficients of two-component interactions. The variable  $n$  in equation 2.6 is total number of the significant glass components excluding silica;  $j$  and  $k$  are individual numbers of the significant glass components, and  $C$  are the component concentrations (excluding silica).

$$\text{Property} = b_0 + \sum_{j=1}^n \left\{ b1_j \cdot C_j + b2_j \cdot C_j^2 + \sum_{k=j+1}^n b3_k \cdot C_j \cdot C_k \right\} \quad (2.6)$$

This equation may be used for glass property modeling in multi-component systems over wide concentration ranges. Sudden property changes such as due to crystallization and phase separation are difficult to describe through multiple regression using polynomial functions [24], so that, advance non-linear functions should be applied in these case. Dreyfus et al. [24] apply neural networks to the prediction of the liquidus temperature of glass forming liquids of oxide blends. They show that neural networks regression is advantageous compared to multiple regression using composition, but if sharp property extremely occur. Polynomial functions do not fit sharp extremely well, that may appear in glasses due to crystallization or phase separation.

In this work, the first order Sheffe' polynomial modeling approach was selected to evaluate liquidus temperature as a function of composition for each primary phase field, because the glass compositions in this study were specifically in short-range of concentrations.

Today the liquidus temperature may be calculated from computer software such as FactSage [25], SciGlass [26] and Uniglass [27]; however, those software still be predicted within limited concentration ranges, and be able to calculate accurately in some glass systems.

## 2.6 E-glass and ECR-glass

### 2.6.1. Definition of glass fibers

Glass Fibers are among the most versatile industrial materials known today. They are produced from raw materials, which are available in virtually unlimited [28]. Glass fibers in this article are derived from compositions containing silica. They exhibit useful bulk properties such as hardness, transparency, resistance to chemical attack, stability, and inertness, as well as desirable fiber properties such as strength, flexibility, and stiffness [29]. Glass fibers fall into two categories, low-cost general-purpose fibers and premium special-purpose fibers. More than 90% of all glass fibers are general-purpose products. These fibers are known by the designation E-glass and are subject to ASTM specifications [30]. The remaining glass fiber is premium special-purpose products. Many, like E-glass, have letter designations implying special properties. Some have trade names, but not all are subject to ASTM specifications. Specifically:

Table 2.1 Definitions of glass fiber followed ASTM

| Letter designation | Property or characteristic     |
|--------------------|--------------------------------|
| E, Electrical      | Low electrical conductivity    |
| S, strength        | High strength                  |
| C, chemical        | High chemical durability       |
| M, modulus         | High stiffness                 |
| A, alkali          | High alkali or soda lime glass |
| D, dielectric      | Low dielectric constant        |

“E” glass definition followed ASTM [30] is a group of oxides include oxide of calcium, aluminum and silicon as major compositions. Table 2.2 divided E-glass into 2 composition range by their applications.

Table 2.2 E-glass compositions classified by application used

| Chemical composition                   | Printed circuit board and aerospace applications (wt %) | General purpose (wt %) |
|--|---|------------------------|
| B <sub>2</sub> O <sub>3</sub>          | 5 - 10  | 0 - 10                 |
| CaO                                    | 16 - 25   | 16 - 25                |
| Al <sub>2</sub> O <sub>3</sub>         | 12 - 16   | 12 - 16                |
| SiO <sub>2</sub>                       | 52 - 56   | 52 - 62                |
| MgO                                    | 0 - 5   | 0 - 5                  |
| Na <sub>2</sub> O and K <sub>2</sub> O | 0 - 2   | 0 - 2                  |
| TiO <sub>2</sub>                       | 0 - 0.8   | 0 - 1.5                |
| Fe <sub>2</sub> O <sub>3</sub>         | 0.05 - 0.4  | 0.05 - 0.8             |
| Fluoride                               | 0 - 1.0   | 0 - 1.0                |

“ECR” glass is developed from E-glass, which is boron-free. Stringent environmental regulations require the addition of costly emission abatement systems to eliminate boron from the off-gases of boron-containing melts. This glass fiber is alternative product which is environment friendly boron-free E-glass. ECR-glass compositions were derived from quaternary phase diagram of SiO<sub>2</sub>-Al<sub>2</sub>O<sub>3</sub>-CaO-MgO system. It is found that this glass has higher chemical resistance than E-glass which derived from ternary phase diagram of SiO<sub>2</sub>-Al<sub>2</sub>O<sub>3</sub>-CaO with high boron containing. ECR glass has longer acid resistance but shorter in alkali [31]. The compositions show in Table 2.3.

สถาบันวิทยบริการ  
จุฬาลงกรณ์มหาวิทยาลัย

Table 2.3 Chemical composition of ECR-glass

| Chemical composition                   | ECR-glass wt % |
|--|----------------|
| B <sub>2</sub> O <sub>3</sub>          | -              |
| CaO                                    | 21-23          |
| Al <sub>2</sub> O <sub>3</sub>         | 10-13          |
| SiO <sub>2</sub>                       | 58-63          |
| MgO                                    | 2-4            |
| Na <sub>2</sub> O and K <sub>2</sub> O | 0-1.2          |
| TiO <sub>2</sub>                       | 1.0-2.5        |
| Fe <sub>2</sub> O <sub>3</sub>         | 0-0.4          |
| Fluoride                               | -              |
| ZnO                                    | 0-3.5          |

### 2.6.2. Glass melting and fiber forming

A glass is an amorphous solid obtained by cooling a melt (i.e., liquid phase) sufficiently fast that crystallization (devitrification) cannot occur. When the melt is cooled slowly, crystallization can occur at the liquidus temperature,  $T_L$ , where crystals and melt are in equilibrium, or below. Glass fibers are therefore obtained at high cooling rates. Chemically, a glass consists of a silica network. Other oxides facilitate melting, homogenizing, removal of gaseous inclusions, and fiber formation at optimum temperatures. This section addresses the generic glass-melting and fiber-forming process, including the viscosity versus temperature profile that is required for general-purpose E-glass glass fiber and more specifically, for E-glass fibers containing 5 to 6% boron oxide. Depending on fiber diameter, optimum fiber formation is achieved with melts having a viscosity ranging from log 2.5 to log 3 P. The generic melting and forming process that is required for boron-free E-glass is the same as the required for boron-containing E-glass, but the viscosity/ temperature profile differs. The relative forming temperature can be deduced from the Fulchuer curve shown in Fig. 2.9. They will be proportionately higher for boron-free E-glass at equal melt viscosities between log 2.5 to log 3.0 P.



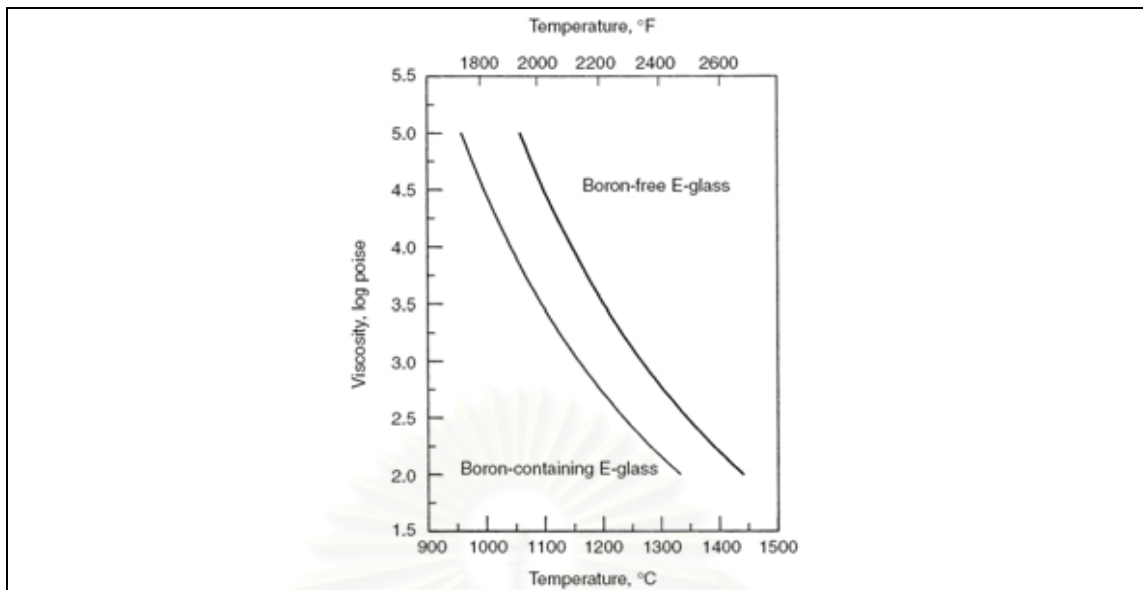


Fig. 2.9 Viscosity of boron-free and boron-containing E-glass [32]

The glass melting begins with the weighing and blending of selected raw materials. In modern fiber-glass plants, this process is highly automated, with computerized weighing units and enclosed material transport systems. The individual components are weighed and delivered to a blending station where the batch ingredients are thoroughly mixed before being transported to the furnace.

In general, fiberglass furnaces are divided into three distinct sections (Fig. 2.10). Batch is loaded into the furnace section for melting, removal of gaseous inclusions, and homogenization. Then, the molten glass flows into the refiner section, where the temperature of the glass is lowered from 1370°C to about 1260°C. The molten glass next goes to the forehearth section located directly above the fiber-forming stations. The temperatures throughout this process are prescribed by the viscosity characteristics of the particular glass. In addition, the physical layout of the furnace can vary widely, depending on the space constraints of the plant. The conversion of molten glass in the forehearth into continuous glass fibers is basically an attenuation process. The molten glass flows through a platinum-rhodium alloy bushing with a large number of holes or tips (400-8000, in typical production). The bushing is heated electrically, and the heat is controlled very precisely to maintain a constant glass viscosity. The fibers are drawn down and cooled rapidly as they exit the bushing.

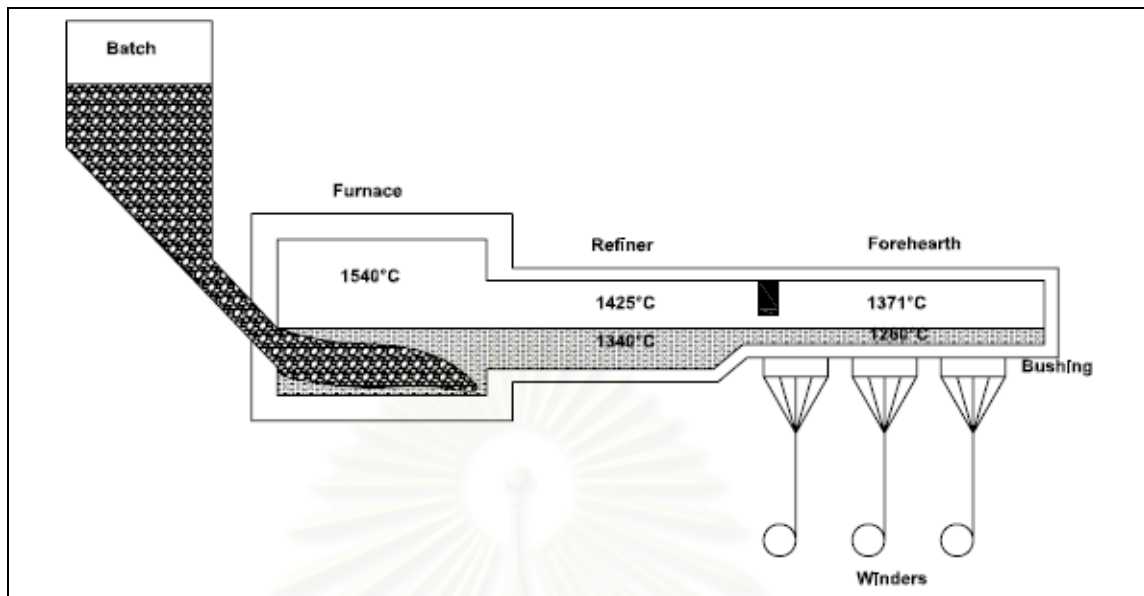


Fig. 2.10 Furnace for glass melting [32]

A schematic of furnace for glass melting in Fig. 2.10 shows the process from start melted through fiber drawn out at forehearth. The temperature must be controlled carefully because if the temperature at some position lowers than liquidus temperature the crystallizations can occur. Thus  $T_L$  of glass compositions must be known to avoid the broken of drawing fiber by crystals defect.

## 2.7 Effect of compositions on melt properties and liquidus temperature of E-glass

As the requirement of industry to minimize production cost especially energy cost and comply with environment emission standards. The melt and fiber-forming temperature (or melt viscosity) must be reduced by modifying or designing a new composition. The melt also must be crystallization resistant as they pass through the furnace and bushings, therefore, liquidus temperature must be considered too. The literatures of new boron-free and essentially boron-free E-glass melts were found in recent year [29, 33, 34]. The log3 fiber-forming temperature is the temperature of a glass melt that has a viscosity of  $10^3$  or (log3) poise. A specific 'delta' between forming and liquidus temperatures is required for a fiberglass melt to remain crystallization resistant in a commercial furnace. The desired delta temperature is furnace dependent, but a delta of  $\geq 60^\circ\text{C}$  is believed to be sufficient to prevent crystals from forming in a

colder spot of a melting furnace [35]. Incumbent E-glass compositions (approximately 6%B<sub>2</sub>O<sub>3</sub>) have low forming temperature (1174 – 1200°C) and high delta temperatures ( $\geq 100^\circ\text{C}$ ). The low forming temperatures are a consequence of the observation that each 1% of B<sub>2</sub>O<sub>3</sub> decrease the forming temperature by 12°C, starting with a B<sub>2</sub>O<sub>3</sub>-free base composition [35].

The effect of SiO<sub>2</sub> and CaO has been documented for a variety of E-glass variants[36, 37, 38]. From this study the compositions had a constant Al<sub>2</sub>O<sub>3</sub> content, a SiO<sub>2</sub> content that decreased from 60.63 to 57.75%, a CaO content that increased from 22.42 to 24.25% at a constant MgO content of 2.5-2.55%, an RO content that increased from 24.92 to 26.80%, and a SiO<sub>2</sub>/RO ratio that decreased from 2.43 to 2.15. It was found that a decrease of SiO<sub>2</sub> by 1% and corresponding increase of RO by 0.63% can be calculated and can be shown to decrease the log3 fiber-forming temperature and delta temperature by 13°C.

The effect of B<sub>2</sub>O<sub>3</sub> also has been documented in variety of E-glass system as the same reference studies in previous paragraph. For this study, the results showed that an increase of B<sub>2</sub>O<sub>3</sub> by 1% generally decreased the log3 fiber-forming temperature by 12°C from 0 to 10% B<sub>2</sub>O<sub>3</sub>. This effect was observed at a delta temperature of approximately 100°C and at a delta temperature of about 65°C.

Wallenberger et al [35] also study the effect of alkali oxides which are Li<sub>2</sub>O and Na<sub>2</sub>O. The Li<sub>2</sub>O is not a common ingredient in E-glass melt; however, because there are factors that limit the use of B<sub>2</sub>O<sub>3</sub>, Li<sub>2</sub>O could become a replacement for B<sub>2</sub>O<sub>3</sub> in an age of increasing energy cost and environmental concern if a cost-considered value-in-use can be shown. Li<sub>2</sub>O, Na<sub>2</sub>O and K<sub>2</sub>O are alkali-metal oxides, and the use of a combined content of 0-2% of alkali-metal oxide is allowed by ASTM E-glass specifications. The decrease of SiO<sub>2</sub> from 60.63 to 59.90% and the simultaneous in alkali oxide from zero to 1.2% dramatically decreased the log3 fiber-forming temperature for Li<sub>2</sub>O- and Na<sub>2</sub>O-modified compositions, but in unequal amounts. The results confirm that Li<sub>2</sub>O is more powerful modifier than Na<sub>2</sub>O. Following Fig. 2.11, the addition of 0.6 wt% Li<sub>2</sub>O to the alkali-oxide-free base composition produced a 36°C lower log3 fiber-forming temperature than the addition of 0.6 wt% Na<sub>2</sub>O, and a 14°C lower liquidus temperature.

Similarly, the addition of 1.2 wt%  $\text{Li}_2\text{O}$  to the alkali-oxide-free base composition produced a  $57^\circ\text{C}$  lower log3 fiber-forming temperature than the addition of 1.2 wt%  $\text{Na}_2\text{O}$ , and a  $23^\circ\text{C}$  lower liquidus temperature. Further more, the liquidus temperature trends to increase with increasing of both alkali oxides content.

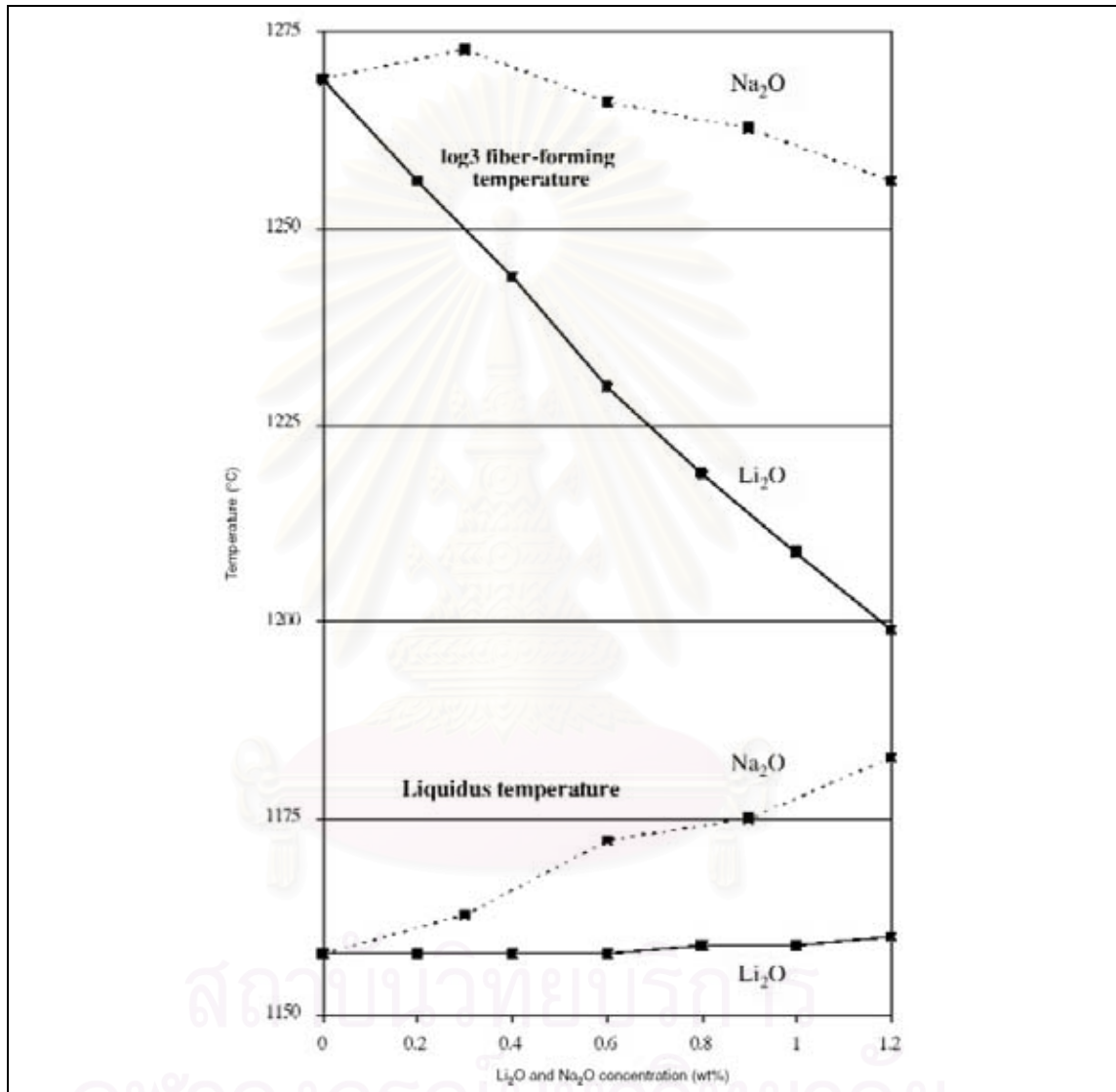


Fig. 2.11 Effect of  $\text{Na}_2\text{O}$  and  $\text{Li}_2\text{O}$  concentration

## CHAPTER III

### EXPERIMENTAL PROCEDURES

#### 3.1 Glass formula selection

Glass compositions based on E-glass and ECR-glass compositions ranges are shown in Table 3.1. Five groups of glass formulas were selected covering E-glass and ECR-glass composition ranges as follows, “E1”, “E2”, “E3”, “E4” and “E5”. Major ingredients in E-glass are  $\text{SiO}_2$ ,  $\text{Al}_2\text{O}_3$ ,  $\text{MgO}$  and  $\text{CaO}$  and  $\text{B}_2\text{O}_3$ . In order to study the effect of alkali oxides ( $\text{Na}_2\text{O}$  and  $\text{K}_2\text{O}$ ), 1 or 3 wt% of alkali oxides was added. Table 3.1 shows the typical chemical compositions of E-glass and ECR-glass and Table 3.2 shows the targeted compositions of selected 25 glass composition. The predicted mineral phases on glass were obtained from calculation method using ‘Uniglass’ software as shown in Table 3.3.

Table 3.1 Chemical compositions of E-glass and ECR-glass (wt %)

| Compositions            | Boron-containing E-glass [39] | Boron-free E-glass [40] | ECR-glass [41] |
|-------------------------|-------------------------------|-------------------------|----------------|
| $\text{SiO}_2$          | 52-56                         | 60.1                    | 58-63          |
| $\text{TiO}_2$          | 0.2-0.5                       | 0.5                     | 1.0-2.5        |
| $\text{Al}_2\text{O}_3$ | 12-15                         | 13.2                    | 10-13          |
| $\text{B}_2\text{O}_3$  | 4-6                           | -                       | -              |
| $\text{Fe}_2\text{O}_3$ | 0.2-0.4                       | 0.2                     | 0-0.4          |
| $\text{MgO}$            | 0.4-4                         | 3.0                     | 2-4            |
| $\text{CaO}$            | 21-23                         | 22.1                    | 21-23          |
| $\text{ZnO}$            | -                             | -                       | 0-3.5          |
| $\text{Na}_2\text{O}$   | 0-1                           | 0.6                     | 0-1.2          |
| $\text{K}_2\text{O}$    | -                             | 0.2                     | 0-1.2          |
| $\text{F}_2$            | 0.2-0.7                       | 0.1                     | -              |

Table 3.2 Chemical compositions of 25 selected glass samples

| Sample code | Chemical compositions (wt%) |                                |                               |      |       |     |                   |                  |
|-------------|-----------------------------|--------------------------------|-------------------------------|------|-------|-----|-------------------|------------------|
|             | SiO <sub>2</sub>            | Al <sub>2</sub> O <sub>3</sub> | B <sub>2</sub> O <sub>3</sub> | MgO  | CaO   | ZnO | Na <sub>2</sub> O | K <sub>2</sub> O |
| E1R         | 52                          | 15                             | 6                             | 4    | 23    | -   | -                 | -                |
| E1N1        | 51.8                        | 14.8                           | 5.8                           | 3.8  | 22.8  | -   | 1                 | -                |
| E1N3        | 51.4                        | 14.4                           | 5.4                           | 3.4  | 22.4  | -   | 3                 | -                |
| E1K1        | 51.8                        | 14.8                           | 5.8                           | 3.8  | 22.8  | -   | -                 | 1                |
| E1K3        | 51.4                        | 14.4                           | 5.4                           | 3.4  | 22.4  | -   | -                 | 3                |
| E2R         | 55                          | 15                             | 6                             | 1    | 23    | -   | -                 | -                |
| E2N1        | 54.8                        | 14.8                           | 5.8                           | 0.8  | 22.8  | -   | 1                 | -                |
| E2N3        | 54.4                        | 14.4                           | 5.4                           | 0.4  | 22.4  | -   | 3                 | -                |
| E2K1        | 54.8                        | 14.8                           | 5.8                           | 0.8  | 22.8  | -   | -                 | 1                |
| E2K3        | 54.4                        | 14.4                           | 5.4                           | 0.4  | 22.4  | -   | -                 | 3                |
| E3R         | 56                          | 13                             | 5                             | 3    | 23    | -   | -                 | -                |
| E3N1        | 55.8                        | 12.8                           | 4.8                           | 2.8  | 22.8  | -   | 1                 | -                |
| E3N3        | 55.4                        | 12.4                           | 4.4                           | 2.4  | 22.4  | -   | 3                 | -                |
| E3K1        | 55.8                        | 12.8                           | 4.8                           | 2.8  | 22.8  | -   | -                 | 1                |
| E3K3        | 55.4                        | 12.4                           | 4.4                           | 2.4  | 22.4  | -   | -                 | 3                |
| E4R         | 60                          | 13                             | -                             | 4    | 23    | -   | -                 | -                |
| E4N1        | 59.75                       | 12.75                          | -                             | 3.75 | 22.75 | -   | 1                 | -                |
| E4N3        | 59.25                       | 12.25                          | -                             | 3.25 | 22.25 | -   | 3                 | -                |
| E4K1        | 59.75                       | 12.75                          | -                             | 3.75 | 22.75 | -   | -                 | 1                |
| E4K3        | 59.25                       | 12.25                          | -                             | 3.25 | 22.25 | -   | -                 | 3                |
| E5R         | 62.0                        | 10                             | -                             | 2    | 23    | 3   | -                 | -                |
| E5N1        | 61.8                        | 9.8                            | -                             | 1.8  | 22.8  | 2.8 | 1                 | -                |
| E5N3        | 61.4                        | 9.4                            | -                             | 1.4  | 22.4  | 2.4 | 3                 | -                |
| E5K1        | 61.8                        | 9.8                            | -                             | 1.8  | 22.8  | 2.8 | -                 | 1                |
| E5K3        | 61.4                        | 9.4                            | -                             | 1.4  | 22.4  | 2.4 | -                 | 3                |

Where R = Regular mean no alkali oxides.  
 N1 and N3 = Glass composition with additional of 1 wt% Na<sub>2</sub>O and 3 wt% Na<sub>2</sub>O  
 K1 and K3 = Glass composition with additional of 1 wt% K<sub>2</sub>O and 3 wt% K<sub>2</sub>O

Table 3.3 Predicted normative mineral contents calculated by “Uniglass”

| Sample code | Components |   |       |      |  |       |       |   |       |
|-------------|------------|---|-------|------|--|-------|-------|---|-------|
|             | 2ZS        | KA6S  | NA6S  | BO   | CM2S   | 2CMS  | CAS   | CS  | S     |
| E1R         | -          | -   | -     | 6.00 | 21.49  | -     | 40.93 | 19.03   | 12.56 |
| E1N1        | -          | -   | 8.46  | 5.80 | 20.41  | -     | 35.89 | 21.29   | 8.14  |
| E1N3        | -          | -   | 25.38 | 5.40 | 15.76  | 3.15  | 25.83 | 24.48   | 0.00  |
| E1K1        | -          | 5.91  | -     | 5.80 | 20.41  | -     | 37.43 | 20.65   | 9.80  |
| E1K3        | -          | 17.73   | -     | 5.40 | 18.27  | -     | 30.43 | 23.90   | 4.28  |
| E2R         | -          | -   | -     | 6.00 | 5.37   | -     | 40.93 | 27.67   | 20.03 |
| E2N1        | -          | -   | 8.46  | 5.80 | 4.30   | -     | 35.89 | 29.94   | 15.61 |
| E2N3        | -          | -   | 25.38 | 5.40 | 2.15   | -     | 25.83 | 34.46   | 6.78  |
| E2K1        | -          | 5.91  | -     | 5.80 | 4.30   | -     | 37.43 | 29.29   | 17.27 |
| E2K3        | -          | 17.73   | -     | 5.40 | 2.15   | -     | 30.43 | 32.54   | 11.75 |
| E3R         | -          | -   | -     | 5.00 | 16.12  | -     | 35.47 | 24.19   | 19.23 |
| E3N1        | -          | -   | 8.46  | 4.80 | 15.04  | -     | 30.44 | 26.45   | 14.81 |
| E3N3        | -          | -   | 25.38 | 4.40 | 12.89  | -     | 20.37 | 30.98   | 5.97  |
| E3K1        | -          | 5.91  | -     | 4.80 | 15.04  | -     | 31.97 | 25.81   | 16.47 |
| E3K3        | -          | 17.73   | -     | 4.40 | 12.89  | -     | 24.97 | 29.06   | 10.95 |
| E4R         | -          | -   | -     | -    | 21.49  | -     | 35.47 | 21.31   | 21.73 |
| E4N1        | -          | -   | 8.46  | -    | 20.15  | -     | 30.30 | 23.67   | 17.43 |
| E4N3        | -          | -   | 25.38 | -    | 17.46  | -     | 19.96 | 28.39   | 8.81  |
| E4K1        | -          | 5.91  | -     | -    | 20.15  | -     | 31.84 | 23.03   | 19.08 |
| E4K3        | -          | 17.73   | -     | -    | 17.46  | -     | 24.57 | 26.47   | 13.78 |
| E5R         | 4.11       | -   | -     | -    | 10.74  | -     | 27.29 | 30.49   | 27.38 |
| E5N1        | 3.83       | -   | 8.46  | -    | 9.67   | -     | 22.25 | 32.75   | 23.03 |
| E5N3        | 3.29       | -   | 25.38 | -    | 7.52   | -     | 12.18 | 37.28   | 14.35 |
| E5K1        | 3.83       | 5.91  | -     | -    | 9.67   | -     | 23.79 | 32.11   | 24.69 |
| E5K3        | 3.29       | 17.73   | -     | -    | 7.52   | -     | 16.79 | 35.36   | 19.32 |
| 2ZS         | =          | 2ZnO·SiO <sub>2</sub>                                 | KA6S  | =    | K <sub>2</sub> O·Al <sub>2</sub> O <sub>3</sub> ·6SiO <sub>2</sub> | NA6S  | =     | Na <sub>2</sub> O·Al <sub>2</sub> O <sub>3</sub> ·6SiO <sub>2</sub> |       |
| BO          | =          | B <sub>2</sub> O <sub>3</sub>                         | CM2S  | =    | CaO·MgO·2SiO <sub>2</sub>  | 2CM2S | =     | 2CaO·MgO·2SiO <sub>2</sub>  |       |
| CA2S        | =          | CaO·Al <sub>2</sub> O <sub>3</sub> ·2SiO <sub>2</sub> | CS    | =    | CaO·SiO <sub>2</sub>   | S     | =     | SiO <sub>2</sub>  |       |

### 3.2 Glass preparation

All glass compositions were prepared from chemical grade oxides. Batch materials were calculated for 100 g of as-fabricated glass. Chemical grade oxides of  $\text{SiO}_2$ ,  $\text{Al}_2\text{O}_3$ ,  $\text{HB}_2\text{O}_3$ ,  $\text{MgCO}_3$ ,  $\text{CaCO}_3$ ,  $\text{ZnO}$ ,  $\text{Na}_2\text{CO}_3$ , and  $\text{K}_2\text{CO}_3$  (chemical identification is shown in Appendix A) were weighed and manually mixed in a plastic bottle. The mixed batch was placed in an 80 cc platinum crucibles and melted at  $1450^\circ\text{C}$  for 1 hour in an electric furnace with  $\text{Mo}_2\text{Si}$  heating elements. The molten glass was then poured onto a clean brass mold and cooled down to room temperature in air. The remaining of mixed batch was loaded and melted at the same condition.

### 3.3 Homogeneity examination of as-fabricated glasses

As-fabricated glass samples were determined on homogeneity and undissolved phases by optical microscope; OM (Olympus BX60M, Olympus optical co. Ltd., Japan) under reflected light with magnifications ranging from 50X to 1000X. In this work, all samples were transparent; therefore, they were not needed further the special preparation such as cross section, finishing or etching. Digital images were taken using a digital camera (Olympus DP12, Olympus optical co. Ltd., Japan).

The X-ray diffractometer (Bruker D8 Advance) was used to confirm the amorphous phase or non-crystallization of as-fabricated glass. The operating condition is:  $10^\circ < 2\theta < 60^\circ$ , step size of  $0.02^\circ$  and 40 KV.

The as-fabricated glass must be homogeneous with non-crystallization and undissolved phases. If the crystallizations or undissolved phases occur, the same batch compositions will be re-melted at higher temperature.

### 3.4 Determination of glass transition temperature and crystallization temperature

Differential thermal analysis (DTA) measures the differences in energies released or absorbed, and the changes in heat capacity of materials as a function of temperature. In this work, DTA (Perkin Elmer, DTA7, USA) was used to examine  $T_g$  (glass transition temperature) and  $T_c$  (crystallization temperature) of selected glass [42].  $T_g$  was determined automatically by computer software [43], which is a midpoint ( $T_m$ )



between extrapolated onset temperature ( $T_i$ ) and extrapolated end temperature ( $T_e$ ) in Fig. 3.1. This method was followed ASTM E 1356 – 03 [44].  $T_c$  was determined by onset temperature as shown in Fig. 3.2, it was performed automatically using computer software [43] similarly as  $T_g$ .

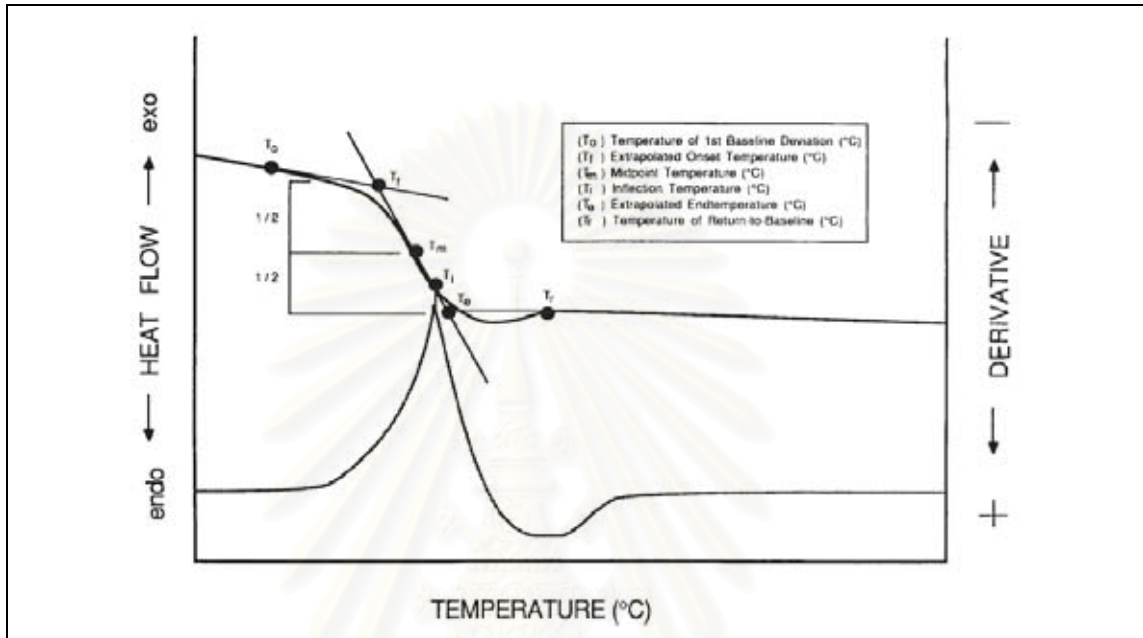


Fig. 3.1 Glass transition region measured temperatures

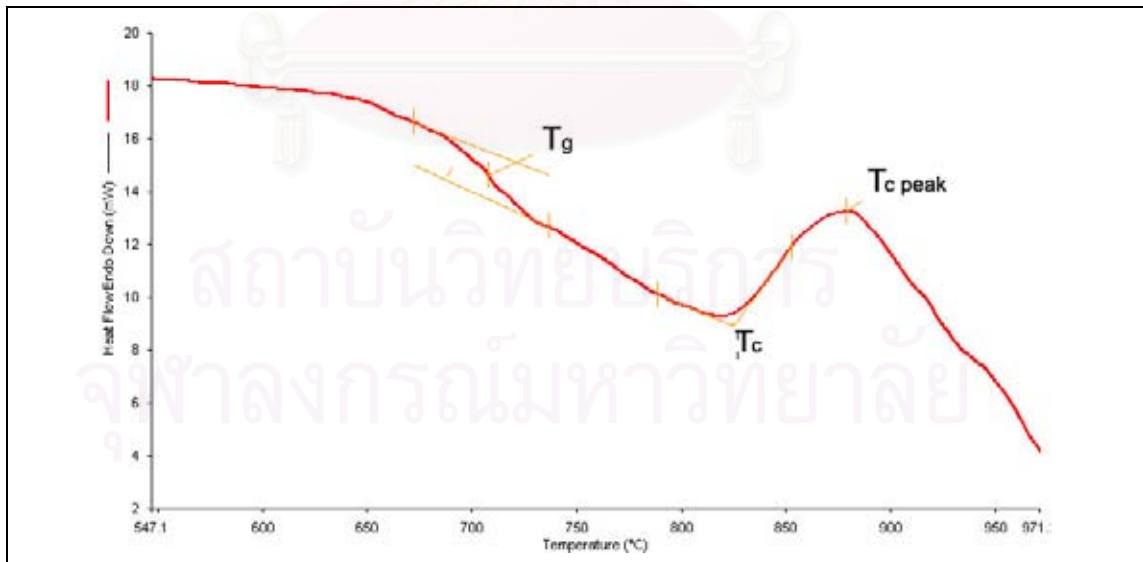


Fig. 3.2  $T_g$  and  $T_c$  determined using computer software [43].

An as-fabricated glass sample was ground manually using an alumina pestle and a mortar, and sieved through sieve number 100 mesh ( $\leq 150 \mu\text{m}$ ). A 20 mg of glass sample powder was loaded in a platinum crucible lining with thin layer of alumina powder in a sample holder of DTA furnace. Standard alumina was used as a reference material. They were heated from room temperature to  $1100^\circ\text{C}$  with a heating rate  $10^\circ\text{C}/\text{min}$ .  $T_g$  and  $T_c$  were determined.

### 3.5 Liquidus temperature determination using uniform temperature method

From section 3.2, approximately 5-10 g of crystal-free sample or as-fabricated glass which was ground and sieved through 100-mesh stainless screen was loaded in a platinum crucible. To begin a uniform temperature process, glass sample was heated from room temperature and held at designed temperature for 24 h in a bottom load furnace as shown in Fig. 3.3. The heat-treated glass was examined using an optical microscope at various magnifications up to 1000X in order to observe and determine appearance of crystals. If no crystallization in heat-treated glass, new glass powder of the same batch was heat treated at  $20^\circ\text{C}$  lower than the initial treatment. The converse of this also true (i.e., if crystals were observed the following heat treatment was performed at  $+20^\circ\text{C}$ ). Assuming that the liquidus temperature lays at half way between the two temperatures measured, which previous temperature detected crystals and higher temperature which crystals were not detected. This step wise approach was used to narrow down the  $T_L$  until a value  $\pm 10^\circ\text{C}$  was obtained.

The standard glass with previously measured  $T_L$  was used to aid in assessing the accuracy of the measurement technique. It is the National Institute of Standards and Technology (NIST) SRM-1461 liquidus measurement standard glass (See Appendix E).

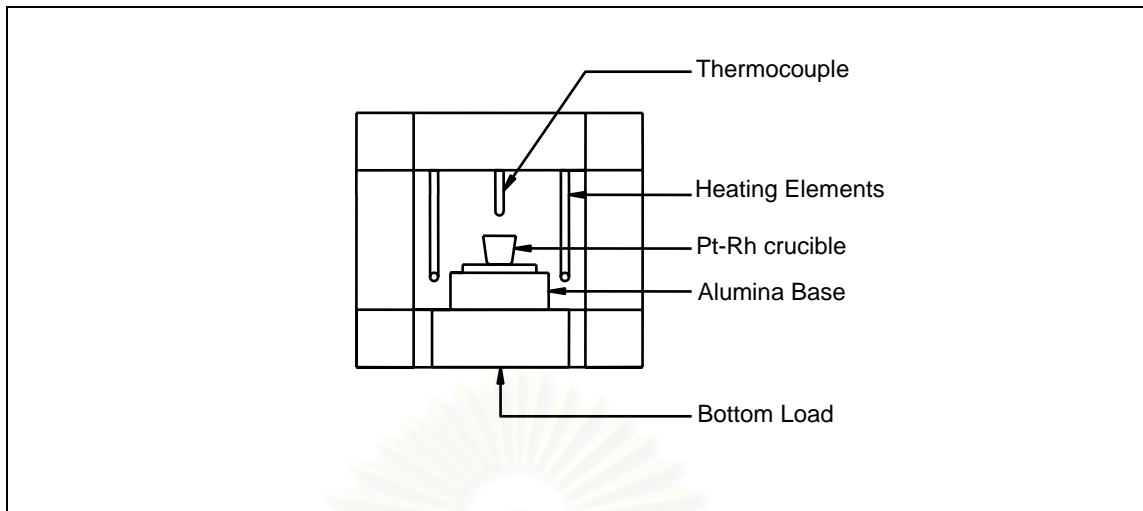


Fig. 3.3 Sketch of bottom load furnace

### 3.6 Primary phase identification

The primary phases in these glasses were determined using three techniques to support. Firstly, the heat treated glass at lower than liquidus temperature obtained from uniform temperature method was ground to process X-ray diffraction. The crystal phases were identified by XRD pattern. Crystals on surface of heat treated glass sample at temperature close to  $T_L$  were examined by OM. The crystal morphology was compared with references [45]. They were confirmed by scanning electron microscope; SEM (JEOL JSM-6400 model) and energy dispersive spectrometry; EDS (OXFORD Instrument ISIS 300). Especially, EDS was used to examine element compositions which were compared with expected crystalline chemical compositions.

สถาบันวิทยบริการ  
จุฬาลงกรณ์มหาวิทยาลัย

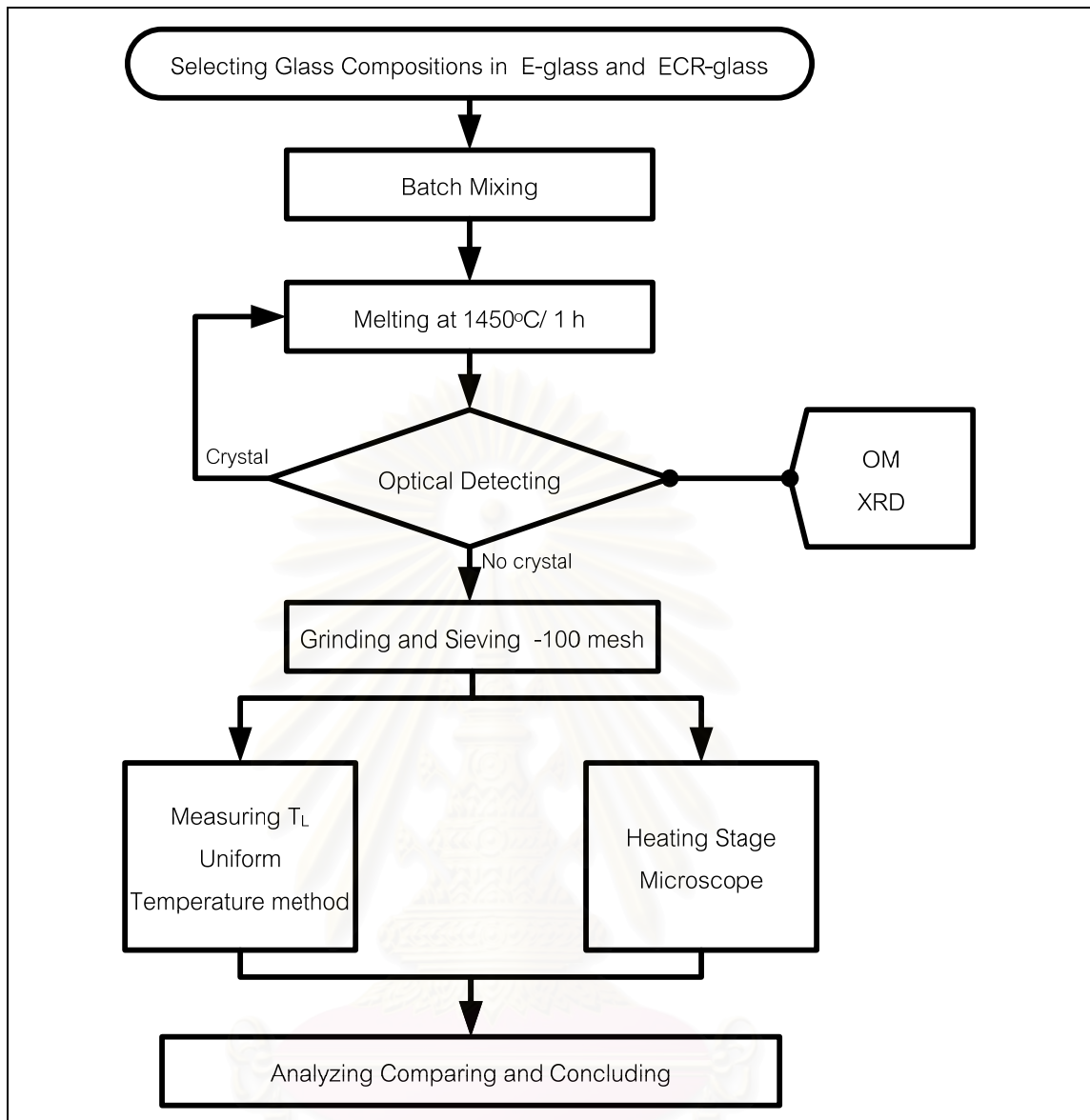


Fig. 3.4 Flow chart of experimental procedure

สถาบันวิทยบริการ  
จุฬาลงกรณ์มหาวิทยาลัย

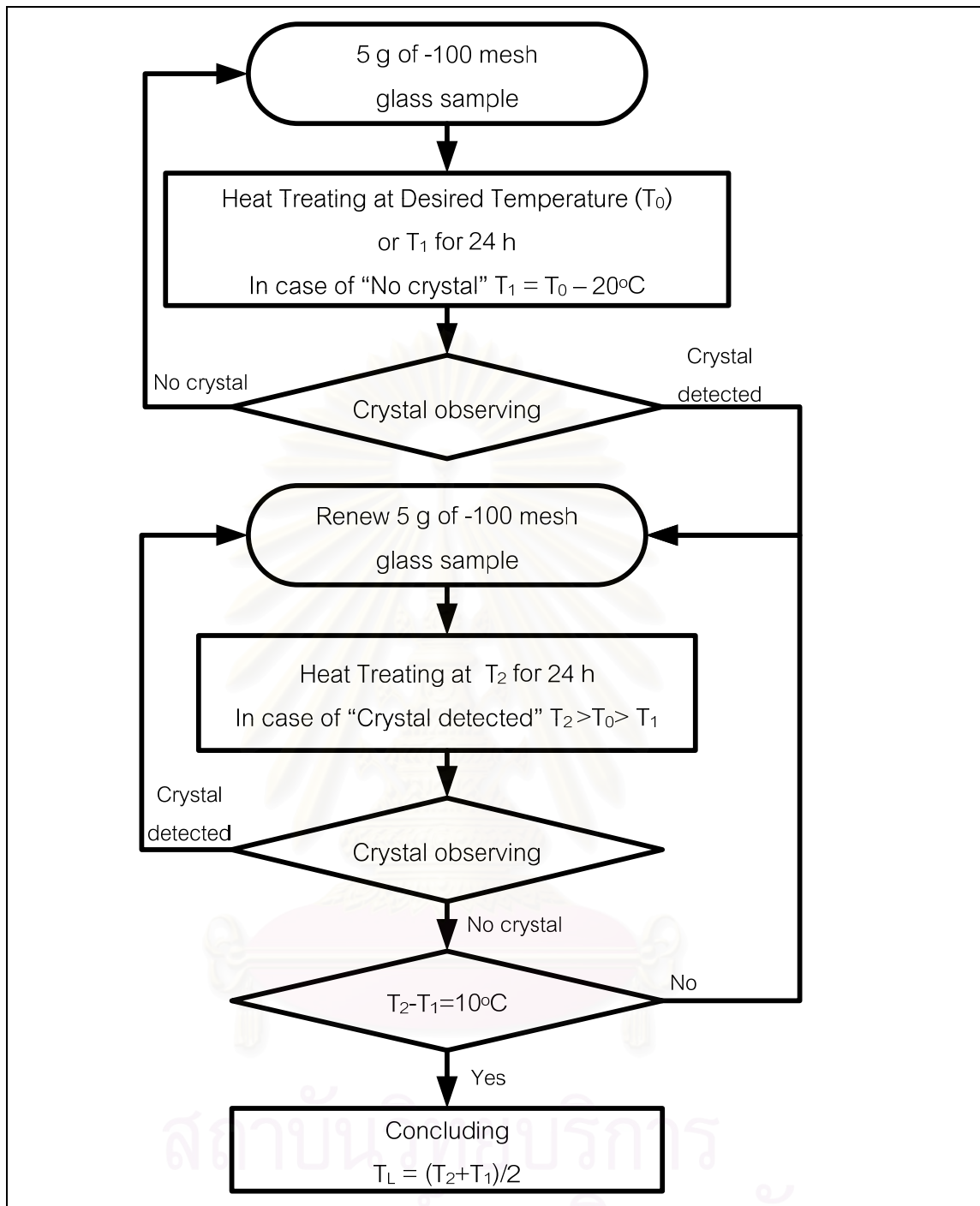


Fig. 3.5 Flow chart of uniform temperature method

### 3.7 Liquidus temperature determination using heating stage microscope

Heating stage microscope is the equipment composed of optical microscope and heating stage. In this work, heating stage could be heated up to 1400°C by Pt-Rd heating element. The sample was a small piece of crystals-containing glass (approximately 2-5 mg). The crystals-containing glass was started by heat treated as-fabricated glass at crystallization temperature region (between  $T_L$  and  $T_c$ ) for 24 h in an electric furnaces. In some cases, samples were come from uniform temperature method, which were heat-treated at lower temperature ( $T_c + 100^\circ\text{C}$ ) with high degree of crystallization. The samples were heated to high temperature with high heating rate approximately 20°C/min. When temperature approached 100°C to  $T_L$  (measured by uniform temperature method) heating rate was slowed down to approximately 1°C/min. The amount of crystals on surface was observed. The temperature was recorded when the amount of crystals started to change. The sample was heated until most of crystals were melted. Then, it was cooled down by 20°C with slow cooling rate and held at this temperature for 5 minutes. If crystallizations were detected, the sample was heated to higher temperature until crystals disappeared. Then, it was cooled down to 10°C higher than previous temperature and checked for crystallizations again. On the other hand, if crystallization points were not detected, the sample was cooled to lower temperature by 10°C per cooling step with 5 minutes of holding time per step, until crystals nucleation points were detected. Finally, the reported  $T_L$  for this method was the temperature that the crystals were disappeared when the sample was heating to higher temperature and the crystals were detected when the sample was cooling down from higher temperature.

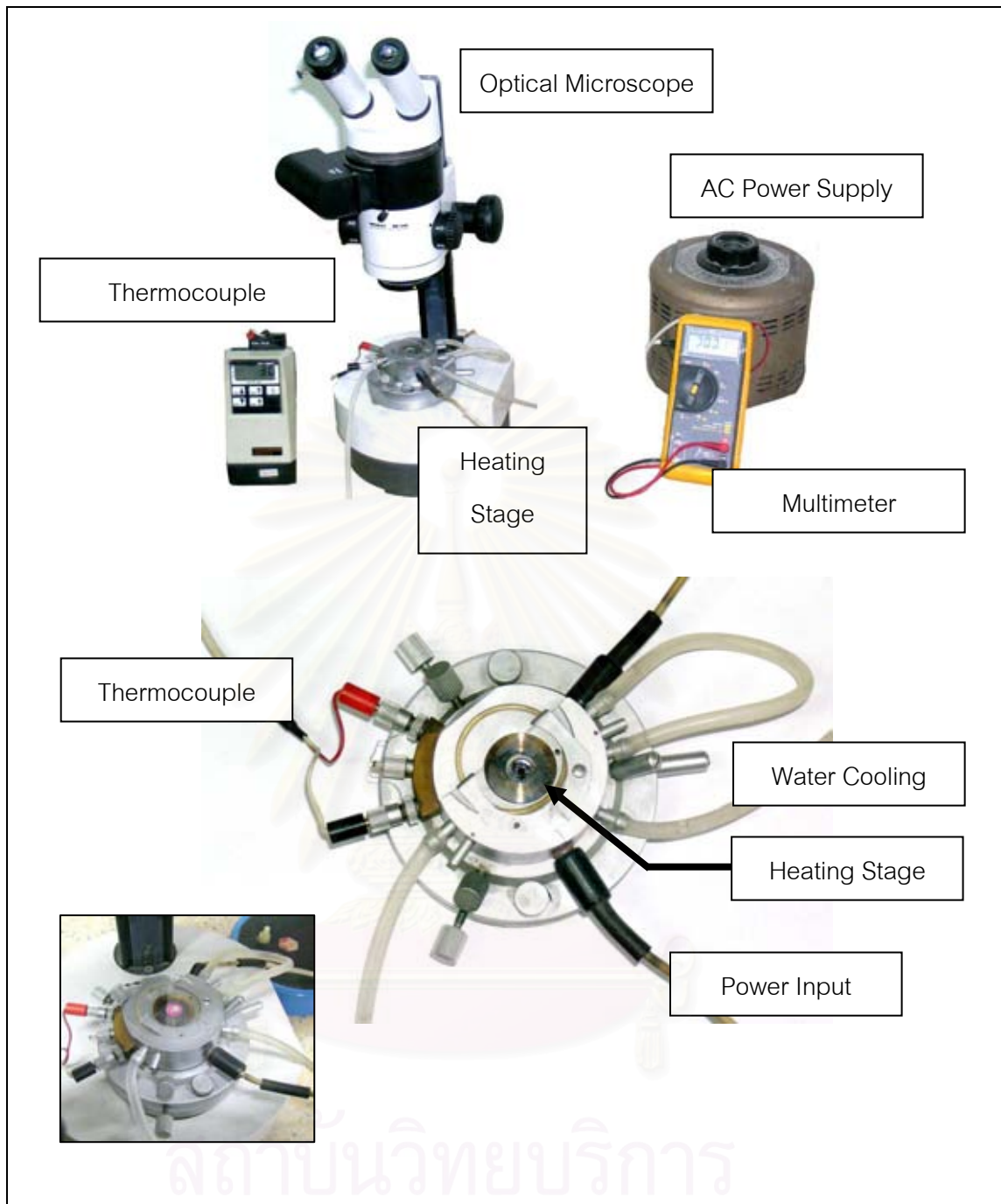


Fig. 3.6 Heating stage microscope

### 3.8 Case study on liquidus temperature of industrial glass

The sample of E-glass from the fiber glass industry was measured using a uniform temperature method. Firstly, the industrial E-glass sample (EFR) was analyzed the chemical composition by XRF. Then, the samples prepared from chemical compositions which was the same as EFR composition. The concentration of iron oxide was varied from 0, 0.3 and 1.3 wt% in order to study its effect on liquidus temperature. Table 3.4 shows the chemical compositions of EFR, EF0, EF03 and EF13 glasses. The mixed compositions were melted followed experimental procedure in section 3.2 and determined liquidus temperature and identified primary phase as followed section 3.5 and 3.6 respectively.

Table 3.4 Comparison of Measured and Targetted chemical compositions (wt%)

| Compositions                   | Samples |        |       |        |
|--------------------------------|---------|--------|-------|--------|
|                                | EFR     | EF0    | EF03  | EF13   |
| Fe <sub>2</sub> O <sub>3</sub> | 0.25    | 0.00   | 0.30  | 1.30   |
| SiO <sub>2</sub>               | 52.93   | 53.00  | 52.96 | 52.84  |
| B <sub>2</sub> O <sub>3</sub>  | 4.99    | 5.00   | 4.96  | 4.84   |
| F                              | 0.81    | 0.80   | 0.76  | 0.64   |
| Na <sub>2</sub> O              | 0.17    | 0.20   | 0.16  | 0.04   |
| MgO                            | 0.14    | 0.20   | 0.16  | 0.04   |
| Al <sub>2</sub> O <sub>3</sub> | 13.77   | 14.00  | 13.96 | 13.84  |
| P <sub>2</sub> O <sub>5</sub>  | 0.00    | 0.00   | 0.00  | 0.00   |
| SO <sub>3</sub>                | 0.00    | 0.00   | 0.00  | 0.00   |
| Cl                             | 0.09    | 0.00   | 0.00  | 0.00   |
| K <sub>2</sub> O               | 0.70    | 0.80   | 0.76  | 0.64   |
| CaO                            | 25.98   | 26.00  | 25.96 | 25.84  |
| TiO <sub>2</sub>               | 0.10    | 0.00   | 0.00  | 0.00   |
| ZrO <sub>2</sub>               | 0.08    | 0.00   | 0.00  | 0.00   |
| Total                          | 100.00  | 100.00 | 99.68 | 100.02 |



## CHAPTER IV

### RESULTS AND DISCUSSIONS

#### 4.1 Observation of as-fabricated glasses

All 25 as-fabricated glasses are shown homogeneous at 1450°C. The optical observation using an optical microscope showed that all as-fabricated glasses are transparent with small amount of bubbles. The molten glasses were easily poured out of the platinum crucible and it could be drawn as long thin fiber. Digital photos of E1R, E2R, E3R, E4R and E5R are shown in Fig. 4.1. The rest of the glass photos are shown in Appendix B.



**E1R**



**E2R**



**E3R**



**E4R**



**E5R**

Fig. 4.1 As-fabricated glasses obtained by melting at 1450°C

In order to check crystallization in the as-fabricated glasses, XRD patterns of all as-fabricated glasses were obtained. Fig. 4.2 shows an amorphous pattern of each glass in E1 group. It was confirmed that crystallization was not presented. Similar patterns of the other glasses are shown in Appendix C.

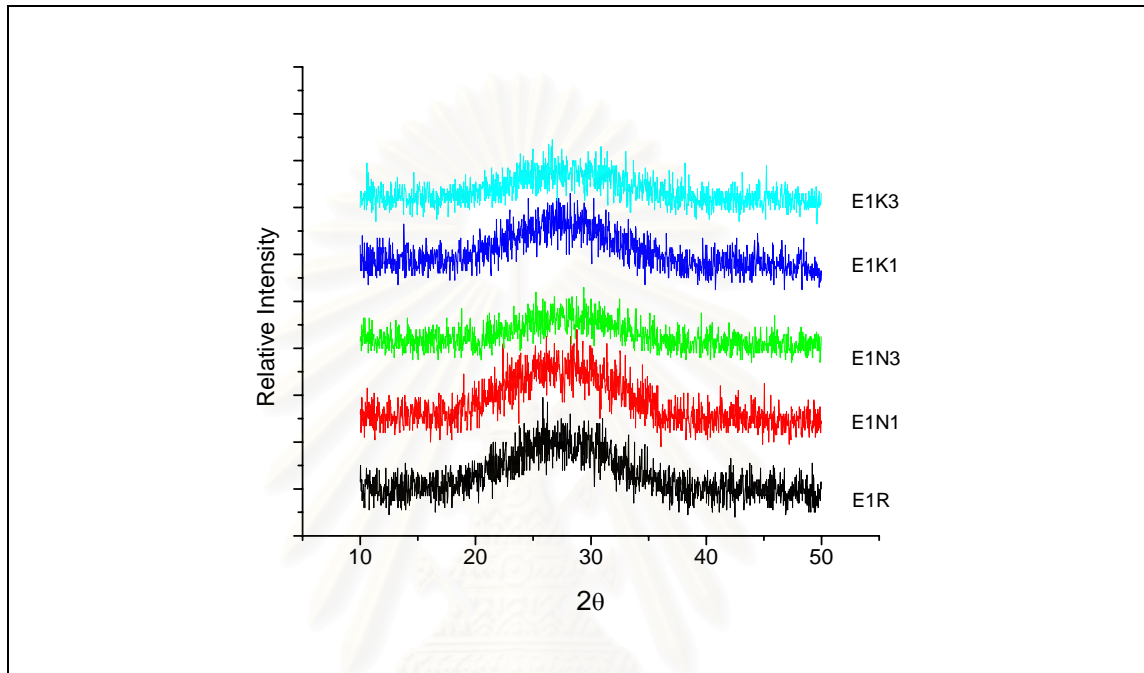


Fig. 4.2 XRD pattern of as-fabricated glasses (E1 group)

#### 4.2 Determination of glass transformation and crystallization temperatures

Fig. 4.3 shows an example of glass transformation temperature ( $T_g$ ), crystallization temperature ( $T_c$ ) and crystallization temperature peak, ( $T_{c\text{ peak}}$ ). In general, crystallization will occur at temperature below  $T_L$ , and  $T_c$  is the temperature that crystallization will happen easiest. Where  $T_c$  is located approximately 50 - 100°C above  $T_g$ . More over,  $T_c$  not only depends on temperature, but also highly depends on time, heating and cooling rates. In order to control the other variables, in this study the constant heating rate was used as 10°C/min. The DTA traces of the other glass samples are shown in Appendix D.

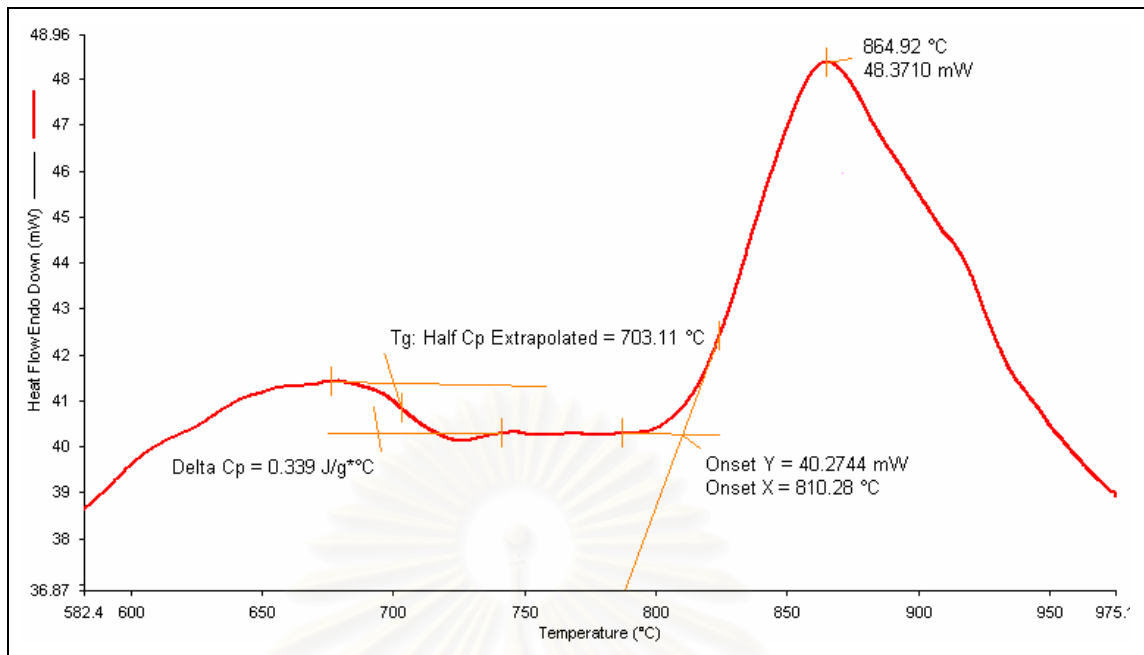


Fig. 4.3  $T_g$ ,  $T_c$  and  $T_{c\text{ peak}}$  in DTA curve of E1R Glass

All  $T_g$  and  $T_c$  results are shown in Table 4.1. The  $T_g$  of E1, E2 and E3 groups ranged from 665 - 730°C with an average of 700°C, while the  $T_g$  of E4 and E5 group were higher and ranged from 718 - 747°C with an averaged of 740°C. In the same pattern,  $T_c$  of E1, E2 and E3 groups ranged from 790 - 825 with an average of 800°C, while the  $T_c$  of E4 and E5 groups ranged from 827- 888°C with an average of 850°C. From these results, these glass could be divided into two groups by the range of both thermal properties. The first one was included E1, E2 and E3 groups which their  $T_g$  and  $T_c$  were lower than the other two groups including E4 and E5 groups. A different between  $T_g$  and  $T_c$  of each glass was approximately 110°C, while the different of  $T_{c\text{ peak}}$  and  $T_c$  was approximately 50°C.

The correlation of alkali oxides on  $T_g$  and  $T_c$  was not shown clearly. Focus on glass samples in the same group,  $T_g$  and  $T_c$  of some samples increased with increasing a concentration of alkali oxides, while some samples showed that their  $T_g$  and  $T_c$  decreased with increasing. However, the difference of  $T_g$  and  $T_c$  in each group were small.

Table 4.1 Thermal analysis results using DTA

| Sample | Measured Temperature (°C) |       |                      |             |                            |
|--------|---------------------------|-------|----------------------|-------------|----------------------------|
|        | $T_g$                     | $T_c$ | $T_{c \text{ peak}}$ | $T_c - T_g$ | $T_c - T_{c \text{ peak}}$ |
| E1R    | 703                       | 810   | 865                  | 107         | 55                         |
| E1N1   | 699                       | 794   | 856                  | 95          | 62                         |
| E1N3   | 693                       | 809   | 862                  | 116         | 53                         |
| E1K1   | 698                       | 812   | 864                  | 114         | 52                         |
| E1K3   | 702                       | 780   | 815                  | 78          | 35                         |
| E2R    | 708                       | 825   | 879                  | 117         | 54                         |
| E2N1   | 703                       | 815   | 860                  | 112         | 45                         |
| E2N3   | 683                       | 793   | 846                  | 110         | 53                         |
| E2K1   | 706                       | 823   | 863                  | 117         | 40                         |
| E2K3   | 697                       | 819   | 871                  | 122         | 52                         |
| E3R    | 704                       | 816   | 875                  | 112         | 59                         |
| E3N1   | 690                       | 806   | 864                  | 116         | 58                         |
| E3N3   | 670                       | 790   | 841                  | 120         | 51                         |
| E3K1   | 730                       | 809   | 868                  | 79          | 59                         |
| E3K3   | 665                       | 792   | 841                  | 127         | 49                         |
| E4R    | 740                       | 854   | 905                  | 114         | 51                         |
| E4N1   | 736                       | 849   | 910                  | 113         | 61                         |
| E4N3   | 718                       | 828   | 874                  | 110         | 46                         |
| E4K1   | 747                       | 860   | 921                  | 113         | 61                         |
| E4K3   | 741                       | 858   | 918                  | 117         | 60                         |
| E5R    | 740                       | 870   | 913                  | 130         | 43                         |
| E5N1   | 730                       | 849   | 900                  | 119         | 51                         |
| E5N3   | 728                       | 827   | 874                  | 99          | 47                         |
| E5K1   | 740                       | 864   | 913                  | 124         | 49                         |
| E5K3   | 740                       | 888   | 938                  | 148         | 50                         |

### 4.3 Liquidus temperature measurement using an uniform temperature method

#### 4.3.1. Liquidus temperature determination

For uniform temperature method, the  $T_L$  was determined at half way of heat-treated temperature that crystallization was detected ( $T_1$ ) and the temperature heat-treated ( $T_2$ ), that crystallization was not detected in heat-treated glass. In this experiment, the interval between  $T_1$  and  $T_2$  was  $10^\circ\text{C}$  in difference. The crystallization was inspected using an optical microscope. The various shapes of crystals in the heat-treated samples were detected and discussed concerning phase identifications in the next part.

First of all, the reference standard material was used to compare  $T_L$  and assess the accuracy of the furnace temperature. The measured  $T_L$  of the SRM-1461 liquidus measurement standard glass was  $1215^\circ\text{C}$ ; halfway between  $1220^\circ\text{C}$  (non-crystal containing) and  $1210^\circ\text{C}$  (crystal containing). The result showed higher  $T_L$  than its certified  $T_L$  ( $1147^\circ\text{C}$ ) which was measured by a gradient temperature method. The difference between two measured  $T_L$  was  $68^\circ\text{C}$ . The repeat of this experiment was done and shown the same result.

The visual observation using an optical microscope pointed out that the crystalline phases of all 25 heat-treated glasses were found on the glass surface, bubble site and crucible wall. It was explained by thermodynamic in term of the free-energy of nucleation or energy barrier as discussed in chapter 2. These crystals were developed from heterogeneous nucleation which its free-energy of crystallization was lower than bulk nucleation or homogeneous nucleation. These crystals were found in form of thin layer of crystal clusters. The crystals were transparent but can be observed by reflecting of polarized light through an optical microscope. The detected size of crystalline phases of heat-treated glasses closed to  $T_L$  were ranged from 30 to  $800\ \mu\text{m}$ . They could be observed clearly via OM with magnifications of 50X to 500X. Fig. 4.4 shows the example of liquidus determination, crystalline phases in glasses which were heat-treated near  $T_L$  ( $T_1$ ) and non-crystalline glasses which were heat-treated at temperature higher than  $T_1$  ( $T_2$ ). Fig. 4.4. shows the liquidus temperature determination

of selected samples which show different crystal shapes and sizes. All visual observations of heat-treated glasses are shown in appendix G.


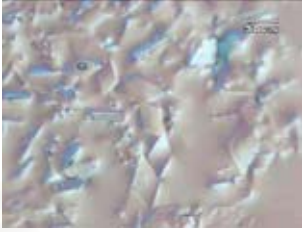

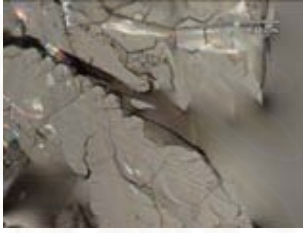
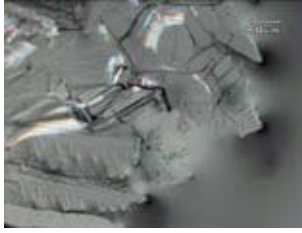

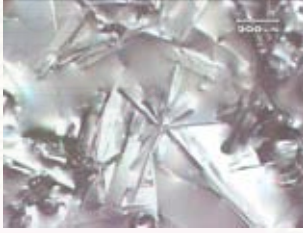



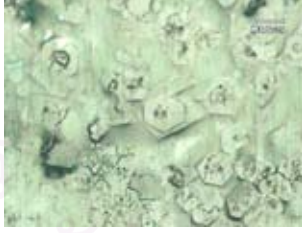



| Sample | $T_2$   | $T_1$  |   |
|--------|---|--|---|
| E1R    |    |    |   |
|        | 1170°C  | 1160°C   |   |
| E2N3   |    |    |    |
|        | 1170°C  | 1160°C   |   |
| E3N1   |  |  |  |
|        | 1130°C  | 1120°C   |   |
| E4K3   |  |  |  |
|        | 1260°C  | 1250°C   | 1240°C  |
| E5K1   |  |  |  |
|        | 1250°C  | 1240°C   |   |

Fig. 4.4 Example of visual observations of heat-treated glass for  $T_L$  determination

Table 4.2  $T_L$  and visual observation of heat-treated glasses

| Samples | Measured $T_L$<br>( $\pm 10^\circ\text{C}$ ) | Visual characterization of crystalline phase heat-treated glasses at near $T_L$ |  |                                |
|---------|--|---|--|--------------------------------|
|         |  | Detected phase  | Shape / position of detected crystals  | Average size ( $\mu\text{m}$ ) |
| E1R     | 1165   | Wollastonite and Anorthite  | Layer of needle and diamond shape crystals on surface                              | 30                             |
| E1N1    | 1145   | Wollastonite and Anorthite  | Layer of needle and diamond crystals on surface                                    | 40                             |
| E1N3    | 1135   | Wollastonite  | Star-like, rectangular and needle on surface and bubble                            | 250                            |
| E1K1    | 1155   | Wollastonite and Anorthite  | Stripe of needle and diamond shape crystals layer on surface                       | 25                             |
| E1K3    | 1115   | Wollastonite  | Stand alone of needle crystal on surface   | 30                             |
| E2R     | 1145   | Anorthite   | Stripe of star-like needle and diamond shape crystals layer on surface             | 20                             |
| E2N1    | 1135   | Wollastonite and Anorthite  | Stripe of star-like needle and diamond shape crystals layer on surface             | 20                             |
| E2N3    | 1165   | Wollastonite  | Dendrite crystal on surface close to crucible wall                                 | 600                            |
| E2K1    | 1145   | Wollastonite and Anorthite  | Stripe of star-like and diamond shape crystals layer on surface                    | 40                             |
| E2K3    | 1185   | Wollastonite  | Dendrite crystal on surface close to crucible wall                                 | 600                            |
| E3R     | 1125   | Wollastonite  | Cluster of rectangular and needle shape crystals on surface                        | 30                             |
| E3N1    | 1125   | Wollastonite  | Star-like, needle and rectangular shape crystals on surface close to crucible wall | 400                            |
| E3N3    | 1165   | Wollastonite  | Layer of hexagon crystals on surface close to crucible wall                        | 400                            |
| E3K1    | 1145   | Wollastonite  | Layer of rectangular crystals on surface close to crucible wall                    | 200                            |
| E3K3    | 1185   | Wollastonite  | Layer of hexagon crystals on surface close to crucible wall                        | 500                            |
| E4R     | 1205   | Wollastonite  | Star-like crystal stand-alone on surface   | 80                             |
| E4N1    | 1195   | Wollastonite  | Star-like crystals on surface and bubbles  | 600                            |
| E4N3    | 1235   | Wollastonite  | Rectangular crystals at bubble sites and surface                                   | 600                            |
| E4K1    | 1215   | Wollastonite  | Rod like crystals stand alone on surface   | 200                            |
| E4K3    | 1255   | Wollastonite  | Rod-like and hexagon crystals stand alone on surface                               | 200                            |

Table 4.2  $T_L$  and Visual observation of heat-treated glasses (cont.)

| Samples | Measured $T_L$<br>( $\pm 10^\circ\text{C}$ ) | Visual characterization of crystalline phase heat-treated glasses at near $T_L$ |   |                                |
|---------|--|---|---|--------------------------------|
|         |  | Detected phase  | Positions of detected crystals                        | Average size ( $\mu\text{m}$ ) |
| E5R     | 1215   | Wollastonite  | Hexagon at bubble site and surface                    | 300                            |
| E5N1    | 1235   | Wollastonite  | Hexagon at bubble site and surface                    | 800                            |
| E5N3    | 1275   | Wollastonite  | Rectangle on surface and bubble site                  | 800                            |
| E5K1    | 1245   | Wollastonite  | Hexagon at bubble site and surface                    | 800                            |
| E5K3    | 1305   | Wollastonite  | Cluster of crystals on surface close to crucible wall | 800                            |

In Table 4.3, the liquidus temperature of each sample was determined at temperature between 'O' (non crystals) and 'X' (detected crystal). The liquidus temperature range of E1 group was from  $1120^\circ\text{C}$  to  $1170^\circ\text{C}$ . The alkali containing samples had lower liquidus temperature than the reference glass (E1R).

The liquidus temperature range of E2 group was from  $1135^\circ\text{C}$  -  $1185^\circ\text{C}$ . In contrast with E1 group, the liquidus temperatures tend to increase with increasing of alkali content. Although the liquidus temperature of 1 wt% alkali oxide containing glasses (E2N1 and E2K1) were lower than the reference glass (E2R), the liquidus temperature of 3 wt% alkali oxide containing glasses (E2N3 and E2K3) were higher. Focus on crystal phase at heat-treated temperature near  $T_L$  presented in Table 4.2, E2N1 and E2K1 were detected both anorthite and wollastonite phases while E2N3 and E2K3 were detected only wollastonite phase. It can be shown that the liquidus temperature of alkali oxide containing glasses in the system of wollastonite primary phase increased with increasing of alkali oxides content.



Table 4.3 Summation of heat-treatment results for E1 and E2 group

| Temp. | E1R | E1N1 | E1N3 | E1K1 | E1K3 | E2R | E2N1 | E2N3 | E2K1 | E2K3 |
|-------|-----|------|------|------|------|-----|------|------|------|------|
| 1200  |     |      |      |      |      |     |      |      |      | O    |
| 1190  |     |      |      |      |      |     |      |      |      | O    |
| 1180  |     |      |      |      |      |     |      | O    |      | X    |
| 1170  | O   |      |      |      |      | O   |      | O    |      |      |
| 1160  | X   |      |      | O    |      | O   | O    | X    | O    | X    |
| 1150  | X   | O    |      | X    |      | X   |      | X    | O    |      |
| 1140  |     | X    | O    | X    |      | X   | O    | X    | X    |      |
| 1130  |     |      | X    | X    | O    | X   | X    | X    | X    |      |
| 1120  |     |      | X    | X    | X    |     | X    | X    |      |      |
| 1110  |     |      |      |      | X    |     |      |      |      |      |
| 1100  |     |      |      |      |      |     |      |      |      |      |

X = Contained crystal and O = Non-crystal

The liquidus temperature range of E3 group was from 1125°C – 1185°C. The liquidus temperature of glasses containing 1 wt% of alkali oxides were slightly higher than the reference glass (E3R). In case of 3 wt% alkali oxides, liquidus temperatures were quite different from the reference glass by 40°C and 60°C for Na<sub>2</sub>O and K<sub>2</sub>O respectively. From Table 4.2, the primary phase of all samples in this group was wollastonite and the increase of alkali oxide affected to increase their liquidus temperatures.

The range of liquidus temperature of E4 group was from 1195°C – 1255°C. The effect of varying alkali oxides were in the same manner of E3 group which liquidus temperature increased with increasing alkali oxides content. The primary phase of all samples in this group was wollastonite.

สถาบันวิทยบริการ  
จุฬาลงกรณ์มหาวิทยาลัย

Table 4.4 Summation of heat-treatment results of E3 and E4group

| Temp. | E3R | E3N1 | E3N3 | E3K1 | E3K3 | E4R | E4N1 | E4N3 | E4K1 | E4K3 |
|-------|-----|------|------|------|------|-----|------|------|------|------|
| 1260  |     |      |      |      |      |     |      |      |      | O    |
| 1250  |     |      |      |      |      |     |      |      |      | X    |
| 1240  |     |      |      |      |      |     |      | O    |      | X    |
| 1230  |     |      |      |      |      |     |      | X    |      | X    |
| 1220  |     |      |      |      |      | O   | O    | X    | O    |      |
| 1210  |     |      |      |      |      | O   | O    |      | X    |      |
| 1200  | O   | O    |      |      | O    | X   | O    |      | X    |      |
| 1190  |     |      |      |      | O    |     | X    |      |      |      |
| 1180  |     |      |      |      | X    |     | X    |      |      |      |
| 1170  |     |      | O    | O    |      | X   |      |      | X    |      |
| 1160  |     | O    | X    |      |      |     |      |      |      |      |
| 1150  | O   |      | X    | O    | X    |     |      |      |      |      |
| 1140  |     |      |      | X    |      |     |      |      |      |      |
| 1130  | O   | O    |      | X    |      |     |      |      |      |      |
| 1120  | X   | X    |      |      |      |     |      |      |      |      |
| 1110  |     |      |      |      |      |     |      |      |      |      |
| 1100  | X   |      |      |      |      |     |      |      |      |      |

X = Non Crystal and O = Contained Crystal

The liquidus temperature range of E5 group was from 1215°C – 1305°C. The summarized crystalline phases detected in heat-treated glass at near  $T_L$  are shown in Fig. 4.5. The liquidus temperatures of this group were highest compared with other groups. In the same way as E3 and E4 group, the liquidus temperature of E5 group increased with increasing of alkali oxides content. The primary phases of all samples in this group were wollastonite.

สถาบันวิทยบริการ  
จุฬาลงกรณ์มหาวิทยาลัย

Table 4.5 Summation of heat-treatment results of E5 group

| Temp. | E5R | E5N1 | E5N3 | E5K1 | E5K3 |
|-------|-----|------|------|------|------|
| 1310  |     |      |      |      | O    |
| 1300  |     |      |      |      | X    |
| 1290  |     |      | O    |      | X    |
| 1280  |     |      | O    |      |      |
| 1270  |     |      | X    |      | X    |
| 1260  |     |      |      |      |      |
| 1250  |     |      | X    | O    | X    |
| 1240  | O   | O    |      | X    |      |
| 1230  |     | X    | X    |      |      |
| 1220  | O   | X    |      |      |      |
| 1210  | X   |      |      |      |      |
| 1200  | X   |      |      |      |      |

X = Contained Crystal and O = Non Crystal

#### 4.3.2. Crystalline phases identification

##### 4.3.2.1. Visual observation and energy dispersive x-ray microanalysis

The visual observation of heat-treated glasses from uniform temperature method could be summarized types and morphologies of crystalline phases are shown in Fig. 4.5. To identify type of crystals, the energy dispersive x-ray microanalysis, EDX (OXFORD Instrument, ISIS 300) was used to analyze atomic ratio compared with chemical contents of crystalline phase, and also compared with the reference books [45, 46]. The results showed that, there were five formats of crystal shapes, classified into two types of crystalline phase. Fig. 4.5 (a) shows anorthite crystals with diamond shape and wollastonite crystals with needle shape. The wollastonite crystals were observed in four different shapes which are rectangular (Fig. 4.5 (b) and (c)), star-like (Fig. 4.5 (d)), dendrite (Fig. 4.5 (e)) and hexagonal (Fig. 4.5 (f)). From the reference book [45], crystal in form of hexagonal shape with cleavage is an  $\alpha$ -wollastonite or pseudowollastonite. Rectangular shape and star-like or needle-like were identified as  $\beta$ -wollastonite [47].

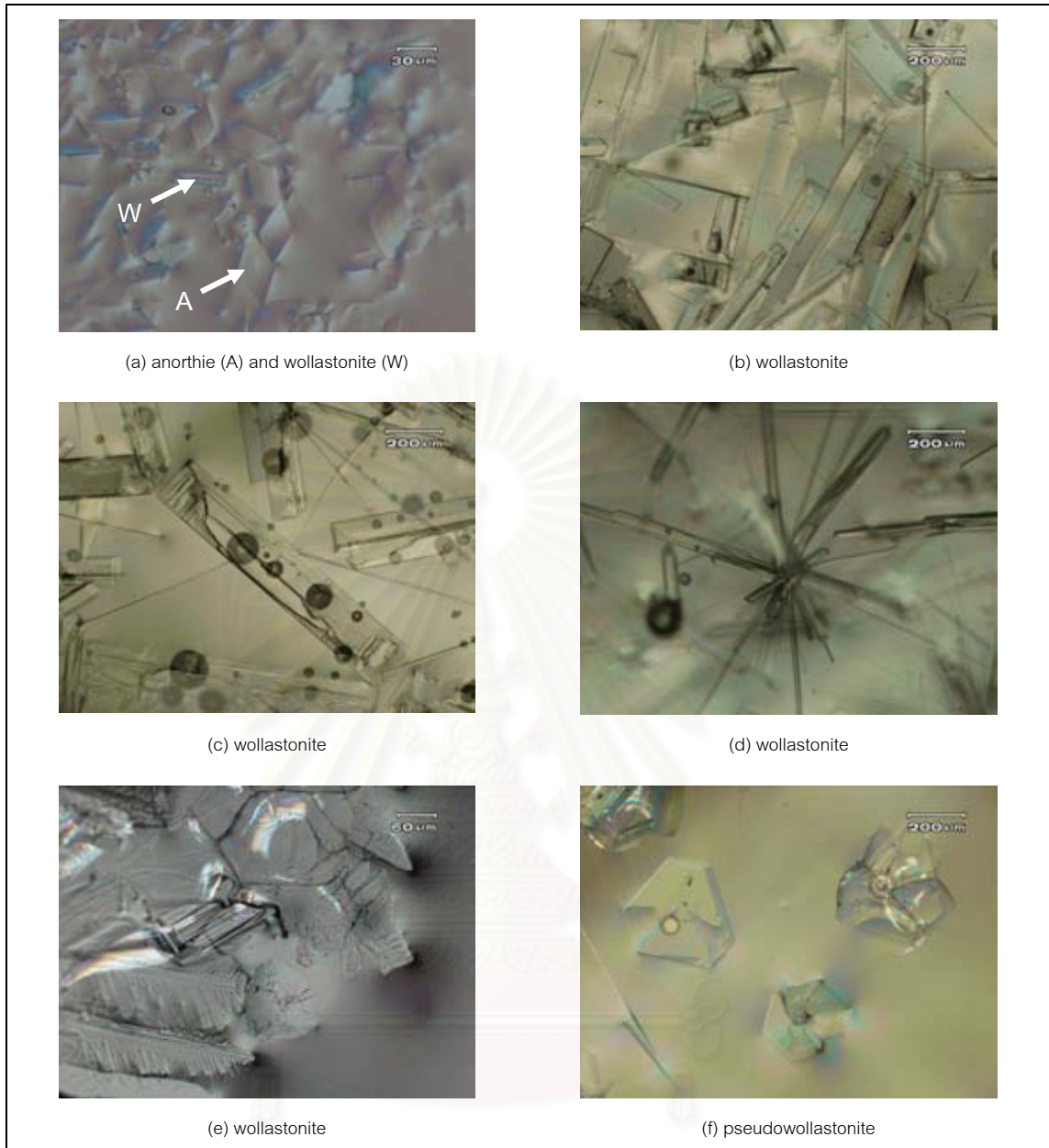


Fig. 4.5 The summarized crystalline phases detected in heat-treated glass at near  $T_L$

Fig. 4.6 shows the analyzed of element concentration by EDX. The theoretical composition of wollastonite is composed of 41.32 %Oxygen, 24.18 %Silicon and 34.5 %Calcium, and anorthite is composed of 46.14%Oxygen, 18.97 %Aluminum, 20.75 %Silicon and 13.72 %Calcium. The analysis results were compared and identified the crystal type.

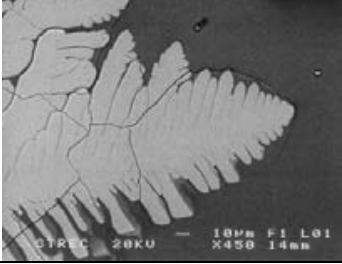

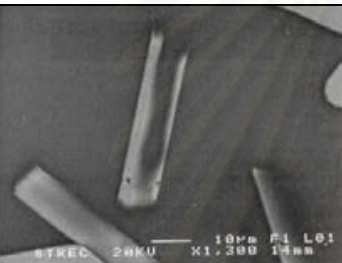
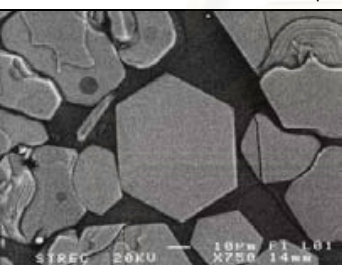
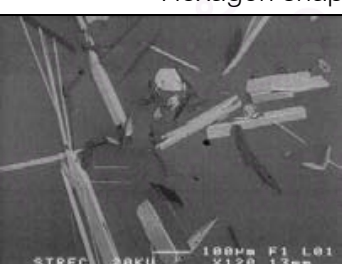
|   |   |
|---|---|
|    | <p>Element %</p> <p>O = 21.71 Si = 30.98</p> <p>Ca = 46.82</p>            |
| <p>Dendrite shape identified as wollastonite.</p>                                   |   |
|    | <p>Element %</p> <p>O = 39.04 Al = 18.73</p> <p>Si = 24.45 Ca = 17.77</p> |
| <p>Diamond shape identified as anorthite.</p>                                       |   |
|   | <p>Element %</p> <p>O = 37.22 Al = 20.10</p> <p>Si = 26.59 Ca = 16.09</p> |
| <p>Rod shape identified as anorthite.</p>   |   |
|  | <p>Element %</p> <p>O = 34.83 Si = 28.85</p> <p>Ca = 36.32</p>            |
| <p>Hexagon shape identified as wollastonite.</p>                                    |   |
|  | <p>Element %</p> <p>O = 38.72 Si = 26.15</p> <p>Ca = 35.13</p>            |
| <p>Star-like shape identified as wollastonite</p>                                   |   |

Fig. 4.6 EDX semi-quantitative analysis aid identifying crystalline phases

In summation, the wollastonite was seem to be the primary phase of this glass system. The increase of alkali oxide contents in each group led to the wollastonite phase transformation. It could be supported by the result of E2 group. While glass with 0 and 1 wt% of alkali oxides obtained anorthite and wollastonite as primary crystalline phases. At highs percentage of alkali oxide (3 wt%) only wollastonite phase was detected. It could be supported by the result of E2 group which contained 0 and 1 wt% of alkali oxides the anorthite phase could be detected with wollastonite phase, while 3 wt% of alkali oxide only wollastonite phase was detected.

#### 4.3.2.2. X-ray diffraction

X-ray diffraction (XRD) was performed on the sample which heat-treated at low temperature (1080°C - 1150°C). Selected glasses of each group, reference glass and glasses with highest percentage of alkali oxides were used to run the XRD. DIFFRAC plus EVA analysis software [48] was used for the analysis. XRD analysis detected two phases in the samples; wollatonite ( $\text{CaO}\cdot\text{SiO}_2$ ) and anorthite ( $\text{CaO}\cdot\text{Al}_2\text{O}_3\cdot 2\text{SiO}_2$ ). Both anorthite and wollastonite phases were found in E1 group (Fig. 4.7). In this group, major wollastonite peaks are higher than anorthite. In case of alkali oxides containing glasses, wollastonite peaks were perform higher than the reference glass (no alkali oxide).

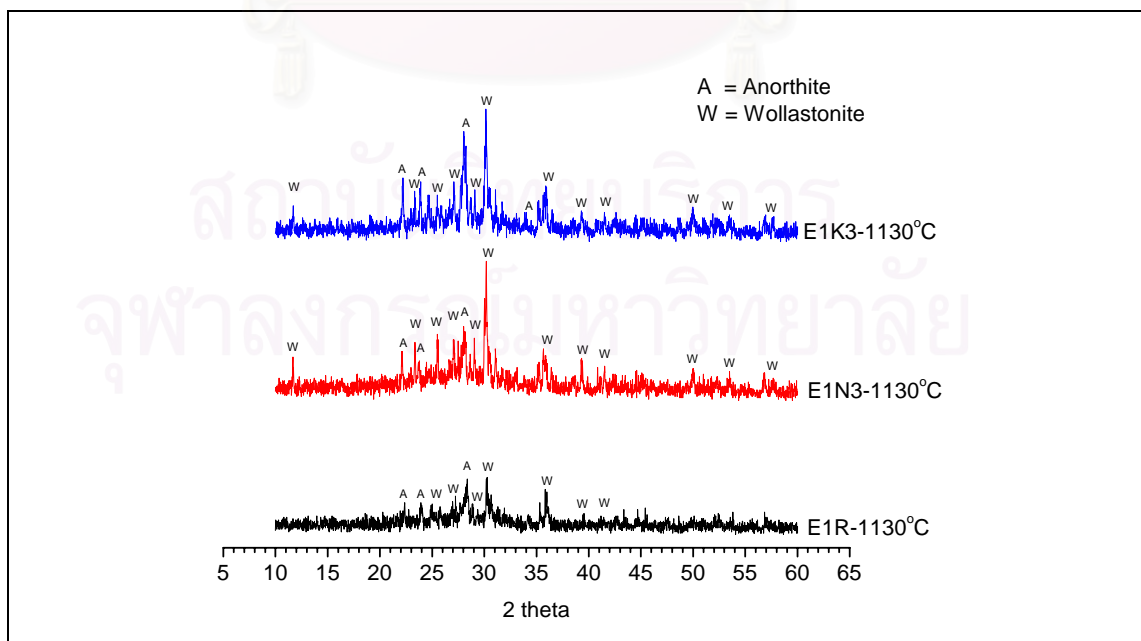


Fig. 4.7 XRD pattern of glass samples in E1 group heat-treated at 1130°C for 24 h

In Fig. 4.8, individual anorthite phase were obtained from E2R heat-treated at 1090°C. Both glasses with alkali oxide (E2N3 and E2K3) performed higher peaks of wollastonite phase as well as E1 group; thus, the alkali oxides lead to crystallization of wollastonite phase.

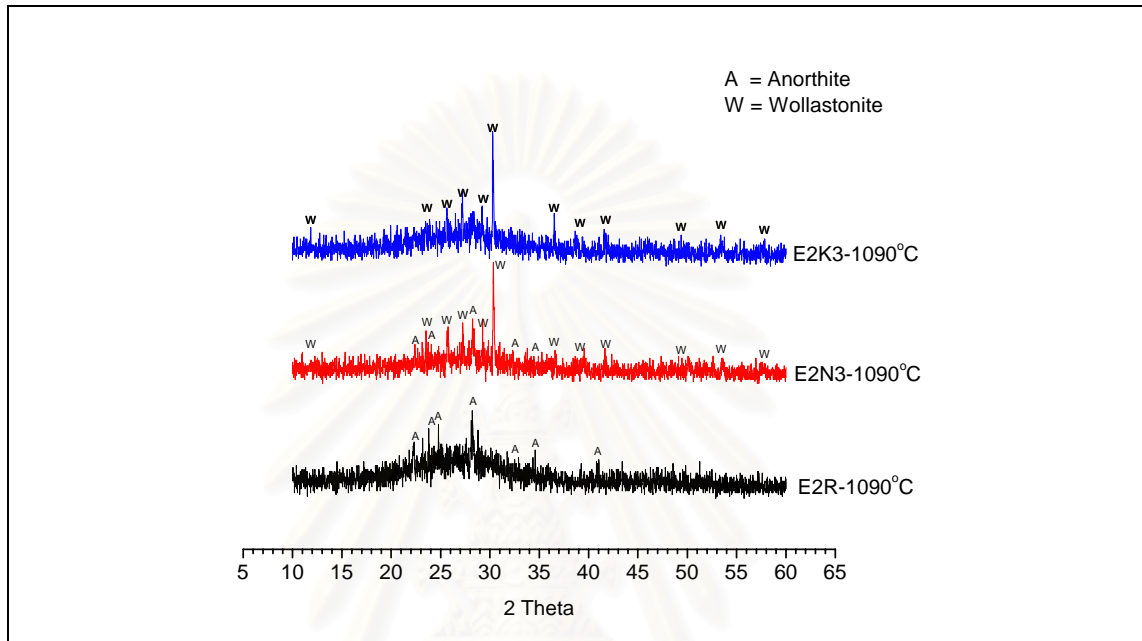


Fig. 4.8 XRD pattern of glass samples in E2 group heat-treated at 1090°C for 24 h

In E3 group (Fig. 4.9), all heat-treated glasses performed only wollastonite phase as well as E5 group (Fig. 4.11). E4 group (Fig. 4.10) showed both anorthite and both wollastonite peaks. Focus on alkali oxides, E4N3 performed higher peak of anorthite phase while it was lower in case of E4K3 glass. From visual observation of crystal morphology in heat-treated glass, however, most crystalline phases were wollastonite.

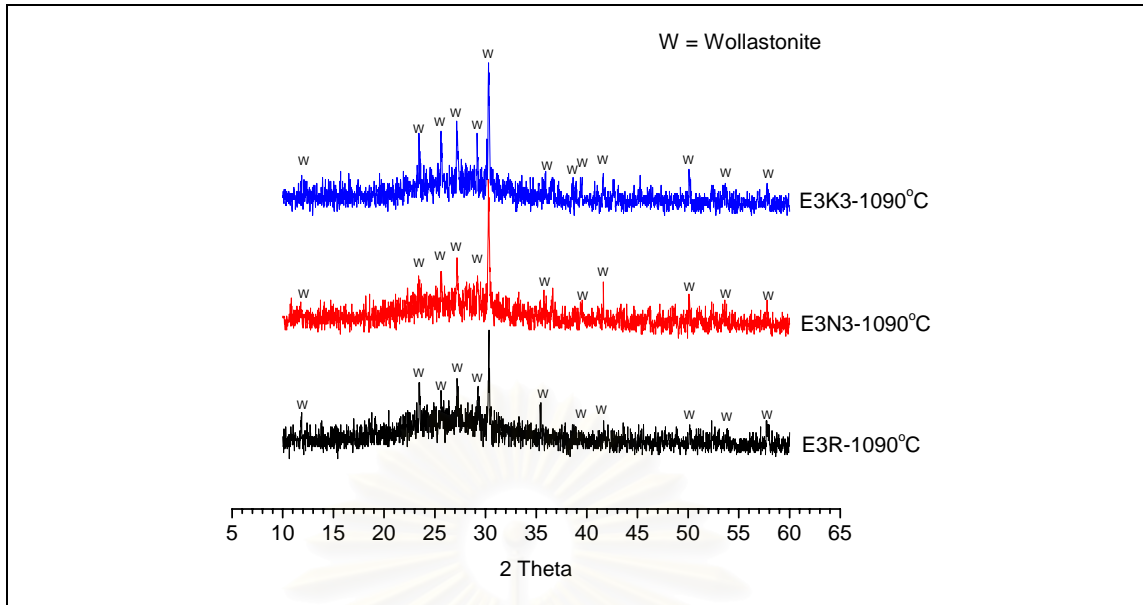


Fig. 4.9 XRD pattern of glass samples in E3 group heat-treated at 1090°C for 24 h

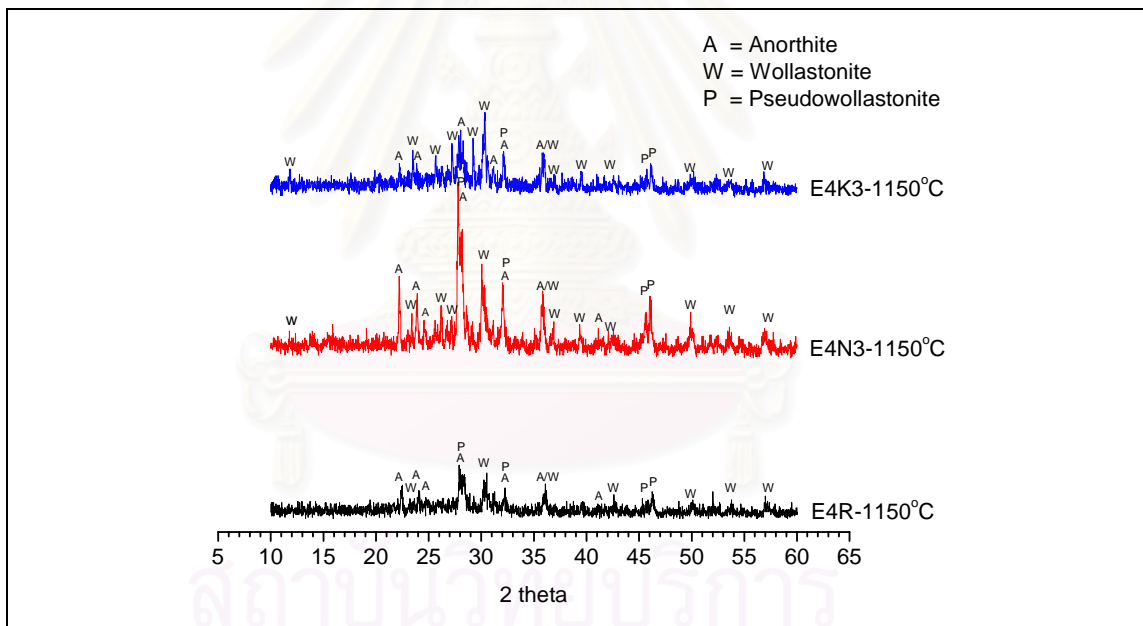


Fig. 4.10 XRD pattern of glass samples in E4 group heat-treated at 1150°C for 24 h



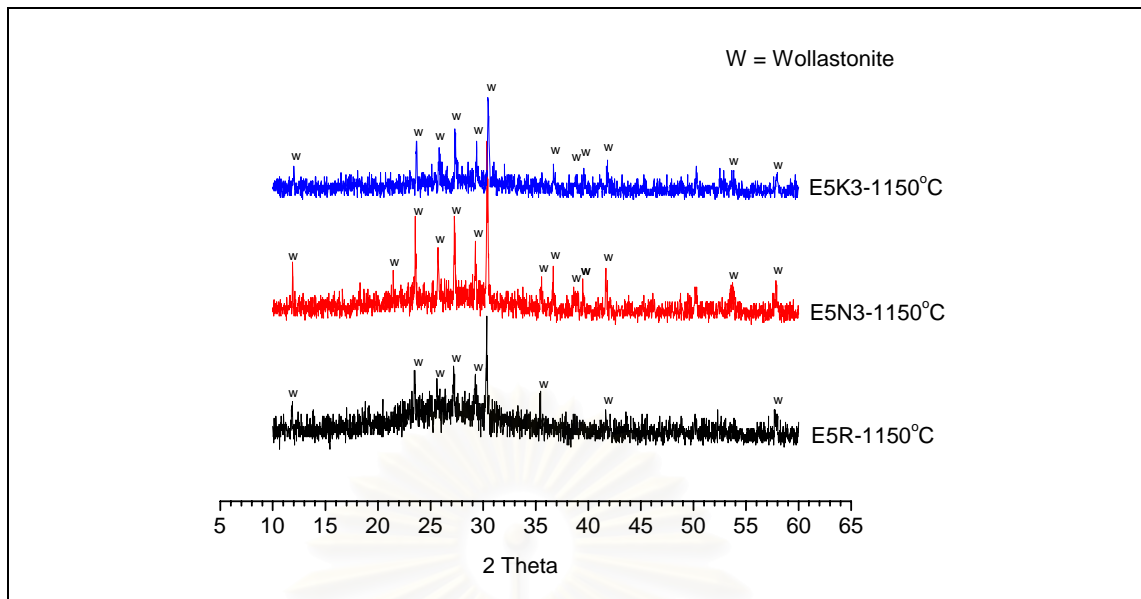


Fig. 4.11 XRD pattern of glass samples in E5 group heat-treated at 1150°C for 24 h

#### 4.4 Effect of glass compositions on liquidus temperature

It was found that a trend of the  $T_L$  of E1 group was decreased with increasing of alkali oxide concentrations. In case of 1 wt%  $\text{Na}_2\text{O}$ , the  $T_L$  decreased by 20°C. For adding 3 wt%  $\text{Na}_2\text{O}$ , the  $T_L$  decreased by 30°C compared with the reference glass (E1R). In the same way, additional of 1 and 3 wt% of  $\text{K}_2\text{O}$  showed the result in decreasing  $T_L$  as well. In contrast, the trend of the  $T_L$  of E2, E3, E4 and E5 group was increase with an increasing of alkali oxides. To explain the reason of this contrast, it can be supported by phase diagram of  $\text{Na}_2\text{O}-\text{CaO}-\text{Al}_2\text{O}_3-\text{SiO}_2$  system. Considering the ratio of anorthite ( $\text{CaO}\cdot\text{Al}_2\text{O}_3\cdot 2\text{SiO}_2$ ) and wollastonite ( $\text{CaO}\cdot\text{SiO}_2$ ) composition in Table 3.3, it shows that the increase of alkali oxides decreased the anorthite ratio, while the wollastonite ratio was increased. The arrow in a circle in Fig. 4.12 shows a direction of increased wollastonite and decreased anorthite ratio while  $\text{Na}_2\text{O}$  slightly increased. Along this direction the liquidus temperature rise from around 1310°C to 1350°C.

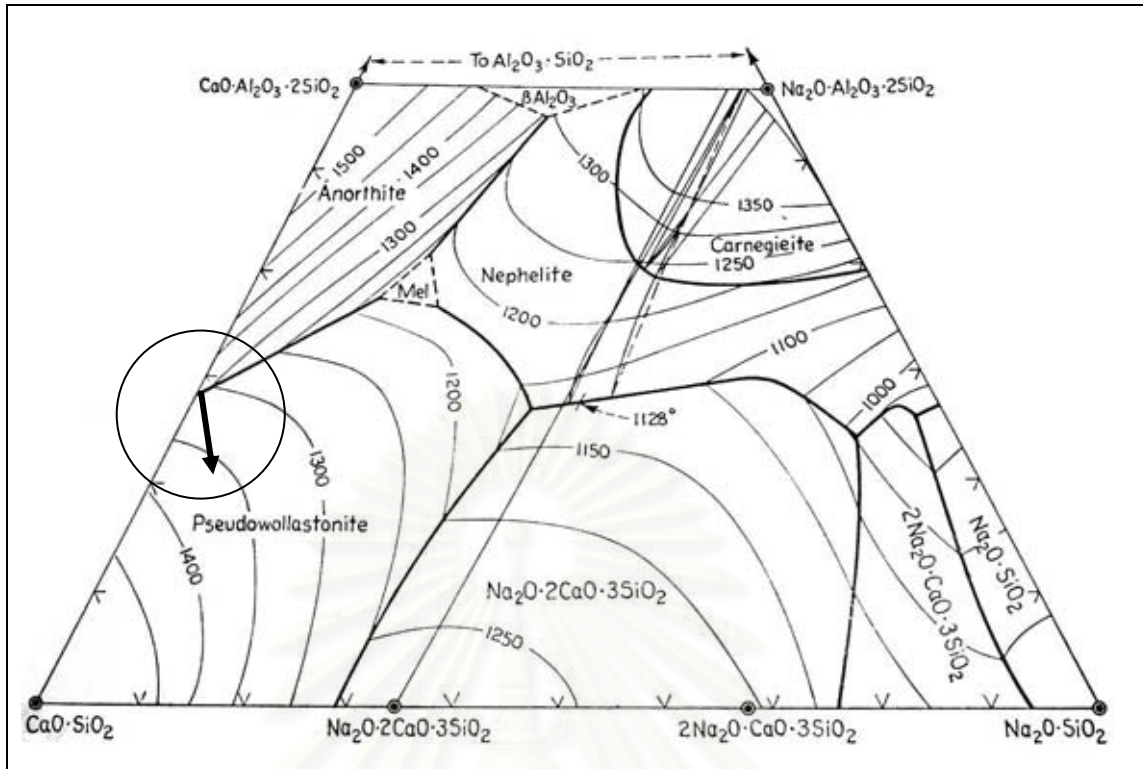


Fig. 4.12 Isothermal section of system  $\text{Na}_2\text{O}-\text{CaO}-\text{Al}_2\text{O}_3-\text{SiO}_2$  phase diagram [49]

Considering  $\text{SiO}_2$  and  $\text{Al}_2\text{O}_3$  contents, while  $\text{SiO}_2$  content was increased from 52 – 60 wt% for E1 – E5 group respectively,  $\text{Al}_2\text{O}_3$  content was gradually decreased from 15 – 10 wt% for E1 - E5 group respectively. This composition change could be shown in Fig. 4.13. The arrow was placed in pseudowollastonite phase field, showed the direction of this discussion, in direction of increasing  $\text{SiO}_2$  with decreasing  $\text{Al}_2\text{O}_3$  the liquidus temperature will increase along this line. In contrast, if  $\text{Al}_2\text{O}_3$  was increased along this arrow the liquidus temperature will decrease.

สถาบันวิทยบริการ  
จุฬาลงกรณ์มหาวิทยาลัย

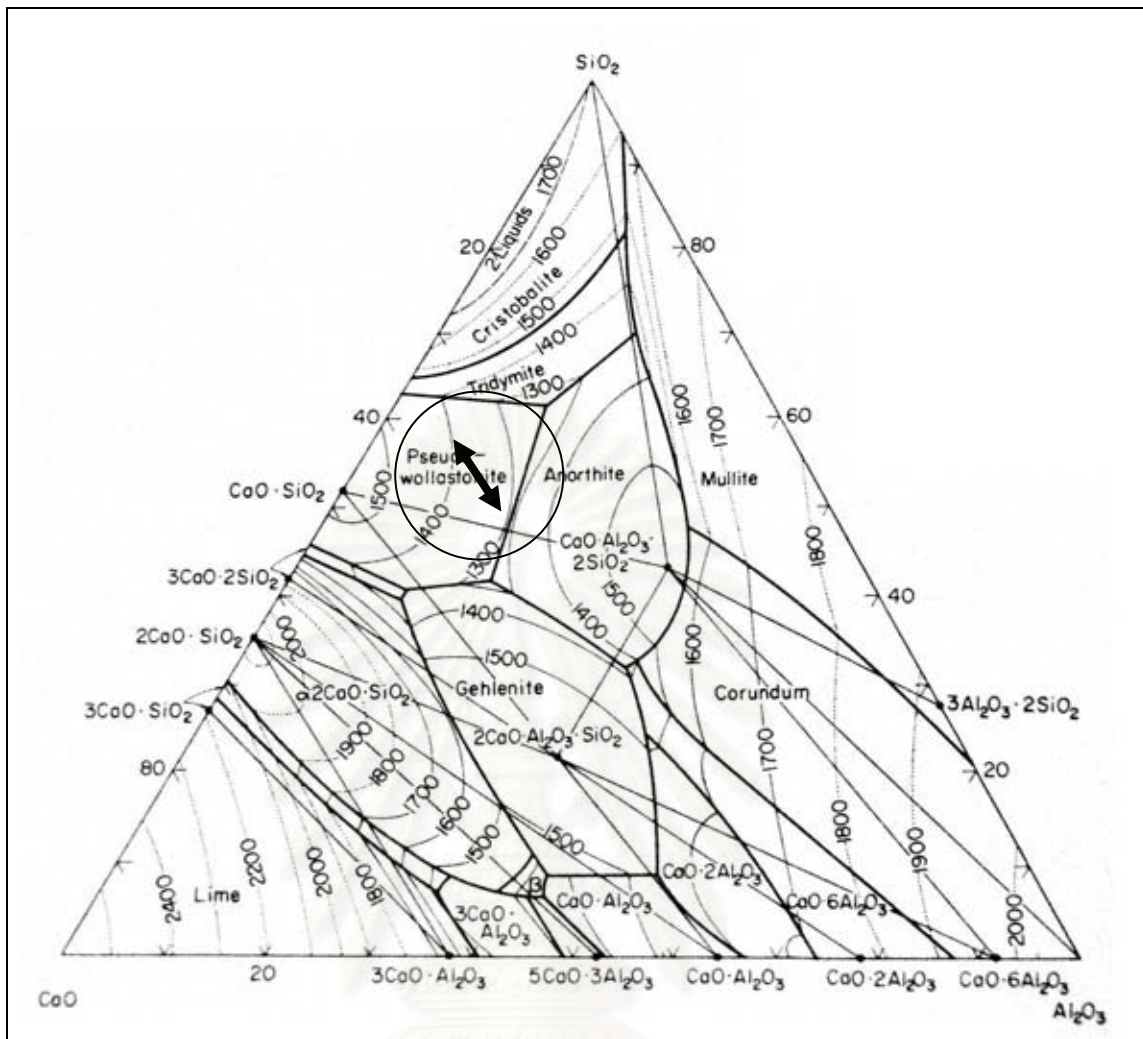


Fig. 4.13 Ternary phase diagram of system  $\text{SiO}_2 - \text{CaO} - \text{Al}_2\text{O}_3$  [49]

#### 4.5 Composition-properties prediction model

##### 4.5.1. Composition-properties modeling using Scheffe' Polynomial

Scheffe' Polynomial [50] was used as the model that allowed the prediction of glass properties such as liquidus temperature, glass transition and durability. This principle is based on the assumption that the relation between the glass composition and a specific property is linear to all component concentrations and all component influences can be summed. The general form of a first order Scheffe' Polynomial is

$$y = \sum_{i=1}^q b_i X_i \quad (4.1)$$

Where  $b_i$  = first order coefficient of component  $i$ ,  $X_i$  = mole fraction of component  $i$ ,  $y$  = glass properties (the liquidus temperature).

$$b = (X'X)^{-1} X'y \quad (4.2)$$

Where  $X$  = glass matrix,  $X'$  =  $X$  transpose,  $y$  = glass property (the liquidus temperature)

The first order form above was used to predict and find the component coefficient for liquidus temperature of glass compositions in this study. All compositions of glasses except E1 group were used to develop the model. The first order coefficients and oxide range for target and measured composition are shown in Table 4.6. The calculation were performed using MATLAB [51] computer software and are found in Appendix G.

Table 4.6 Component coefficients for first order liquidus temperature models

| Oxide                          | Composition Range | Component Coefficient |
|--------------------------------|-------------------|-----------------------|
| SiO <sub>2</sub>               | 54.4-62           | 22.3968               |
| Al <sub>2</sub> O <sub>3</sub> | 9.4-15            | -20.154               |
| B <sub>2</sub> O <sub>3</sub>  | 0-6               | -3.5775               |
| MgO                            | 0.4-2             | -36.1411              |
| CaO                            | 22.4-23           | 11.2552               |
| ZnO                            | 0-3               | -52.883               |
| Na <sub>2</sub> O              | 0-3               | 5.7698                |
| K <sub>2</sub> O               | 0-3               | 14.0198               |

The liquidus temperatures were calculated or predicted using compositions as follow.

$$T_L = 22.3968X_{SiO_2} - 20.154X_{Al_2O_3} - 3.5775X_{B_2O_3} - 36.1411X_{MgO} + 11.2552X_{CaO} - 52.883X_{ZnO} + 5.7698X_{Na_2O} + 14.0198X_{K_2O} \quad (4.3)$$

The results of calculated  $T_L$  were showed in Table 4.7 and the comparison of calculated  $T_L$  and measured  $T_L$  are plotted in Fig. 4.14. The first order model was fitted with 98.57%  $R^2$ . The standard error (S) were also calculated which showed a value of

18.18. The analysis of this model indicated that the  $T_L$  of composition range followed Table 4.6 increased with increasing concentration of  $\text{SiO}_2$ ,  $\text{CaO}$ ,  $\text{Na}_2\text{O}$  and  $\text{K}_2\text{O}$  and decreased with increasing  $\text{Al}_2\text{O}_3$ ,  $\text{B}_2\text{O}_3$ ,  $\text{MgO}$  and  $\text{ZnO}$ .

Table 4.7 Measured  $T_L$  and calculated  $T_L$  of glasses E2, E3, E4 and E5 group

| Sample code | Chemical compositions (wt%) |                         |                        |              |              |              |                       |                      | Measured $T_L$ ( $^{\circ}\text{C}$ ) | Calculated $T_L$ ( $^{\circ}\text{C}$ ) |
|-------------|-----------------------------|-------------------------|------------------------|--------------|--------------|--------------|-----------------------|----------------------|---------------------------------------|---|
|             | $\text{SiO}_2$              | $\text{Al}_2\text{O}_3$ | $\text{B}_2\text{O}_3$ | $\text{MgO}$ | $\text{CaO}$ | $\text{ZnO}$ | $\text{Na}_2\text{O}$ | $\text{K}_2\text{O}$ |                                       |   |
| E2R         | 55                          | 15                      | 6                      | 1            | 23           | -            | -                     | -                    | 1145                                  | 1135.54                                 |
| E2N1        | 54.8                        | 14.8                    | 5.8                    | 0.8          | 22.8         | -            | 1                     | -                    | 1135                                  | 1144.74                                 |
| E2N3        | 54.4                        | 14.4                    | 5.4                    | 0.4          | 22.4         | -            | 3                     | -                    | 1165                                  | 1163.15                                 |
| E2K1        | 54.8                        | 14.8                    | 5.8                    | 0.8          | 22.8         | -            | -                     | 1                    | 1145                                  | 1150.34                                 |
| E2K3        | 54.4                        | 14.4                    | 5.4                    | 0.4          | 22.4         | -            | -                     | 3                    | 1185                                  | 1179.95                                 |
| E3R         | 56                          | 13                      | 5                      | 3            | 23           | -            | -                     | -                    | 1125                                  | 1134.59                                 |
| E3N1        | 55.8                        | 12.8                    | 4.8                    | 2.8          | 22.8         | -            | 1                     | -                    | 1125                                  | 1143.80                                 |
| E3N3        | 55.4                        | 12.4                    | 4.4                    | 2.4          | 22.4         | -            | 3                     | -                    | 1165                                  | 1162.20                                 |
| E3K1        | 55.8                        | 12.8                    | 4.8                    | 2.8          | 22.8         | -            | -                     | 1                    | 1145                                  | 1149.40                                 |
| E3K3        | 55.4                        | 12.4                    | 4.4                    | 2.4          | 22.4         | -            | -                     | 3                    | 1185                                  | 1179.00                                 |
| E4R         | 60                          | 13                      | -                      | 4            | 23           | -            | -                     | -                    | 1205                                  | 1196.68                                 |
| E4N1        | 59.7                        | 12.7                    | -                      | 3.75         | 22.7         | -            | 1                     | -                    | 1195                                  | 1209.21                                 |
| E4N3        | 59.2                        | 12.2                    | -                      | 3.25         | 22.2         | -            | 3                     | -                    | 1235                                  | 1234.28                                 |
| E4K1        | 59.7                        | 12.7                    | -                      | 3.75         | 22.7         | -            | -                     | 1                    | 1215                                  | 1214.81                                 |
| E4K3        | 59.2                        | 12.2                    | -                      | 3.25         | 22.2         | -            | -                     | 3                    | 1255                                  | 1251.08                                 |
| E5R         | 62.0                        | 10                      | -                      | 2            | 23           | 3            | -                     | -                    | 1215                                  | 1242.73                                 |
| E5N1        | 61.8                        | 9.8                     | -                      | 1.8          | 22.8         | 2.8          | 1                     | -                    | 1235                                  | 1246.36                                 |
| E5N3        | 61.4                        | 9.4                     | -                      | 1.4          | 22.4         | 2.4          | 3                     | -                    | 1275                                  | 1253.62                                 |
| E5K1        | 61.8                        | 9.8                     | -                      | 1.8          | 22.8         | 2.8          | -                     | 1                    | 1245                                  | 1251.96                                 |
| E5K3        | 61.4                        | 9.4                     | -                      | 1.4          | 22.4         | 2.4          | -                     | 3                    | 1305                                  | 1270.42                                 |

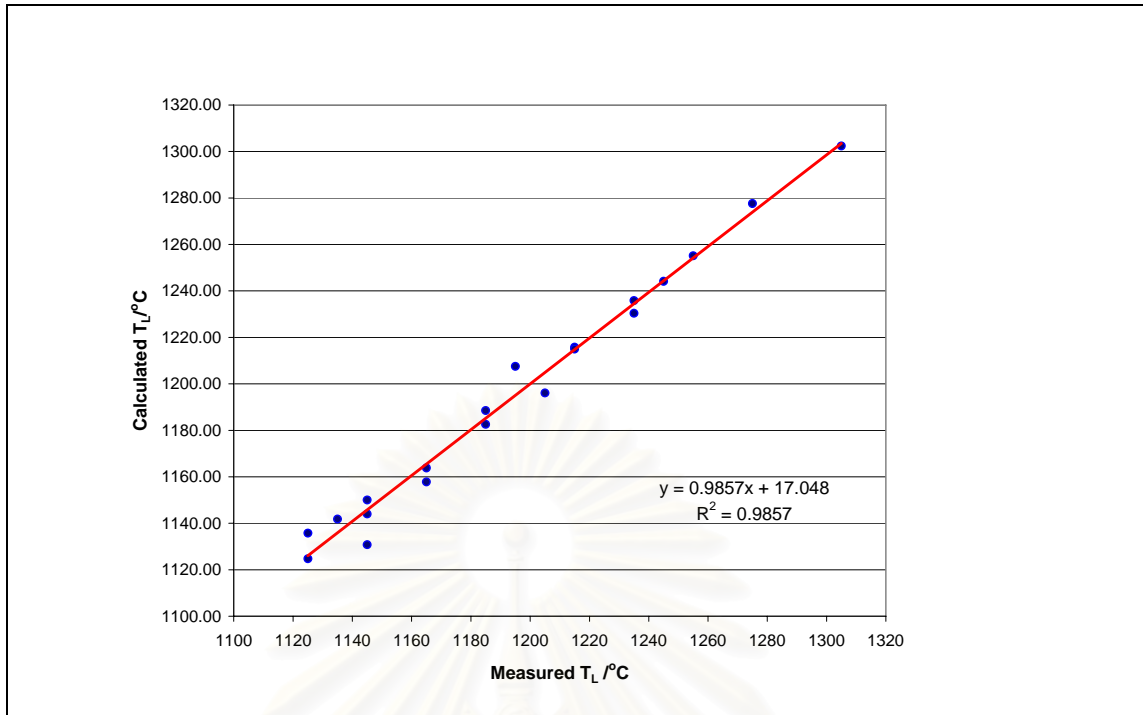


Fig. 4.14 Plot of Calculated  $T_L$  vs. Measured  $T_L$

#### 4.5.2. Prediction $T_L$ from relation between $T_g$ and $T_L$

Thermodynamic considerations one can immediately infer that it always be the case that  $T_g < T_L$  which already know that was inferred by Gibb. Tammann [52] suggest formula

$$\frac{T_g}{T_m} \approx \frac{2}{3} \quad (4.4)$$

Sakka and Mackenzie [53] who were used and confirmed the equation 4.1 and this equation has been confirmed numerous times as showed in Fig. 4.15.

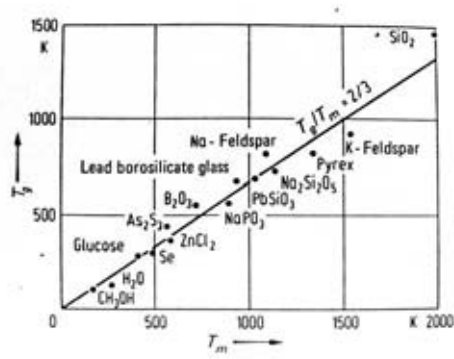


Fig. 4.15 Ratio of transformation temperature  $T_g$ : melt or liquidus temperature  $T_m$

The ratio of transformation temperature  $T_g$  and uniform temperature measured  $T_L$  were shown in Table 4.8. The average of  $T_g/T_L$  was 0.60 or  $3/5$ . This value was used to calculate for  $T_L$  prediction and shown in Table 4.9.

สถาบันวิทยบริการ  
จุฬาลงกรณ์มหาวิทยาลัย

Table 4.8  $T_g$ ,  $T_L$  and ratio of transformation temperature  $T_g$ : Liquidus temperature  $T_L$ 

| Sample             | $T_g$ | $T_L$ | $T_g/T_L$ |
|--------------------|-------|-------|-----------|
| E1R                | 703   | 1165  | 0.60      |
| E1N1               | 699   | 1145  | 0.61      |
| E1N3               | 693   | 1135  | 0.61      |
| E1K1               | 698   | 1155  | 0.60      |
| E1K3               | 702   | 1115  | 0.63      |
| E2R                | 708   | 1145  | 0.62      |
| E2N1               | 703   | 1135  | 0.62      |
| E2N3               | 683   | 1165  | 0.59      |
| E2K1               | 706   | 1145  | 0.60      |
| E2K3               | 697   | 1185  | 0.59      |
| E3R                | 704   | 1125  | 0.63      |
| E3N1               | 690   | 1125  | 0.61      |
| E3N3               | 670   | 1165  | 0.58      |
| E3K1               | 730   | 1145  | 0.64      |
| E3K3               | 665   | 1185  | 0.56      |
| E4R                | 740   | 1205  | 0.61      |
| E4N1               | 736   | 1195  | 0.62      |
| E4N3               | 718   | 1235  | 0.58      |
| E4K1               | 747   | 1215  | 0.61      |
| E4K3               | 741   | 1255  | 0.59      |
| E5R                | 740   | 1215  | 0.61      |
| E5N1               | 730   | 1235  | 0.59      |
| E5N3               | 728   | 1275  | 0.57      |
| E5K1               | 740   | 1245  | 0.59      |
| E5K3               | 740   | 1305  | 0.57      |
| Average            |       |       | 0.60      |
| Standard deviation |       |       | 0.02      |



Table 4.9 Comparison measured  $T_L$  and predicted  $T_L$  by  $T_g/T_L$  ratio

| Sample | Measure $T_L$ | Predicted $T_L$ |
|--------|---------------|-----------------|
| E1R    | 1165          | 1168            |
| E1N1   | 1145          | 1161            |
| E1N3   | 1135          | 1151            |
| E1K1   | 1155          | 1160            |
| E1K3   | 1115          | 1166            |
| E2R    | 1145          | 1176            |
| E2N1   | 1135          | 1168            |
| E2N3   | 1165          | 1135            |
| E2K1   | 1145          | 1173            |
| E2K3   | 1185          | 1158            |
| E3R    | 1125          | 1169            |
| E3N1   | 1125          | 1146            |
| E3N3   | 1165          | 1113            |
| E3K1   | 1145          | 1213            |
| E3K3   | 1185          | 1105            |
| E4R    | 1205          | 1229            |
| E4N1   | 1195          | 1223            |
| E4N3   | 1235          | 1193            |
| E4K1   | 1215          | 1241            |
| E4K3   | 1255          | 1231            |
| E5R    | 1215          | 1229            |
| E5N1   | 1235          | 1213            |
| E5N3   | 1275          | 1209            |
| E5K1   | 1245          | 1229            |
| E5K3   | 1305          | 1229            |

The plot of measured  $T_L$  vs calculated  $T_L$  by  $T_g/T_L$  ratio was shown in Fig. 4.16. From this graph, their R-square was very low. It was noticed that  $T_g$  of glasses were slightly different, in the other hand the  $T_L$  were more different. In addition, the direction of change in  $T_g$  values of some compositions were found contrary in  $T_L$ .

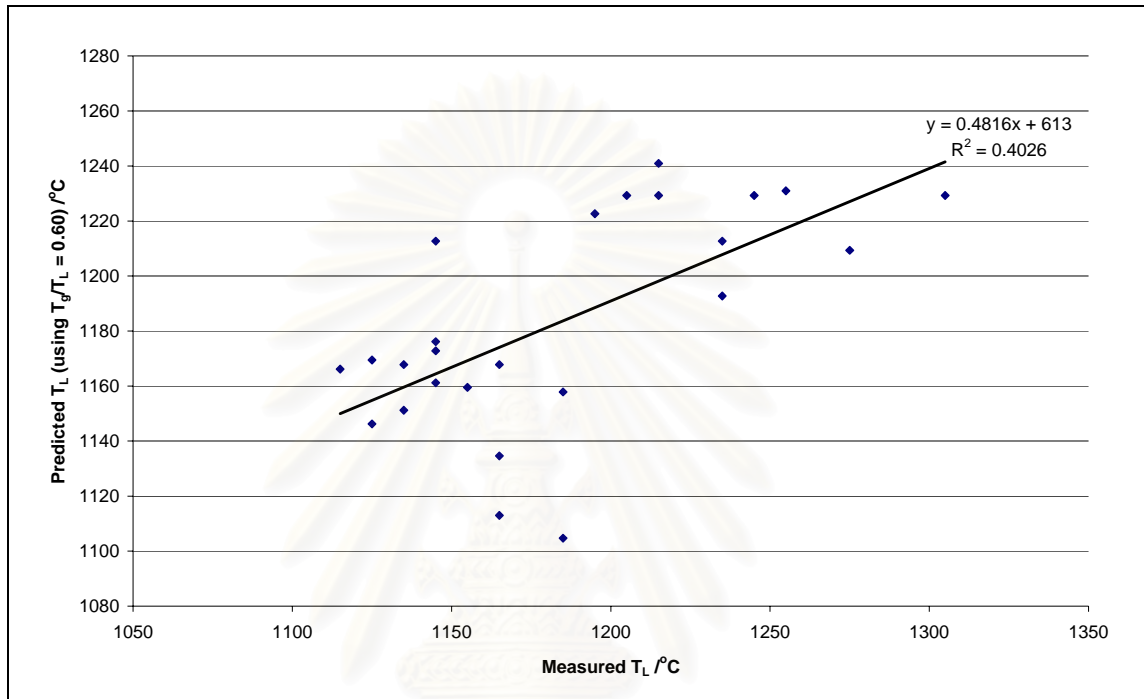


Fig. 4.16 Plot of measured  $T_L$  vs. predicted  $T_L$  (using  $T_g/T_L = 0.60$  or  $3/5$ )

#### 4.6 Liquidus temperature measurement using heating stage microscope

As discussed in section 2.3 regard to homogeneous crystallization, when temperature was cooled below liquidus temperature nuclei are not present in metastable zone or undercooling zone due to nucleation rate equal to zero. However, crystals growth in this region is as the result of nuclei containing. Focus on heterogeneous nucleation, the free energy of crystallization is lower than the free energy of homogenous crystallization. The heterogeneous nucleation can occurred in the metastable zone; therefore, the effect of 'supercooling' seems to decrease. In addition, the crystals will melt into liquid at constant temperature in heating temperature condition, so that, the  $T_L$  was determined as temperature that remaining crystals was completely melted, in some

case that crystals were very large size; consequently, those required a longer time to melt. The  $T_L$  for this case was obtained from contact area between molten glass and platinum plate that found the change of small size of crystals and its disappearance when heating to higher temperature.

Unfortunately, there were limitations of this experiment. Firstly, the AC power supply could not be finely controlled the output voltage. The output voltage can be changed were in the minimum of 0.2 volt. The temperature change was approximately  $100^\circ\text{C}/\text{volt}$  for range of 9.0 – 11.0 volt. Therefore, the temperature which was controlled by this power supply was not finely controlled. Secondly, the highest temperature limit was  $1400^\circ\text{C}$ . Considering  $T_L$  results from uniform temperature method which  $T_L$  must be lowers than  $1200^\circ\text{C}$ , just only six glasses were selected from group E1 and E2 to measure  $T_L$  in this experiment. The last one is that microscope in this experiment could not be operated in polarized light. The crystals were inspected by reflecting of light on surface of the molten glass. Although the crystallization in molten glass could not be observed, the result of crystal observation of heat-treated glass at temperature near  $T_L$ , in uniform temperature method section, was confirmed that remaining crystals were located on the surface of glass and crucible contact are.

The aluminum metal, certified standard materials with melting point of  $660.1^\circ\text{C}$ , were used to aid in assessing the accuracy of the measurement technique. It was found that the thin piece of aluminum metal was rapidly deformed at  $701^\circ\text{C}$  (Fig. 4.17) so that the measured melting point was  $701^\circ\text{C}$ . The result showed  $40^\circ\text{C}$  higher than certified temperature. Since the thermocouple was embedded in the stage below the supported Pt-plate as a result temperature was lower than the thermocouple temperature.

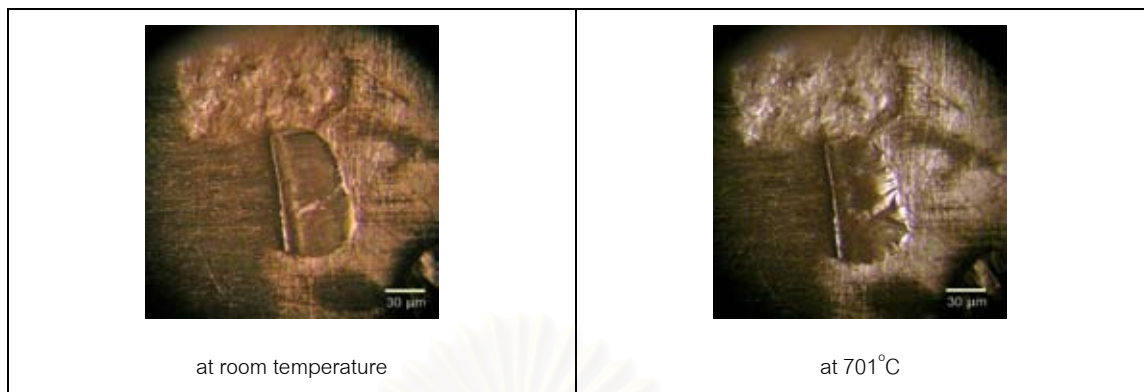


Fig. 4.17 Melting point measurement of aluminum standard material using a heating stage microscope

The results of liquidus temperature of six selected glasses were shown in Table 4.10. Liquidus temperatures measured by a heating stage microscope of E1 group showed lower  $T_L$  in case of alkali-containing glasses which were E1N3 and E1K3. For E2 group, the liquidus of alkali-containing glasses (E2N3 and E2K3) showed higher  $T_L$  than reference sample (E2R). Both group had similar trend of  $T_L$  as result from uniform temperature method. The liquidus temperature measured by heating stage microscope,  $T_{L-HS}$  was higher than liquidus temperature measured by a uniform temperature method,  $T_{L-UT}$  by  $113^\circ\text{C}$  on average. It was probably that the temperature of sample and heating stage measured by thermocouple may be different as shown by the result of aluminum standard material. In addition, non-equilibrium condition of this experiment was affected deficiency by too short of crystallization time and delayed of heat transfer depended to size of a sample.

Fig. 4.18 shows the step to determine liquidus temperature of E2K3. The samples used were crystals containing glasses at  $1090^\circ\text{C}$  for 24 h. In this figure, (a) is the starting point to observe crystal transformation. The sample was heated gradually up to higher temperature and simultaneously observed the change of size and shape of crystals. At the 2<sup>nd</sup> Step, it was found that crystals were decreased and melted. The sample was cooled down to lower temperature at  $1290^\circ\text{C}$  on the 3<sup>rd</sup> step. It was found the growth of crystals. Finally, the sample was heated to high temperature interval

between 1325°C and 1290°C which was 1300°C. At this temperature crystal were melted completely and no crystallization after holding at these temperatures for 10 minutes, thus, it was summarized that  $T_L$  was 1300°C. However measured  $T_{L-HS}$  may slightly lower than 1300°C, the limitation of temperature controller by output voltage could not finely adjust. Therefore the report of  $T_{L-HS}$  was 1290 - 1300°C in this case. Other samples were run in the same way followed these steps. The primary crystalline phase that happened on the surface of all six samples was needle-like crystal of  $\beta$ -wollastonite.

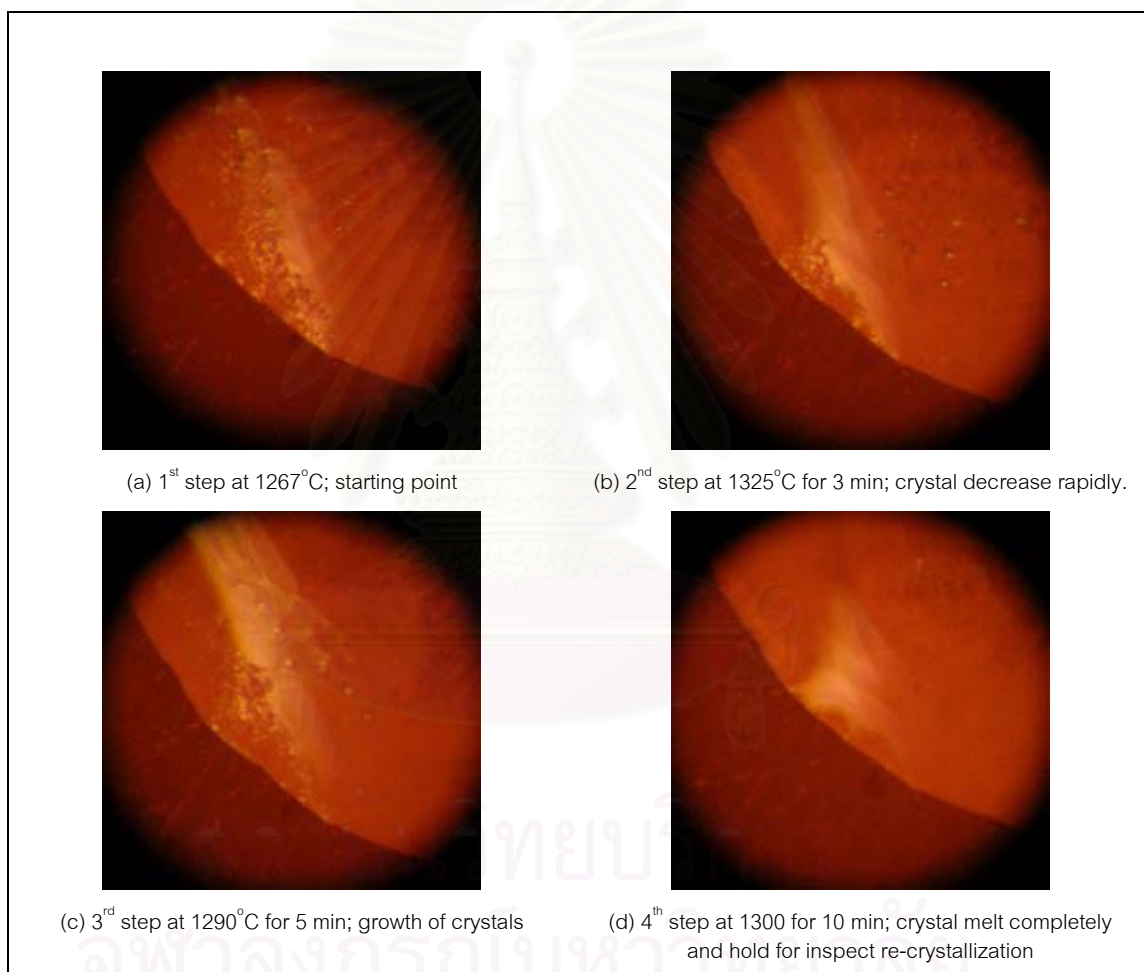


Fig. 4.18 Step to observed and determined liquidus temperature of E2K3 using heating stage microscope.

Table 4.10 Measured  $T_L$  using heating stage microscope

| Sample                                     | $T_{L-HS}$ ( $^{\circ}C$ ) | $T_{L-UT}$ ( $^{\circ}C$ ) | $T_{L-HS(max)} - T_{L-UT}$ ( $^{\circ}C$ ) |
|--|----------------------------|----------------------------|--|
| E1R heat-treated at 1080 $^{\circ}C$ /24h  | 1260-1280                  | 1165                       | 115  |
| E1N3 heat-treated at 1080 $^{\circ}C$ /24h | 1240-1252                  | 1135                       | 117  |
| E1K3 heat-treated at 1080 $^{\circ}C$ /24h | 1222-1235                  | 1125                       | 110  |
| E2R heat-treated at 1090 $^{\circ}C$ /24h  | 1256-1260                  | 1145                       | 115  |
| E2N3 heat-treated at 1090 $^{\circ}C$ /24h | 1280-1300                  | 1165                       | 135  |
| E2K3 heat-treated at 1090 $^{\circ}C$ /24h | 1290-1300                  | 1185                       | 115  |

$T_{L-HS}$  = The liquidus temperature measured by heating stage microscope,  $T_{L-UT}$  = The liquidus temperature measured by a uniform temperature method and  $T_{L-HS(max)}$  = The highest temperature of  $T_{L-HS}$  range

#### 4.7 Case study on liquidus temperature of industrial glass

##### 4.7.1. Observation of as-receive industrial glass and as-fabricated glasses

The photographs of E-glass sample from glass-fiber-production plant and as-fabricated glasses are shown in Fig. 4.19. Excluding EFR sample that came from industrial plant, all as-fabricated samples (EF0, EF03 and EF13) could be melted at 1450 $^{\circ}C$  without undissolved phase or crystallization. The EF0 sample which was non-iron oxide containing glass was colorless and transparent. The EF03 sample containing 0.3 wt%  $Fe_2O_3$  showed light tone of green color similar to EFR sample which contained 0.3 wt%  $Fe_2O_3$  (known by XRF result). The EF13, which included 1.3 wt%  $Fe_2O_3$ , showed darker green and yellow tone. The molten glasses were poured out of the platinum crucible easily and it could be drawn as a long thin fiber.

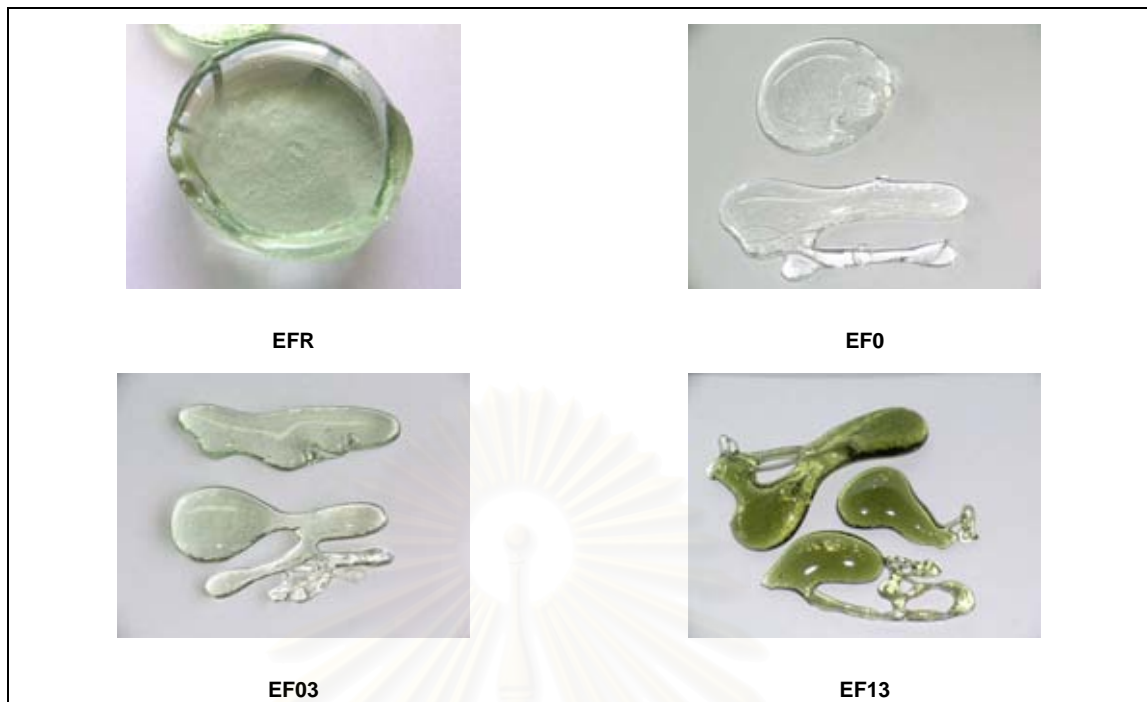


Fig. 4.19 Industrial E-glass (EFR) and as-fabricated glasses after melted at 1450°C

#### 4.7.2. Chemical analysis results

The glass samples were analyzed for chemical compositions by XRF and prepared by compressing powder method. The results showed that the difference of  $\text{SiO}_2$  contents between measured and target compositions was 4 wt% in average while CaO content was increased approximately 5 wt% for all three samples. The variations of less than 1 wt% of measured compositions such as F,  $\text{Na}_2\text{O}$ ,  $\text{K}_2\text{O}$  and MgO may be a result of decrease in main components such as  $\text{SiO}_2$ , CaO,  $\text{Al}_2\text{O}_3$  and  $\text{B}_2\text{O}_3$  and trace component come from impurities in chemical batches.

Table 4.11 Comparing between Measured and Target compositions (wt%)

| Compositions                   | EFR    | EF0    |        |       | EF03  |        |       | EF13   |        |       |
|--------------------------------|--------|--------|--------|-------|-------|--------|-------|--------|--------|-------|
|                                | M      | T      | M      | T-M   | T     | M      | T-M   | T      | M      | T-M   |
| Fe <sub>2</sub> O <sub>3</sub> | 0.25   | 0.00   | 0.00   | 0.00  | 0.30  | 0.26   | -0.04 | 1.30   | 1.14   | -0.16 |
| SiO <sub>2</sub>               | 52.93  | 53.00  | 49.13  | -3.87 | 52.96 | 49.42  | -3.54 | 52.84  | 48.77  | -4.07 |
| B <sub>2</sub> O <sub>3</sub>  | 4.99   | 5.00   | 4.00   | -1.00 | 4.96  | 3.50   | -1.46 | 4.84   | 4.20   | -0.64 |
| F                              | 0.81   | 0.80   | 0.28   | -0.52 | 0.76  | 0.22   | -0.54 | 0.64   | 0.13   | -0.51 |
| Na <sub>2</sub> O              | 0.17   | 0.20   | 0.74   | 0.54  | 0.16  | 0.72   | 0.56  | 0.04   | 0.57   | 0.53  |
| MgO                            | 0.14   | 0.20   | 0.27   | 0.07  | 0.16  | 0.24   | 0.08  | 0.04   | 0.14   | 0.10  |
| Al <sub>2</sub> O <sub>3</sub> | 13.77  | 14.00  | 15.00  | 1.00  | 13.96 | 14.98  | 1.02  | 13.84  | 14.86  | 1.02  |
| P <sub>2</sub> O <sub>5</sub>  | 0.00   | 0.00   | 0.01   | 0.01  | 0.00  | 0.02   | 0.02  | 0.00   | 0.02   | 0.02  |
| SO <sub>3</sub>                | 0.00   | 0.00   | 0.19   | 0.19  | 0.00  | 0.20   | 0.20  | 0.00   | 0.16   | 0.16  |
| Cl                             | 0.09   | 0.00   | 0.07   | 0.07  | 0.00  | 0.08   | 0.08  | 0.00   | 0.07   | 0.07  |
| K <sub>2</sub> O               | 0.70   | 0.80   | 0.93   | 0.13  | 0.76  | 0.91   | 0.15  | 0.64   | 0.76   | 0.12  |
| CaO                            | 25.98  | 26.00  | 31.06  | 5.06  | 25.96 | 31.41  | 5.45  | 25.84  | 30.94  | 5.10  |
| TiO <sub>2</sub>               | 0.10   | 0.00   | 0.01   | 0.01  | 0.00  | 0.01   | 0.01  | 0.00   | 0.01   | 0.01  |
| ZrO <sub>2</sub>               | 0.08   | 0.00   | 0.05   | 0.05  | 0.00  | 0.05   | 0.05  | 0.00   | 0.04   | 0.04  |
| Total                          | 100.00 | 100.00 | 101.74 |       | 99.68 | 101.76 |       | 100.02 | 101.81 |       |

T = Target compositions, M = Measured compositions and D = Different between T and M

#### 4.7.3. Measurement of liquidus temperature using a uniform temperature method

The liquidus temperature of EFR was 1085°C close to a liquidus temperature of E-glass in literature which is between 1065-1077°C [32], while the liquidus temperatures of EF0, EF03 and ER13 were higher up to 1195°C as shown in Table 4.12.

The crystalline phase observation was found that at low temperature the heat-treated glass contain various shapes of crystals such as hexagon, rectangular, star-like and needle-like. The crystal detected at temperature close to  $T_L$  was a needle-like crystal and hexagonal crystal.

The liquidus temperature of EFR was lower than other samples in this case. It may be explained by CaO/SiO<sub>2</sub> ratio according to ternary phase diagram in Fig. 4.13. In



pseudowollastonite phase field if CaO were increased with decreasing of SiO<sub>2</sub>, it will tend to increase the liquidus temperature. Consequently, the liquidus temperatures of EF0, EF03 and EF13 glasses with lower SiO<sub>2</sub> but higher in CaO concentrations, were higher than EFR.

Table 4.12 T<sub>L</sub> and Visual observation of heat-treated glasses

| Samples | Measured T <sub>L</sub><br>(±10°C) | Visual characterization of crystalline phase heat-treated glasses at near T <sub>L</sub> |   |                   |
|---------|------------------------------------|--|---|-------------------|
|         |                                    | Detected phase   | Shape / position of detected crystals                   | Average size (μm) |
| EFR     | 1085                               | Wollastonite   | Needle-like and hexagon on the surface                  | 180               |
| EF0     | 1195                               | Wollastonite   | Rectangular and hexagon on surface                      | 800               |
| EF03    | 1185                               | Wollastonite   | Star-like, rectangular and needle on surface and bubble | 120               |
| EF13    | 1185                               | Wollastonite   | Layer of hexagon on the surface                         | 120               |

Table 4.13 Summation of heat-treatment results of industrial glass and EF group

| Temp. | EFR | EF0 | EF03 | EF13 |
|-------|-----|-----|------|------|
| 1200  |     | O   | O    | O    |
| 1190  |     | X   | O    | O    |
| 1180  |     | X   | X    | X    |
| 1170  |     |     |      |      |
| 1160  |     | X   |      |      |
| 1150  |     |     |      |      |
| 1140  |     | X   | X    | X    |
| 1130  |     |     |      |      |
| 1120  |     |     |      |      |
| 1100  | O   |     |      |      |
| 1000  |     |     |      |      |
| 1090  | O   |     |      |      |
| 1080  | X   |     |      |      |

X = Contained Crystal and O = No Crystal detected

In order to study the effect of iron oxide on the liquidus temperature of E-glass composition, the results show that the T<sub>L</sub> of samples contained iron oxides of 0.3 and 1.3 wt% were slightly lower than EF0 sample (Table 4.2).




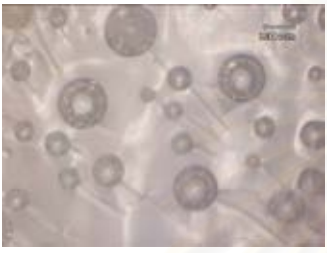
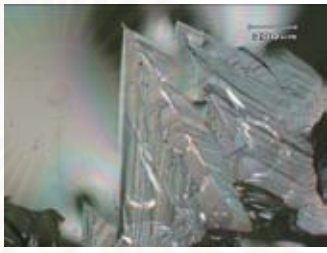
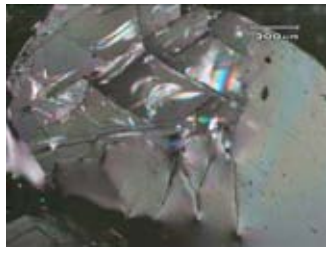

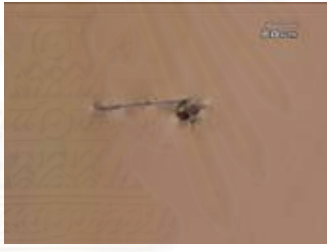
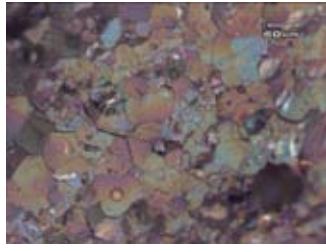

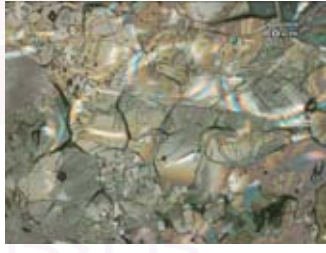
| Sample | $T_2$   | $T_1$  |  |
|--------|---|--|--|
| EFR    |    |    |   |
|        | 1100°C  | 1090°C   | 1080°C   |
| EF0    |    |    |   |
|        | 1200°C  | 1190°C   | 1180°C   |
| EF03   |   |   |  |
|        | 1190°C  | 1180°C   | 1170°C   |
| EF13   |  |  |  |
|        | 1190°C  | 1180°C   |  |

Fig. 4.20 Visual observations of heat-treated glass for  $T_L$  determination

#### 4.7.4. Primary phase identification

The study of primary phase will give the information for modifying or designing glass compositions based on phase diagram considering the liquidus temperature. Fig. 4.21 shows the XRD patterns of glass samples which were heat-treated at lower

temperature than their liquidus temperatures. The XRD patterns of EFR show highest intensity of cristobalite phase and  $\beta$ -wollastonite as a second phase. The XRD patterns of heat-treated EF0, EF03 and EF13 at  $1140^{\circ}\text{C}/24\text{h}$  show only pseudowollastonite phase. The high intensity of cristobalite peak may be explained by EFR was obtained directly from an industrial furnace that may include of cristobalite nuclei from raw materials or from the refractory in the furnace chamber. The temperature that glass sample was pulled out was not determined as the cristobalite phase may have been presented before the heat treatment.

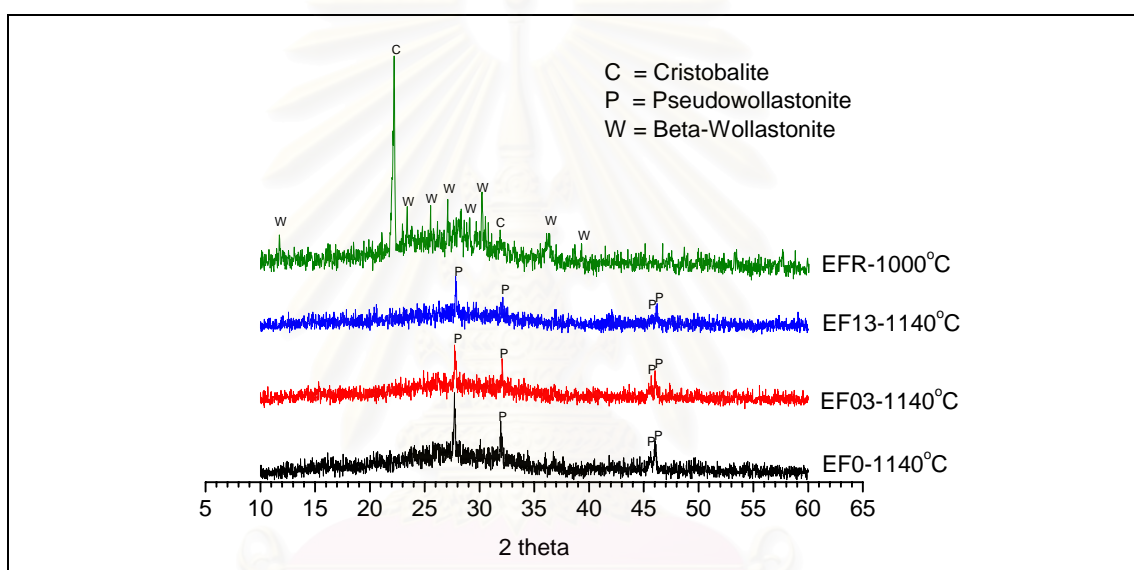


Fig. 4.21 XRD Pattern of glass samples heat-treated at  $1140^{\circ}\text{C}/24\text{h}$  for EF0, EF03 and EF13, and  $1000^{\circ}\text{C}/24\text{h}$  for EFR.

## CHAPTER V

### CONCLUSIONS

#### 5.1 Conclusions

In order to compare the liquidus temperature of glasses in E-glass and ECR-glass composition range, the liquidus temperatures were measured using both a uniform temperature method and a heating stage microscope. In addition, the regression model was used to predict and study the relation between compositions and liquidus temperature. The following conclusions have been drawn from this study.

1. The 25 glass compositions melted at  $1450^{\circ}\text{C}$  showed homogeneous and transparent with colorless appearance.
2. Primary phases of these glasses system were wollastonite.
3. Alkali oxide ( $\text{Na}_2\text{O}$  and  $\text{K}_2\text{O}$ ) were led to increase  $T_L$ .
4.  $\text{K}_2\text{O}$  had more influence on  $T_L$  than  $\text{Na}_2\text{O}$ .
5. The liquidus temperature of these glass compositions were between  $1130^{\circ}\text{C}$  and  $1310^{\circ}\text{C}$  using a uniform temperature method.
6. The detected crystals in heat-treated glass closed to  $T_L$ , were observed on surface and crucible contacted area.
7. Scheffe' Polynomial was used to predict the liquidus temperature of these glass compositions; however, the accuracy will be valid in a short range of compositions.
8. Because the limitation of the temperature used for heating stage microscope was  $1400^{\circ}\text{C}$ , liquidus temperature of the samples with higher  $T_L$ , E3 - E5 group, could not be measured.
9. The liquidus temperatures of glass samples measured by using the heating stage microscope are higher than those using a uniform temperature method.

The case study of industrial E-glass was concluded as follow;

10. Three glasses compositions melted at 1450°C showed the homogeneous and transparent with colorless for non-containing iron oxide glass, light green for 0.3 wt% iron oxide glass and darker green for 1.3 wt% iron oxide glass.
11. The liquidus temperature of iron oxide glass was slightly decreased by iron oxide by 10°C when compared with non iron oxide glasses. But it was not different of liquidus temperatures in case of 0.3 wt% iron oxide containing and 1.3 wt% iron oxide containing.
12. The liquidus temperature of industrial E-glass sample was 1085°C lower than EF03 which was the simulated composition, the chemical composition of EF03 showed higher in CaO and lower in SiO<sub>2</sub>. It was supported by ternary phase diagram of CaO-SiO<sub>2</sub>-Al<sub>2</sub>O<sub>3</sub> in pseudowollastonite phase field.
13. The primary crystalline phase of all three fabricated glasses were both type of  $\alpha$ -wollastonite and  $\beta$ -wollastonite. For industrial glass the primary phases were cristobalite and  $\beta$ -wollastonite.

## 5.2 Future works

The follows are recommendation for future work.

Glass fiber forming required the temperature of log 3 forming, so that, to design the compositions of glass fiber the log 3 forming should be considered. The good glass fiber composition should have a lower  $T_L$  and log 3 forming temperature. In addition the temperature of log 3 of forming and  $T_L$  should not be too much in different.

Liquidus temperature of the same compositions should be re-measure using a gradient temperature method to compare the result.

## REFERENCES

- [1] ไอเคพีซีที แอดไวเซอร์, บริษัท. รายงานภาวะอุตสาหกรรม งานการสำรวจข้อมูลการผลิตรายปี ปี พ.ศ. 2545. กรุงเทพฯ: กรมส่งเสริมอุตสาหกรรม, 2547.
- [2] Zachariasen, W.H. The Atomic Arrangement in Glass. J. Am.Chem. Soc. 54 (1932): 3841-3851.
- [3] Kingery, W.D. Introduction to Ceramics. 2<sup>nd</sup> ed. New York: Wiley-Interscience Publication, 1976.
- [4] Pual, A. Chemistry of Glasses. 2<sup>nd</sup> ed. New York: Chapman and Hall, 1990.
- [5] Holloway, D.G. The Physical Properties of Glass. London: Wykeham publications (London), 1973.
- [6] ASTM-C162. Standard Terminology of Glass and Glass Products. ASTM International. 1999.
- [7] ASTM-C829. Standard Practices for Measurement of Liquidus Temperature of Glass by the Gradient Furnace. ASTM International. 2000.
- [8] Schulz, R.L.; Brown, K. G. and Jantzen, C.M. Technical Report on the Impact of MgO on Defense Waste Processing Facility (DWPF) Glass Liquidus Temperature and Durability (U). South Carolina: Westinghouse Savannah River, 2000.
- [9] Crum, J.V. Liquidus Temperature Model for High-Level Waste Glasses That Precipitate Zirconium-Containing Crystalline Phase: Environmental Issue and Waste Management Technologies III. (n.d.) : 271-277.
- [10] Edward Orton Jr. Ceramic Foundation. Liquidus Furnace Model GTF-MD Series Brochure. [online]. Available from: <http://www.ortonceramic.com/Glass/z04gBrochure-LiqFce.pdf>. [2005, January 14].
- [11] Lehmann, O. Molecularphysik, Engelmann, Leipzig (1888); see pp. 90-93 of ref 4.

- [12] Priven, A.I. Calculation of the properties of oxide glasses and melts from composition: problems and prospects. Glass Physics and Chemistry (Translation of Fizika i Khimiya Stekla) 24 (1998): 67-72.
- [13] Cable, M. Materials Science and Technology. in J. Zarzicki (ed.), Glasses and Amorphous Materials, New York: VCH, 1991.
- [14] Lakatos, T.; Johansson, G. and Simmingsköld: Viscosity temperature relations in the glass system SiO<sub>2</sub>-Al<sub>2</sub>O<sub>3</sub>-Na<sub>2</sub>O-K<sub>2</sub>O-CaO-MgO in the composition range of technocal glasses. Glass Technology 13 (1972): 88-95.
- [15] Priven, A.I. and Priven, A. I. Comparative characterization of methods for calculating the viscosity of silicate glass-forming melts. Glass Physics and Chemistry (Translation of Fizika i Khimiya Stekla) 23 (1997): 333-343.
- [16] Backman, R.; Karlsson K.H.; Cable, M. and Pennington, N. Glastech. Ber. 63K (1990) 460.
- [17] Backman, R.; Karlsson, K.H. and Cable, M. Model for Liquidus Temperature of Multicomponent Silicate Glasses, Phys. Chem. Glasses. 38 (1997): 103.
- [18] Hrma, P.R. and Piepel, G. F. Property/Composition and Temperature on the Properties of High Level Waste Glasses Melting at 1150°C, PNNL Report 103059 to the US Department of Energy, vol. 1 and 2, Contract DE-AC06-76RLO 1830, December 1994.
- [19] Vienna, J. D.; Hrma, P. R. et al. Effect of Composition and Temperature on the Properties of High Level Waste (HLW) Glass Melting above 1200°C (Draft). PNNL Report 10987 to the US Department of Energy, Contract DE-AC06-76RLO 1830, February 1996.
- [20] Hrma, P. and Robertus, R. J. Waste glass design based on property composition functions. Ceram. Eng. Sci. Proc. 14 (1993): 187-203.

- [21] Hrma, P.; Piepel, G.F.; Redgate, P.E.; Smith, D. E.; Schweiger, M.J.; Vienna, J.D. and Kim, D.S. Prediction of processing properties for nuclear waste glasses. Ceramic Transactions 61: 505-513.
- [22] Fluegel, A.; Varshneya, A. K.; Seward, T. P. and Earl, D. A. Viscosity of commercial glasses in the softening range. Ceramic Transactions 141 (2004): 379-386
- [23] Kucuk, A.; Clare, A. G. and Jones, L. An estimation of the surface tension of silicate glass melts at 1400°C using statistical analysis. Glass Technol. 40 (Oct 1999): 149-153.
- [24] Dreyfus, C. and Dreyfus G. A Machine Learning Approach to the Estimation of the Liquidus Temperature of Glass-Forming Oxide Blends. J. Non-Cryst. Solids. 318 (2003): 63-78.
- [25] Pelton, A. D.; Bale, C. W. and Thompson, W. T. FactSage. [Computer software]. Montreal: Ecole Polytechnique. <http://www.crct.polymtl.ca>. 2002.
- [26] SciGlass. Glass property information system version 3.5. [Computer software]. MA: SciVision. 2000.
- [27] Reinhard Conradt. UNIGLASS version May 2002. [Computer software]. Aachen: Dept. of Glass and Ceramic Composites, Inst. of Mineral Engineering. RWTH. 2002.
- [28] Loewenstein, K. L. The Manufacturing Technology of Continuous Glass Fibers. 3<sup>rd</sup> revised ed. Elsevier, 1993.
- [29] Wallenberger, F.T. Structural Silicate and Silica Glass Fibers. in F.T. Wallenberger (ed.) Advanced Inorganic Fibers Processes, Structures, Properties, Applications, pp. 129-168. Kluwer Academic Publishers, 1999.
- [30] ASTM-D578. Standard Specification for Glass Fiber Strands. ASTM International. 2000.



- [31] Dockum, J.F. Fiberglass: Handbook of Reinforcement for Plastics. New York: Van Nostrand Reinhold Company, 1987: 233-286.
- [32] Frederick, W. T., James W.C., and Li Hong. Glass Fibers: ASM Handbook. Vol. 21: composites. Ohio: ASM International, 2003.
- [33] Sproull, J.F. Fiber Glass Compositions. U.S. Pat. No.4,543,106, Sept.17, 1985.
- [34] Eastes, W.L.; Hofmann, D.A. and Wingert, J.W. Boron-Free Glass Fibers, U.S. Pat. No. 5,789,325, Aug.4, 1998.
- [35] Wallenberger, F.T.; Hicks, R.J. and Bierhals, A.T. Effect of Oxides on Decreasing Melt Viscosity and Energy Demand of E-glass. Am. Ceram. Soc. Bull. 85 (2006): 38-41.
- [36] Wallenberger, F.T.; Hicks, R.J. and Bierhals, A.T. Design of Environmentally Friendly Fiberglass Compositions Derived from the Ternary SiO<sub>2</sub>-Al<sub>2</sub>O<sub>3</sub>-CaO Phase Diagram: Structures, Properties and Crystallization Potential of Eutectic and Selected Multi-Oxide E-Glass Compositions. J. Non-Cryst. Solids. 349 (2004): 377-387.
- [ 37 ] Wollenberger, F.T.; Hicks, R.J. and Bierhals, A.T. Design of Energy and Environmentally Friendly Fiberglass Compositions Derived from the Quaternary SiO<sub>2</sub>-Al<sub>2</sub>O<sub>3</sub>-CaO-MgO Phase Diagram-Part I: Structures, Properties and Crystallization Potential of Eutectic and Selected Multi-Oxide E-Glass Compositions. in Ceramic Transactions, vol.170, Melt Chemistry, Relaxation and Solidification Kinetics of Glasses. Edited by H.Li, C.S. Ray, D.M. Strachan, R. Weber and Y. Yue. American Ceramic Society, Westerville, Ohio, 2004.
- [38] Wollenberger, F.T.; Hicks, R.J. and Bierhals, A.T. Design of Environmentally Friendly Fiberglass Compositions Derived from the Quaternary SiO<sub>2</sub>-Al<sub>2</sub>O<sub>3</sub>-CaO-MgO Phase Diagram-Part II: Fluorine-Free E-Glass Compositions

Containing Low Levels of Boron and Lithium Oxide. Glastech. Ber. Glass Sci. Technol. 77C (2004): 170-183.

- [39] Loewenstein, K.L. The Manufacturing Technology of Continuous Glass Fibers. 3rd revise ed. Elsevier, 1993.
- [40] Eastes, W.L.; Hofman, D.A. and Wingert, J.W. Boron-Free Glass Fibers. U.S. Patent 5,789,329. 1998.
- [41] Katz and Milewski. Handbook of Reinforcement for Plastics. 1987.
- [42] Vogel, W. Chemistry of Glass. Ohio: The American Ceramic Society, 1985.
- [43] Perkin Elmer, Inc. Thermal Analysis: Pyris software version 7.0.0.0110. [Computer software]. USA: Perkin Elmer, 2004.
- [44] ASTM E 1356 – 03. Standard Practices for Measurement of Liquidus Temperature of Glass by the Gradient Furnace. ASTM International. 2000.
- [45] Volgel, Werner. Glassfehler. Springer-Verlag Berlin Heidelberg. Germany, 1993.
- [46] Hlavac, Jan. The Technology of Glass and Ceramics (Glass Science and Technology; 4). New York: Elsevier Science Publishing Company, 1983.
- [47] Uhlmann, D.R. and Beall G.H. Nucleation and Crystallization in Glasses. Edit by J.H. Simmons. USA: The American Ceramic Society, 1982.
- [48] Bruker Axs GMBH. Diffraclus EVA (version 7). [Computer software]. Germany: Bruker Axs, 2002.
- [49] Levin, Ernest M.; Robbins, Carl R. and McMurdie, Howard F. Phase Diagrams for Ceramists. USA: The American Ceramic Society, 1964.
- [50] Scheffe, The Analysis of Variance. New York: John Wiley & Son Inc, 1959
- [51] Math Works, Inc. MATLAB (version 6.5.0.180913a Release 13 ). [Computer software]. USA: Math Works, 2002.

[52] Tammann, G. Der Glasszustand. Leipzig: L. VoB. 1933.

[53] Sakka, S. and Mackenzie, J.D. Relation between apparent glass transition temperature and liquidus temperature for inorganic glasses. J. Non-Cryst. Solids 6 (1971): 145-162.



สถาบันวิทยบริการ  
จุฬาลงกรณ์มหาวิทยาลัย



APPENDICES

สถาบันวิทยบริการ  
จุฬาลงกรณ์มหาวิทยาลัย

## APPENDIX A

Supplier and lot number of batch chemicals

| Chemicals                       | Suppliers          | Purity (%pure) |
|---------------------------------|--------------------|----------------|
| SiO <sub>2</sub>                | Fisher             | ≥98            |
| Al <sub>2</sub> O <sub>3</sub>  | APS, Australia     | ≥95%           |
| HB <sub>2</sub> O <sub>3</sub>  | Fisher             | 99.99          |
| MgCO <sub>3</sub>               | Fluka, Switzerland | 40.0% MgO      |
| CaCO <sub>3</sub>               | Fluka, Switzerland | ≥99%           |
| ZnO                             | Fluka, Switzerland | ≥99            |
| Na <sub>2</sub> CO <sub>3</sub> | Fluka, Switzerland | ≥99%           |
| K <sub>2</sub> CO <sub>3</sub>  | APS, Australia     | ≥99%           |



สถาบันวิทยบริการ  
จุฬาลงกรณ์มหาวิทยาลัย

## APPENDIX B

Visual observations of 25 glass compositions, the photographs were taken by digital camera (Nikon model coolpix 5400).



E1R



E1N1



E1N3



E1K1



E1K3

As - fabricated E1 glass sample group



E2R



E2N1



E2N3



E2K1



E2K3

As - fabricated E2 glass sample group



**E3R**



**E3N1**



**E3N3**



**E3K1**



**E3K3**

---

As - fabricated E3 glass sample group



**E4R**



**E4N1**



**E4N3**



**E4K1**



**E4K3**

---

As - fabricated E4 glass sample group



E5R



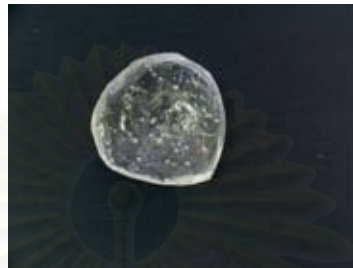
E5N1



E5N3

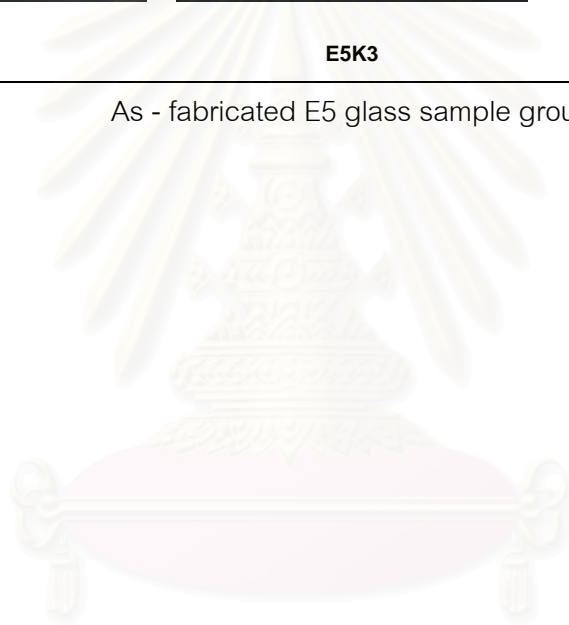


E5K1



E5K3

As - fabricated E5 glass sample group

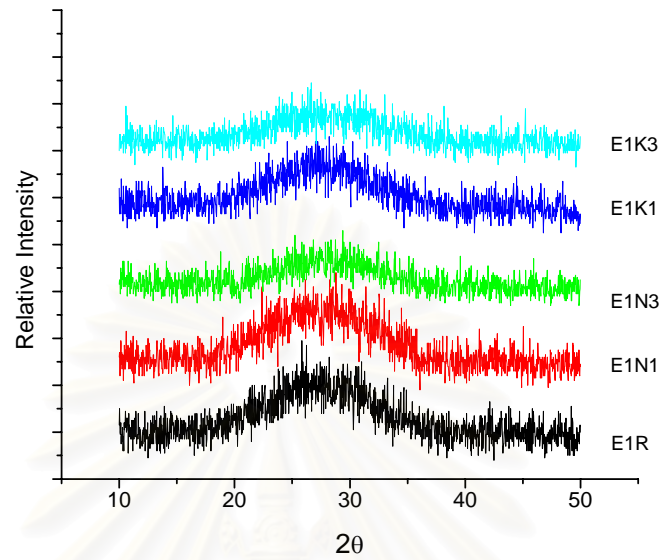


สถาบันวิทยบริการ  
จุฬาลงกรณ์มหาวิทยาลัย

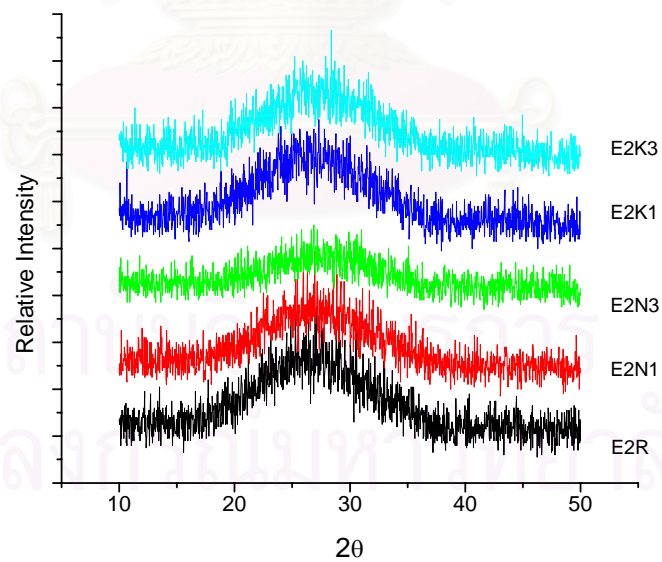


## APPENDIX C

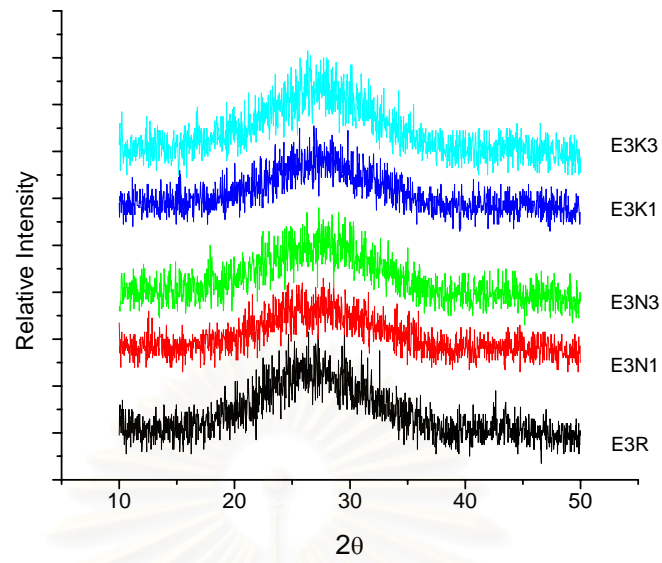
XRD pattern of as-fabricated glasses in each group



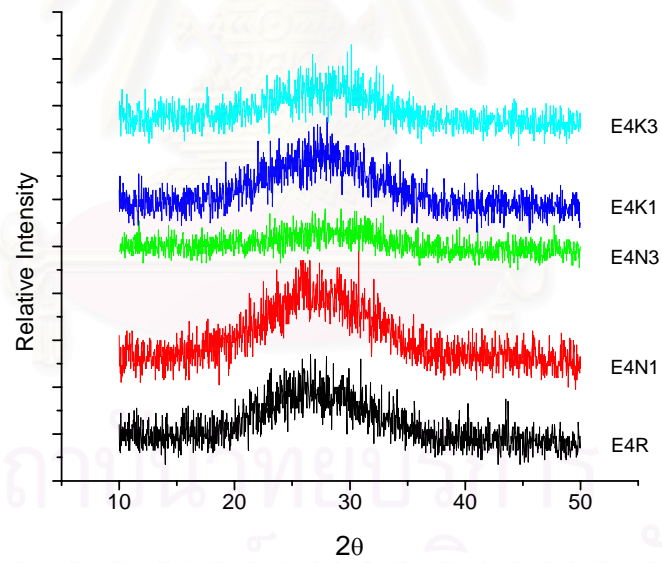
XRD pattern of as- fabricated E1 group



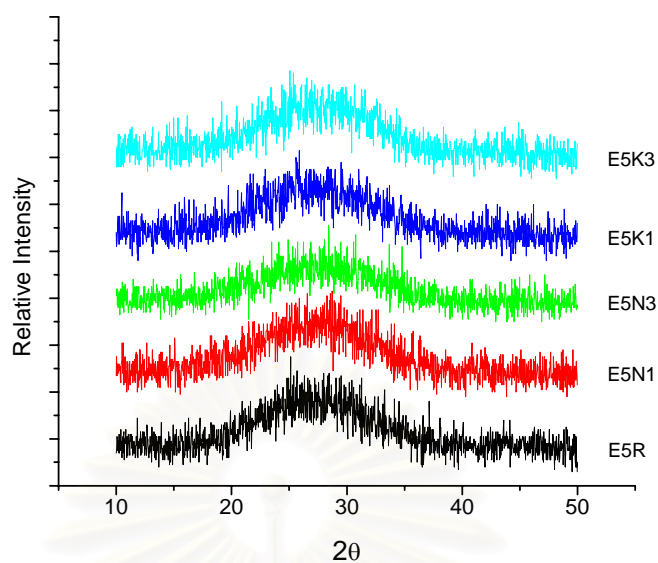
XRD pattern of as - fabricated E2 group



XRD pattern of as - fabricated E3 group



XRD pattern of as - fabricated E4 group



XRD pattern of as - fabricated E5 group

สถาบันวิทยบริการ  
จุฬาลงกรณ์มหาวิทยาลัย

## APPENDIX D

List of heat treatment temperature using in uniform temperature method

| Samples | Heat treatment temperature ( °C)   | Samples | Heat treatment temperature ( °C) |
|---------|------------------------------------|---------|----------------------------------|
| E1R     | 1170 1160 1150                     | E4R     | 1220 1210 1200                   |
| E1N1    | 1150 1140                          | E4N1    | 1220 1210 1200 1190 1180         |
| E1N3    | 1140 1130 1120                     | E4N3    | 1230 1220                        |
| E1K1    | 1150 1140 1130 1120                | E4K1    | 1220 1210 1200                   |
| E1K3    | 1120 1110                          | E4K3    | 1250 1240 1230                   |
| E2R     | 1170 1160 1150 1140 1130           | E5R     | 1240 1220 1210 1200              |
| E2N1    | 1160 1150 1140 1130 1120           | E5N1    | 1240 1230 1220                   |
| E2N3    | 1180 1170 1160 1150 1140 1130 1120 | E5N3    | 1290 1280 1270 1250 1230         |
| E2K1    | 1150 1140 1130                     | E5K1    | 1250 1240                        |
| E2K3    | 1190 1180 1170                     | E5K3    | 1310 1300 1290 1270 1250         |
| E3R     | 1150 1130 1120 1100                |         |                                  |
| E3N1    | 1160 1130 1120 1100                |         |                                  |
| E3N3    | 1170 1160 1150                     |         |                                  |
| E3K1    | 1170 1150 1140 1130                |         |                                  |
| E3K3    | 1200 1190 1180                     |         |                                  |

สถาบันวิทยบริการ  
จุฬาลงกรณ์มหาวิทยาลัย

## APPENDIX E



National Institute of Standards &amp; Technology

## Certificate

## Standard Reference Material 1416

## Aluminosilicate Glass for Liquidus Temperature

(In Cooperation with the American Society for Testing and Materials)

This Standard Reference Material (SRM) is a mixed alkaline earth aluminosilicate glass that is certified for the liquidus temperature. It is for use in checking test methods and in calibrating equipment specified in ASTM 829 Standard Practices for Measurement of Liquidus Temperature by the Gradient Furnace Method. Each SRM unit consists of 22 lengths of approximately 12.7 cm (5 in) of glass tubing totalling approximately 250 g.

The certified value for the gradient liquidus temperature is:

$$1147 \pm 4 \text{ } ^\circ\text{C}$$

The certified value is the interlaboratory mean of results. The expanded uncertainty of the certified value was computed according to the NIST uncertainty policy, as described in NIST Technical Note 1297 [1, 2]. It is the root sum of squares of the within and between-laboratory standard uncertainties, 0.66 and 1.29  $^\circ\text{C}$  respectively, expanded by a t-multiplier based on five degrees of freedom. The certified value and expanded uncertainty give a 95% confidence interval for the mean.

Glass for this SRM was supplied by Corning, Inc., Corning, NY. NIST technical coordination for this SRM was performed by M.J. Cellarosi, Ceramics Division. The ASTM coordination of cooperative analyses leading to certification was performed by H.E. Hagy, Chairman, and A.C. Siefert, Research Associate, of ASTM C14.91 Subcommittee on Standard Reference Materials.

Statistical analysis of the certification data was performed by L.M. Oakley of the NIST Statistical Engineering Division.

The technical and support aspects involved in the preparation, certification, and issuance of this SRM were coordinated through the Standard Reference Materials Program by J.S. Kane.

**Instructions for Use:** The glass tubing provided must be crushed with a clean mortar and pestle and sieved to obtain particles finer than 0.85 mm (#20 sieve) for measurement, as specified in ASTM C829. The method specifies preparation of 70 g of glass for a measurement sequence. The crushed glass is hygroscopic, and therefore should be stored in a desiccator if measurements are not made immediately.

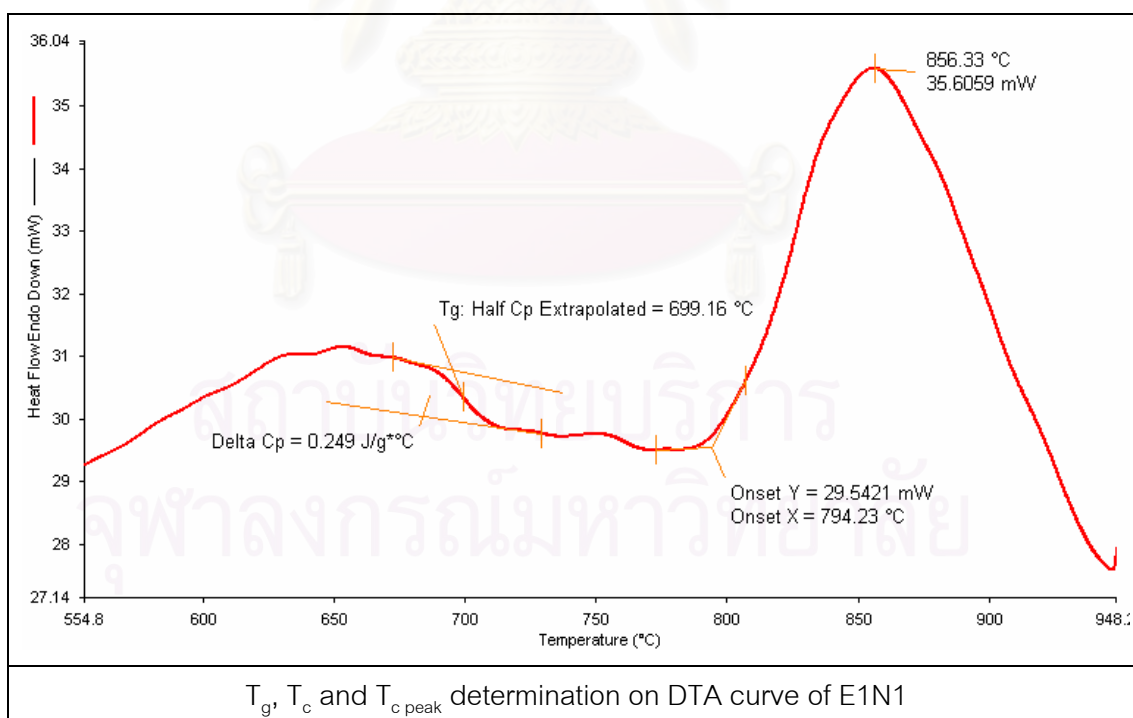
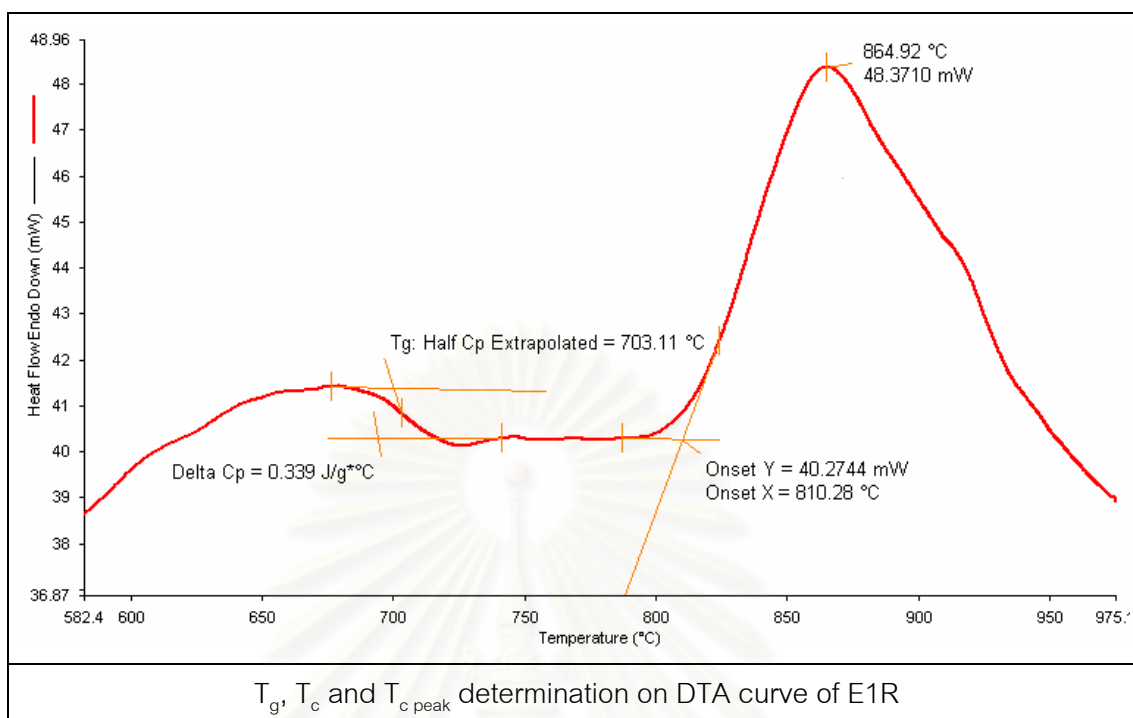
An index-matching fluid with refractive index of 1.54 should be used to help in detecting the presence of crystals and thereby in determining the position of the crystalline boundary in a known temperature gradient zone. For optimum detection of the crystalline boundary, it is recommended that the initial temperature be set for 1 h at 20  $^\circ\text{C}$  above the temperature range of interest, after which the temperature should be lowered to the zone containing the liquidus temperature.

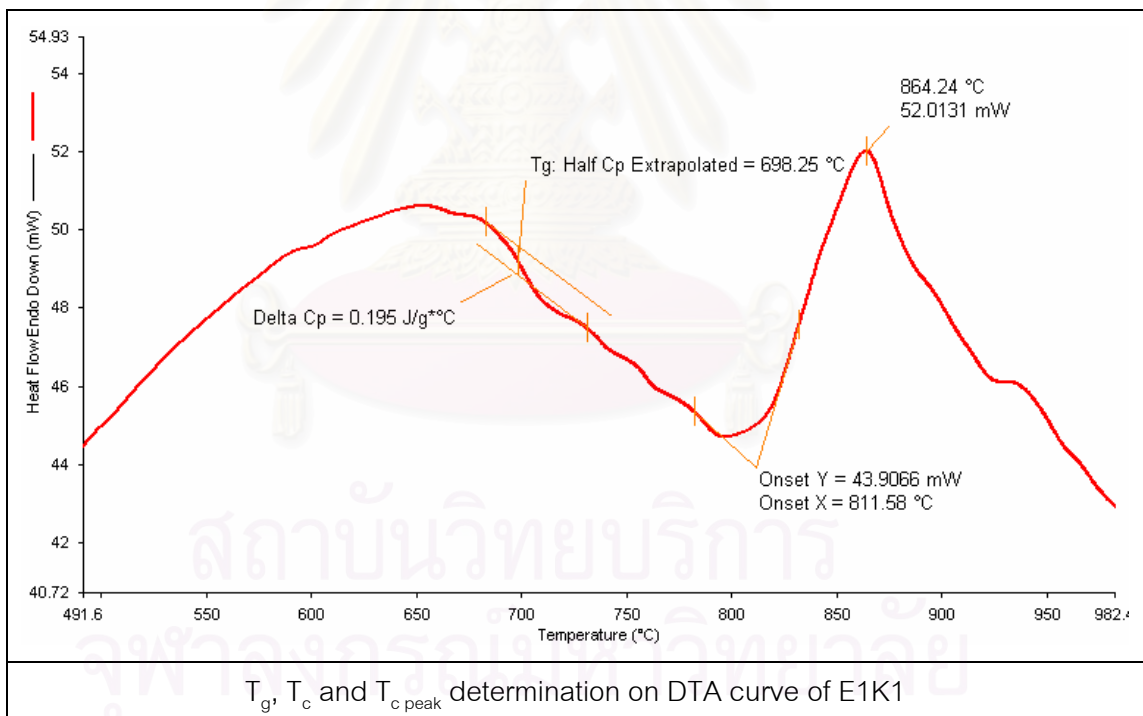
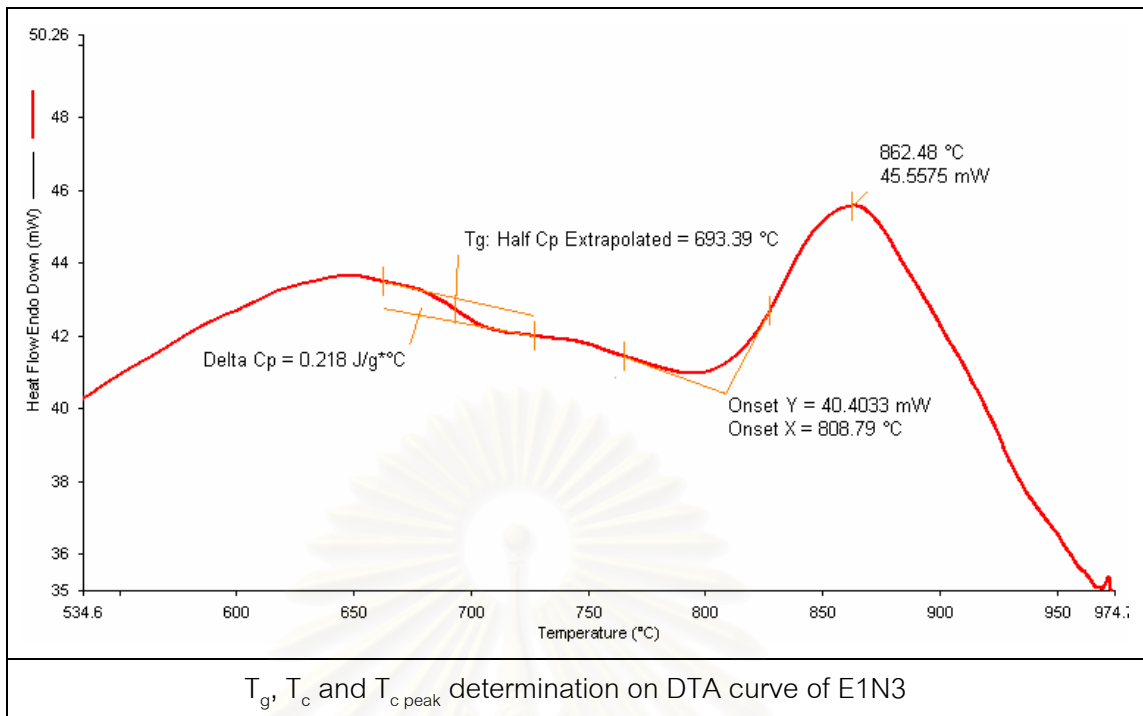
Gaithersburg, MD 20899  
May 17, 1994

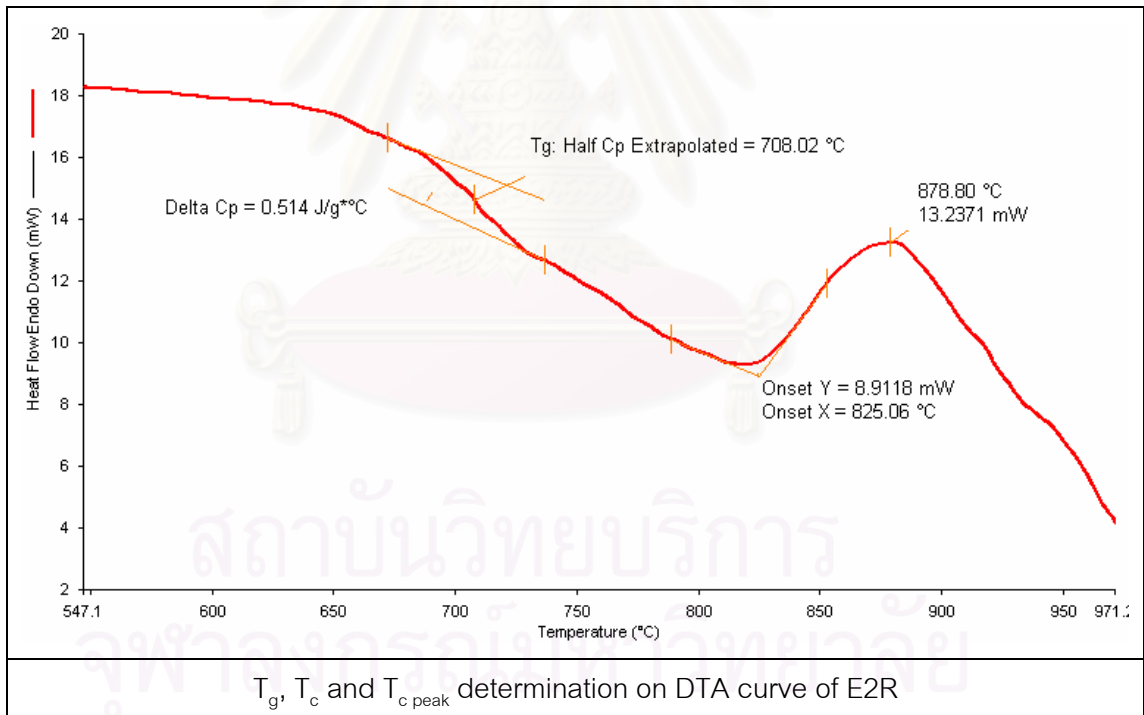
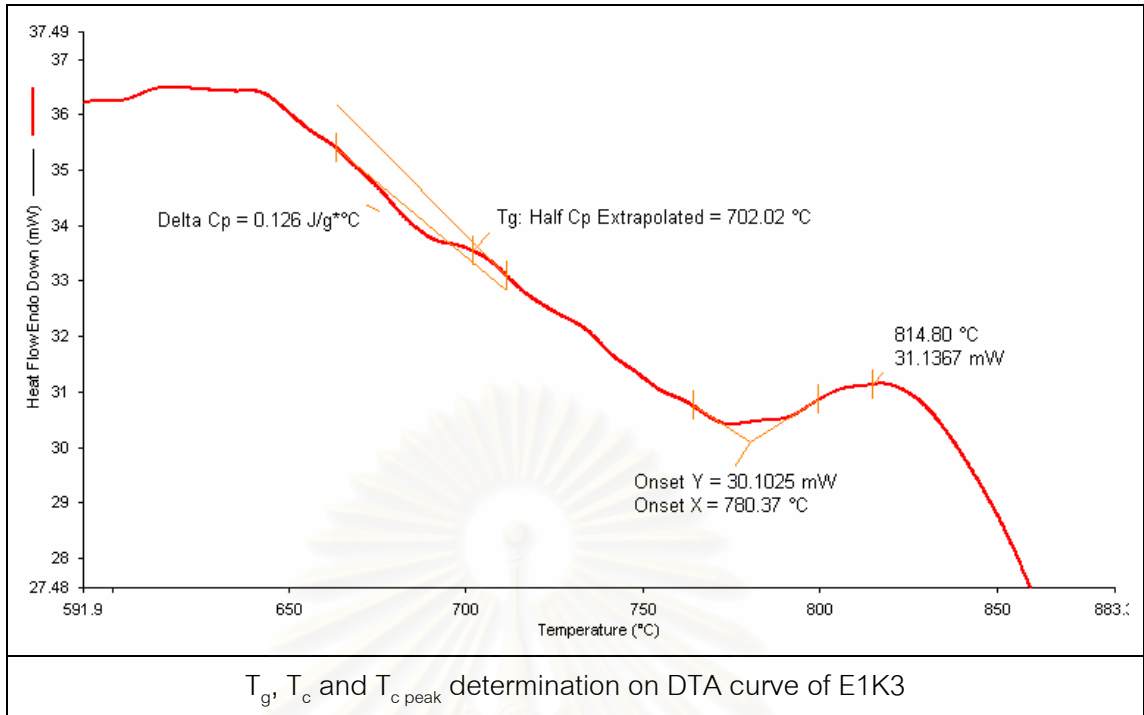
Thomas E. Gills, Chief  
Standard Reference Materials Program

(over)

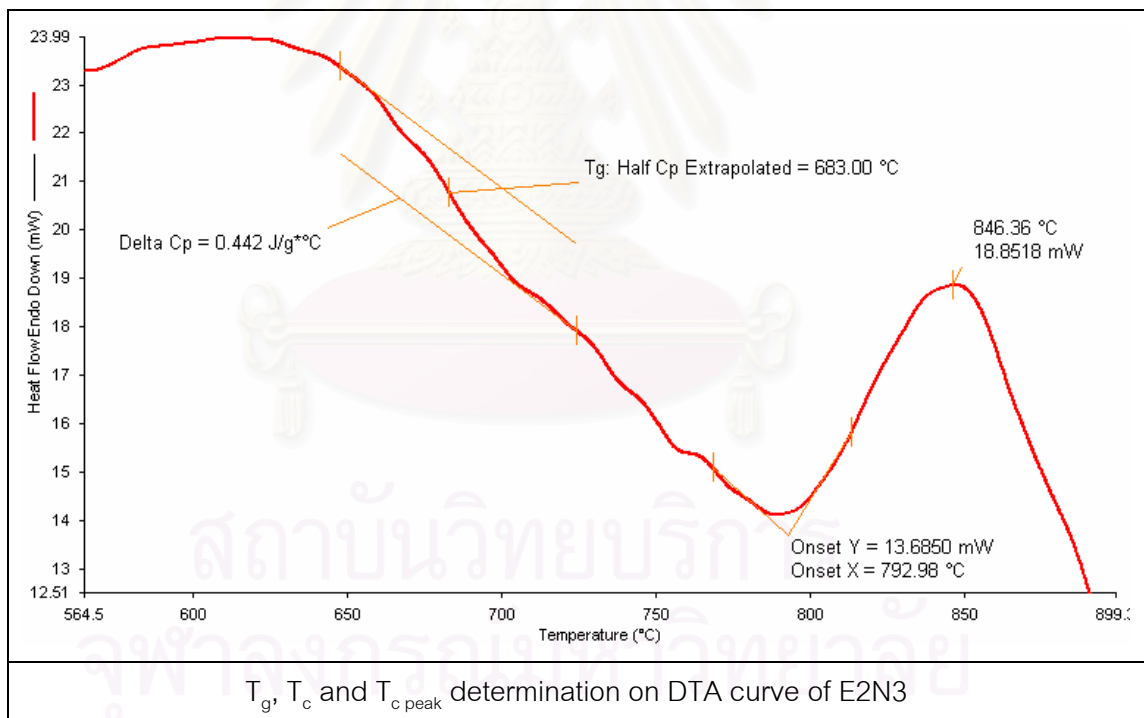
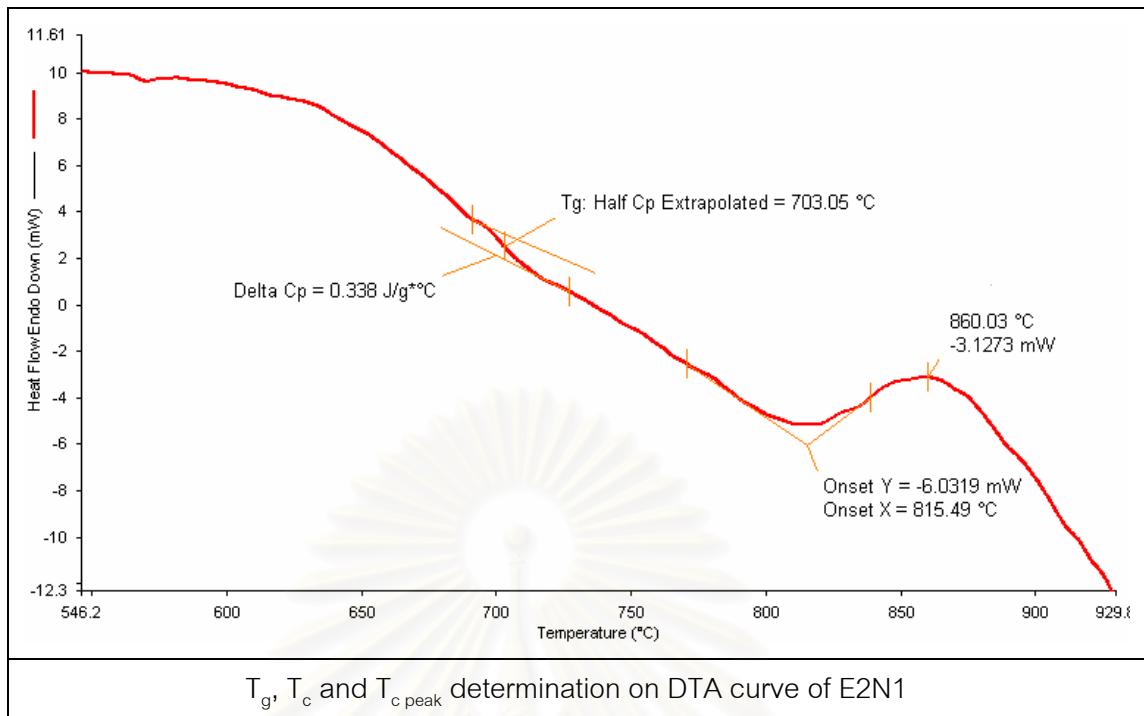
## APPENDIX F

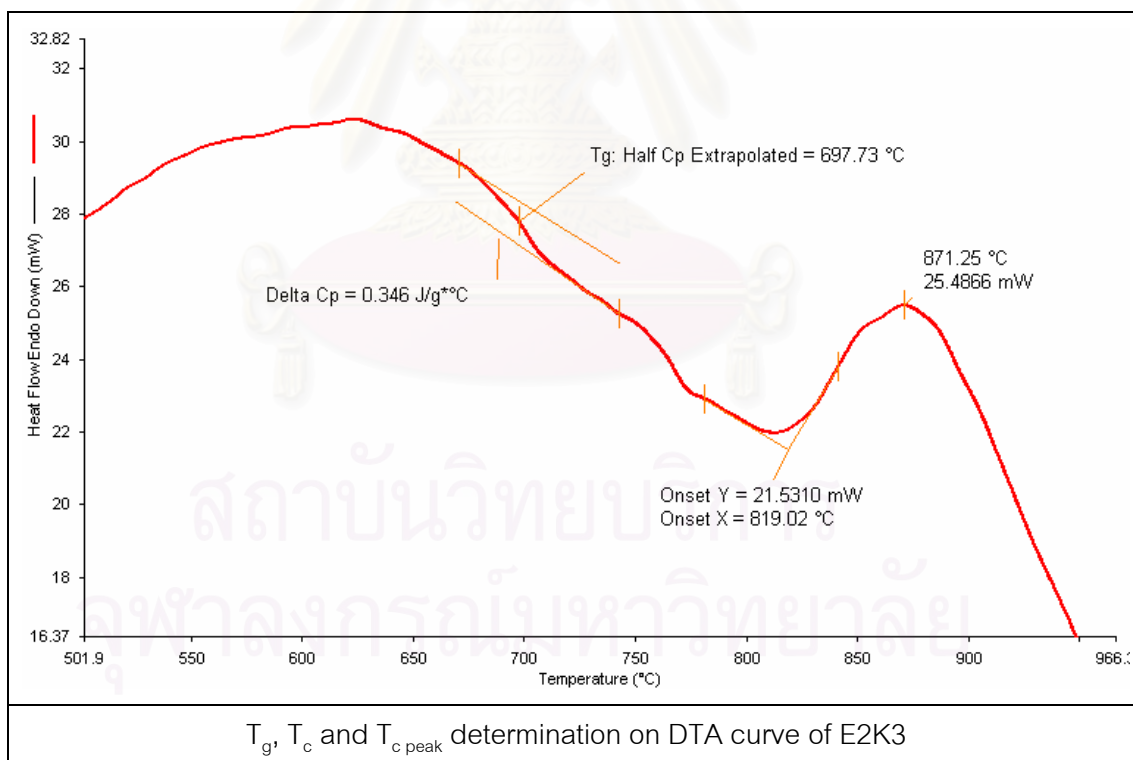
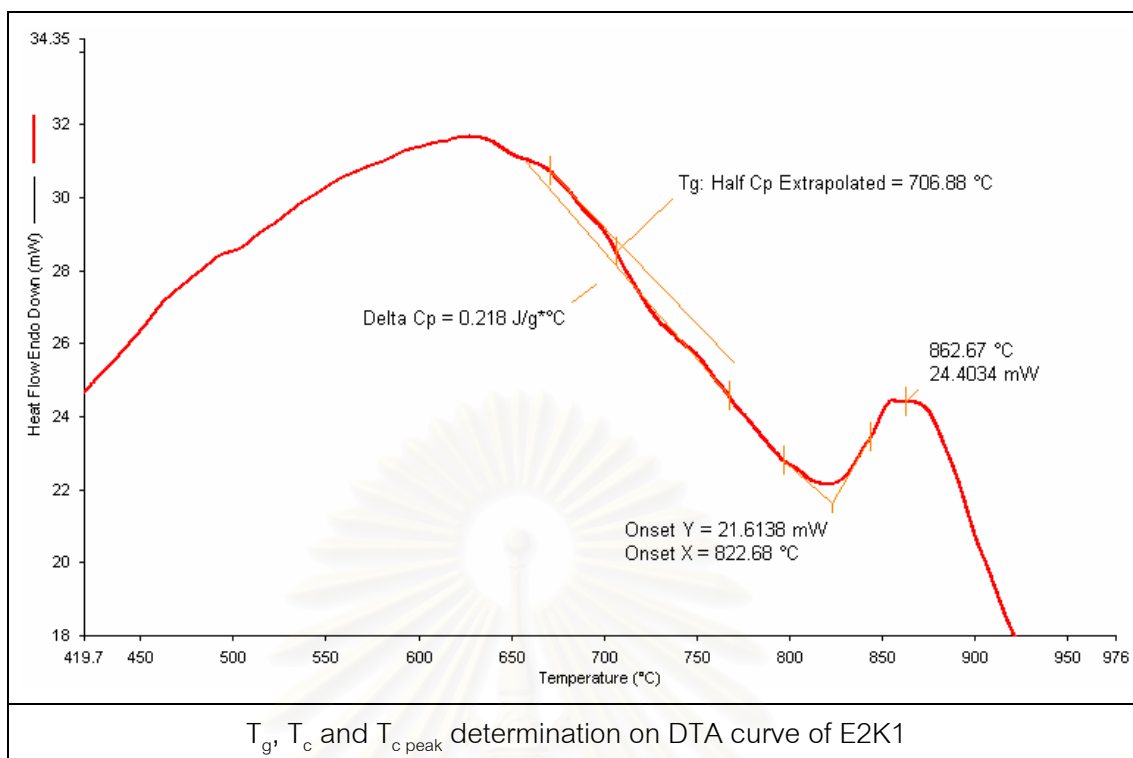


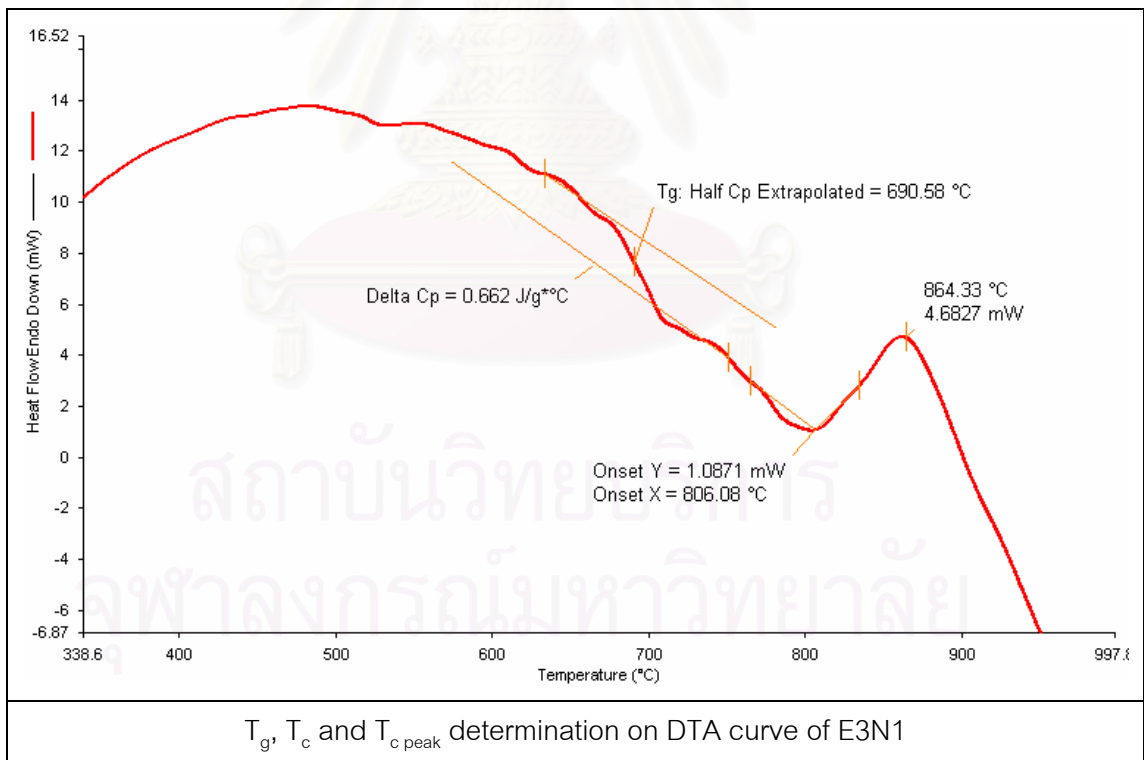
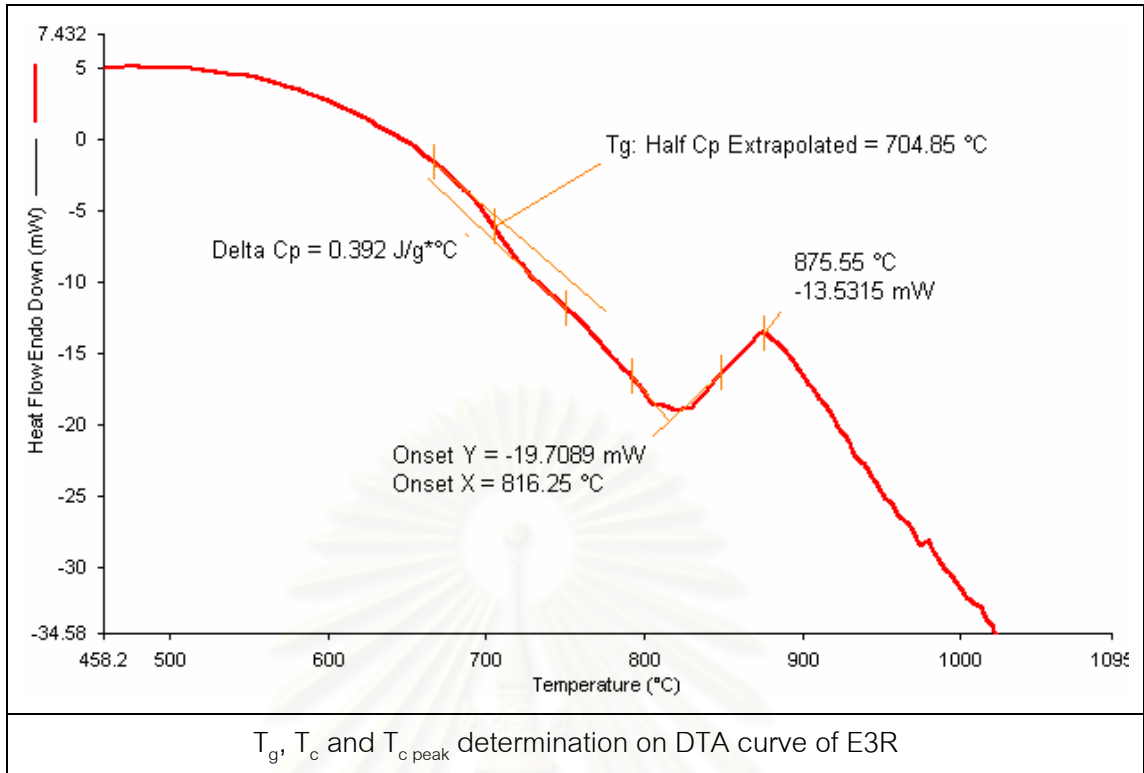


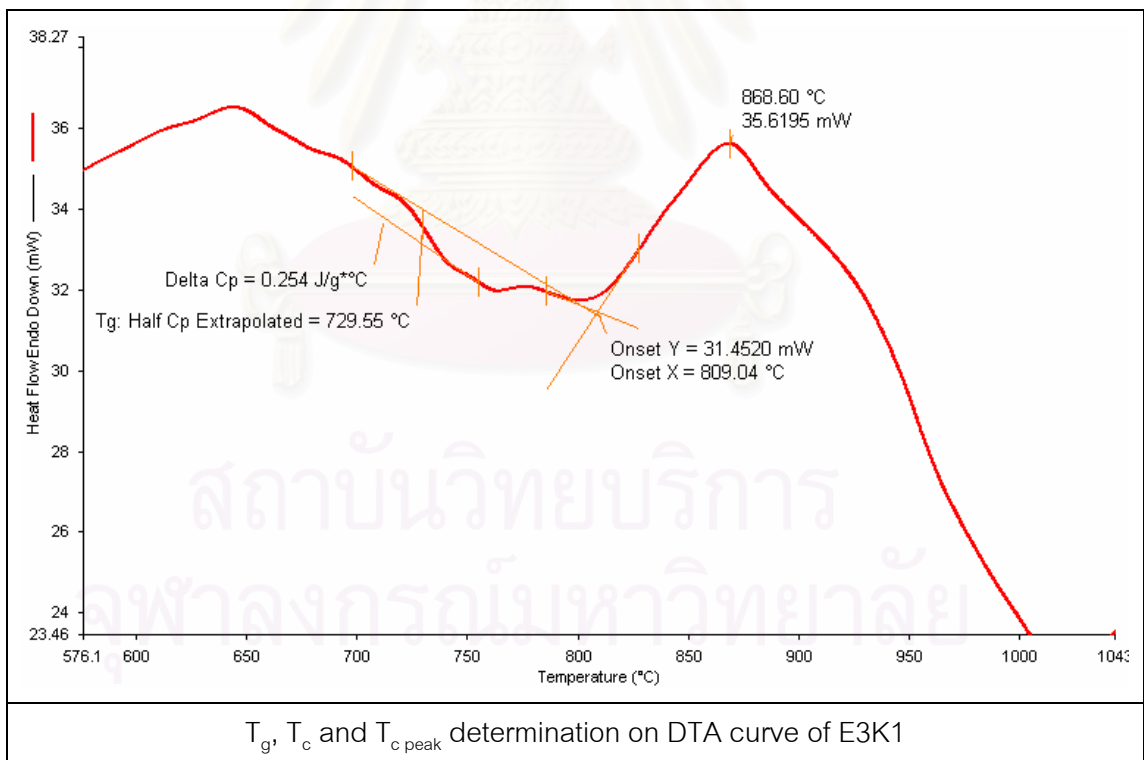
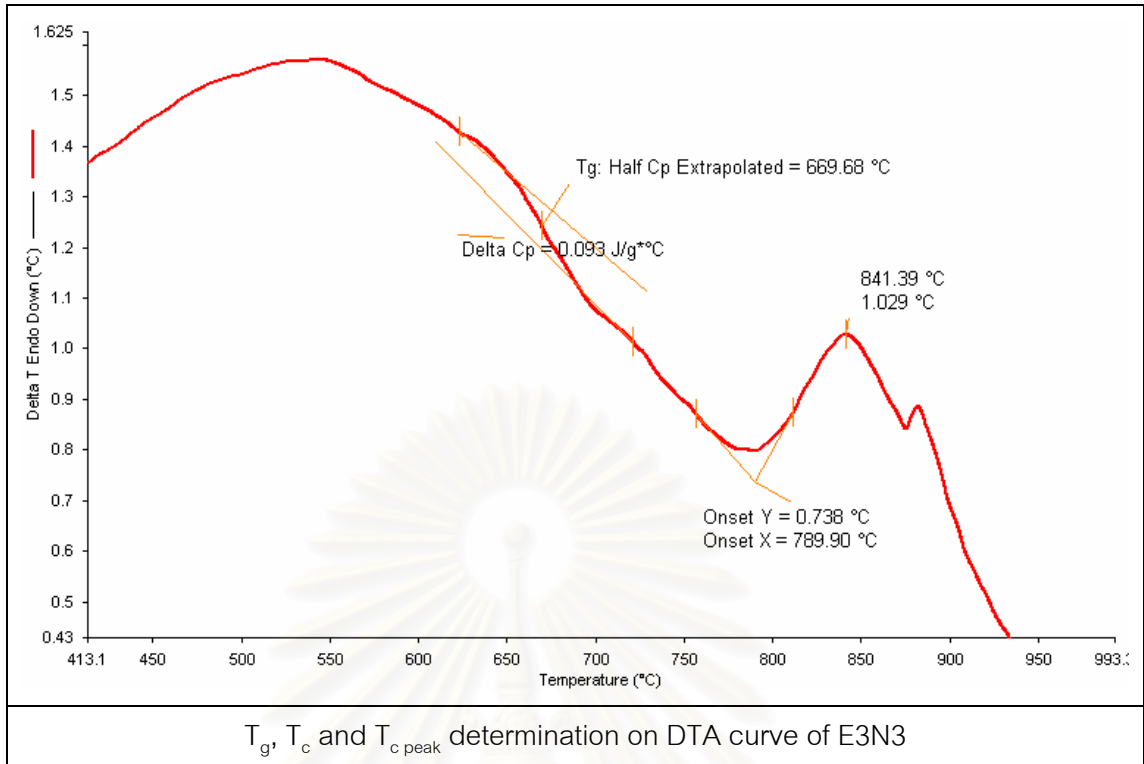


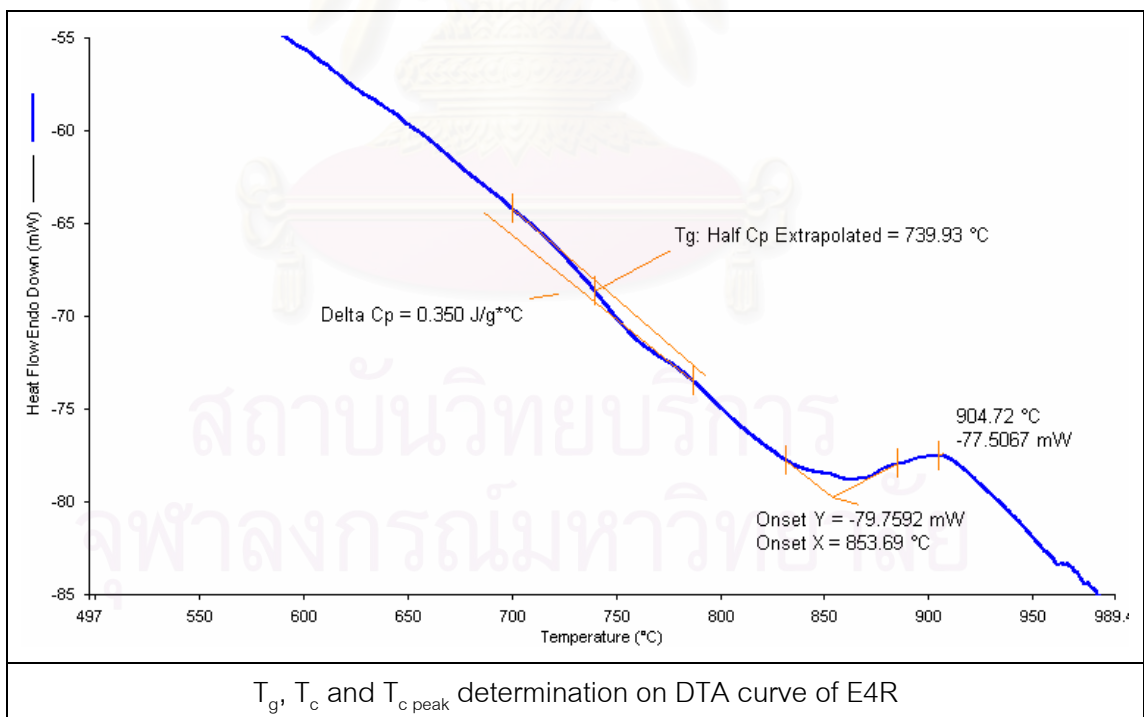
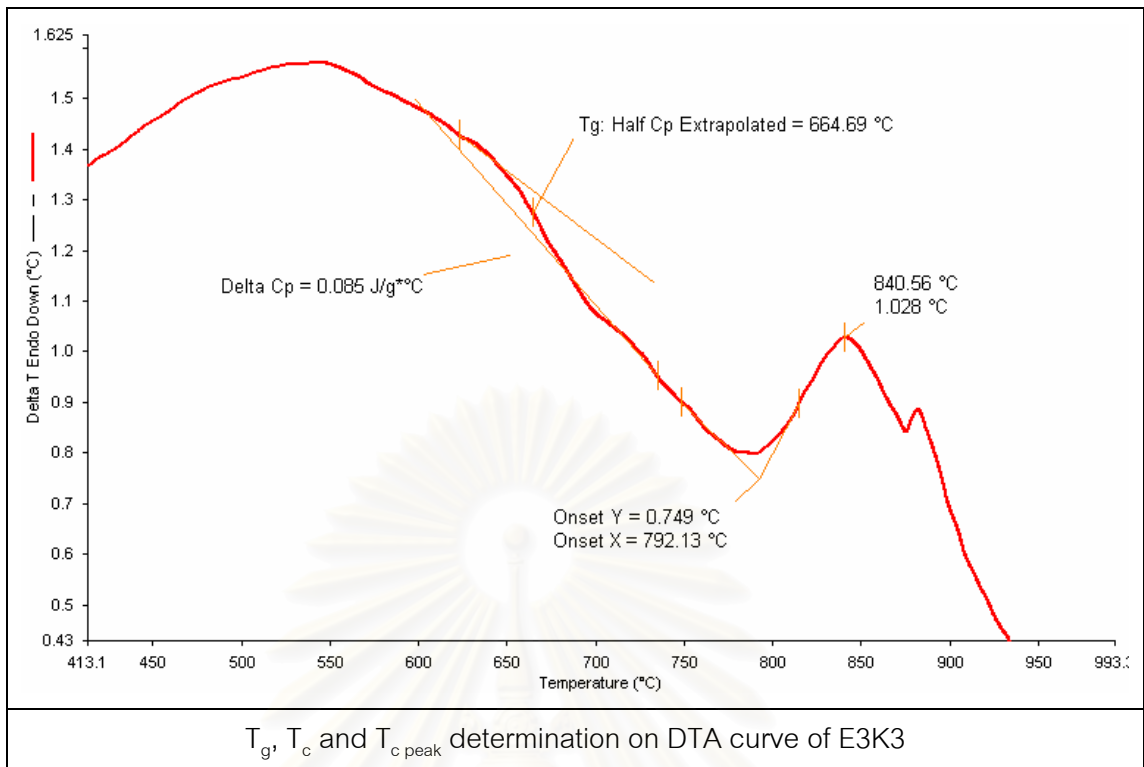


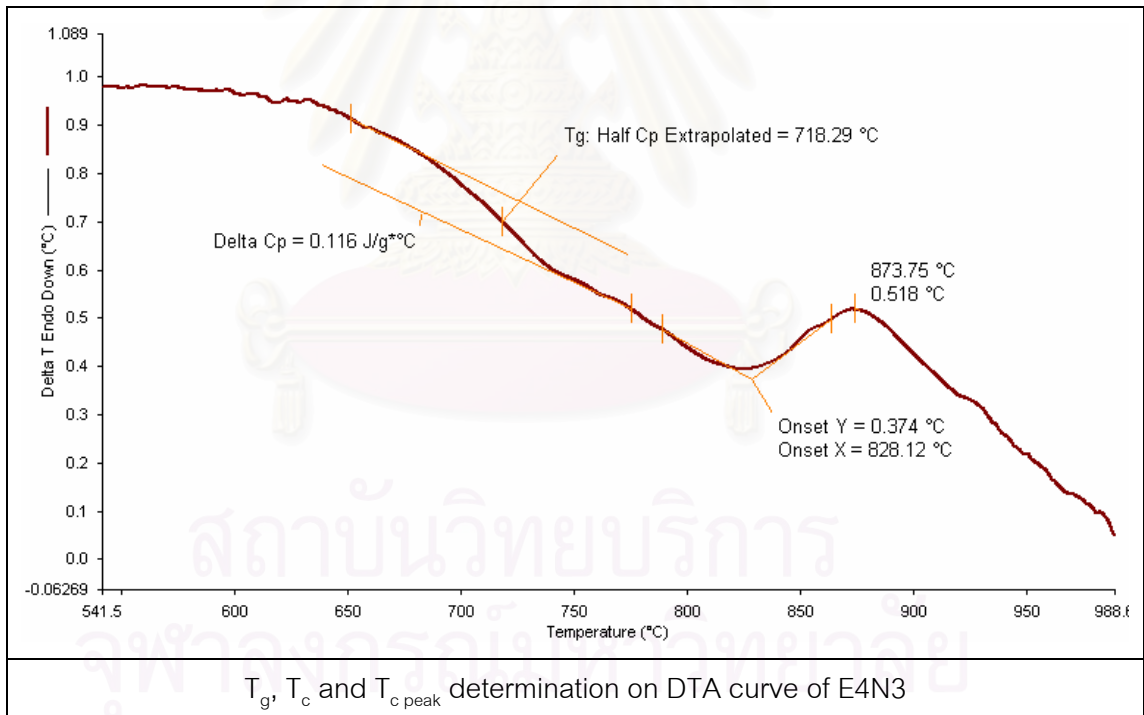
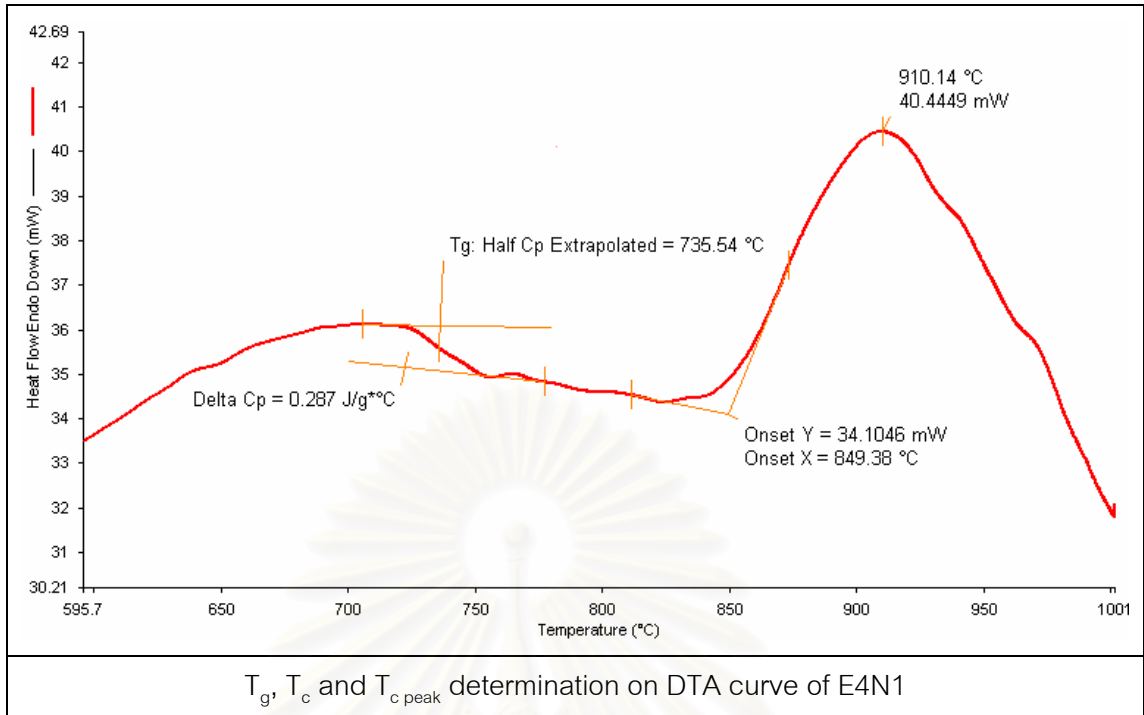


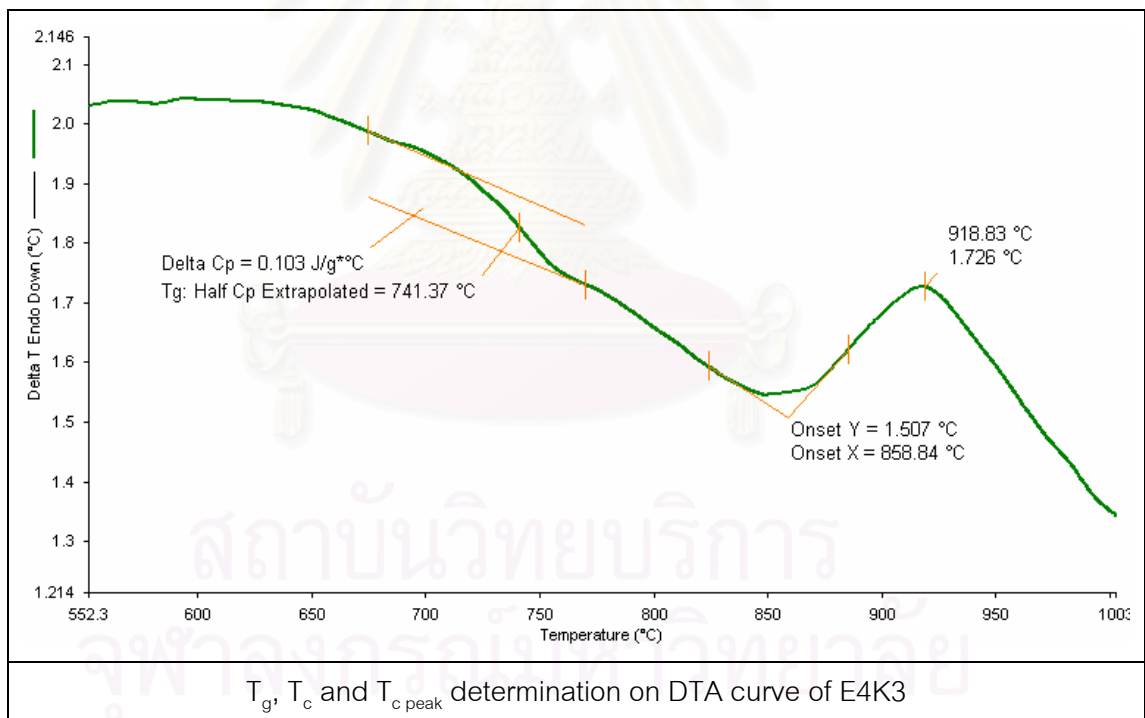
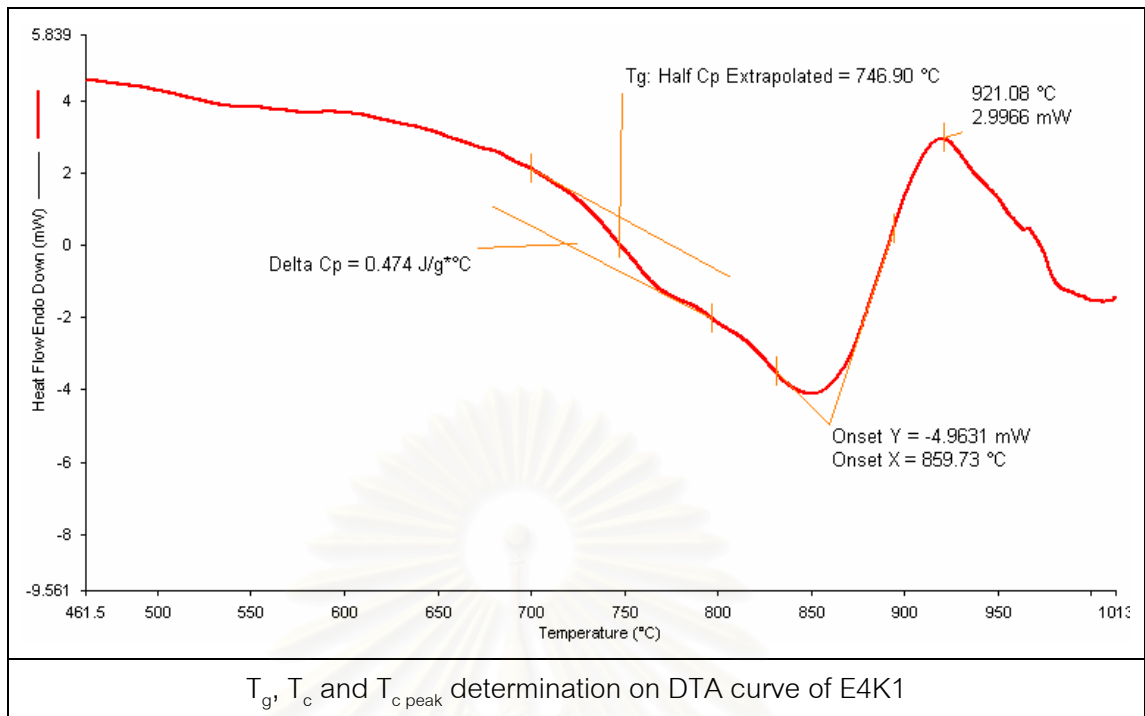


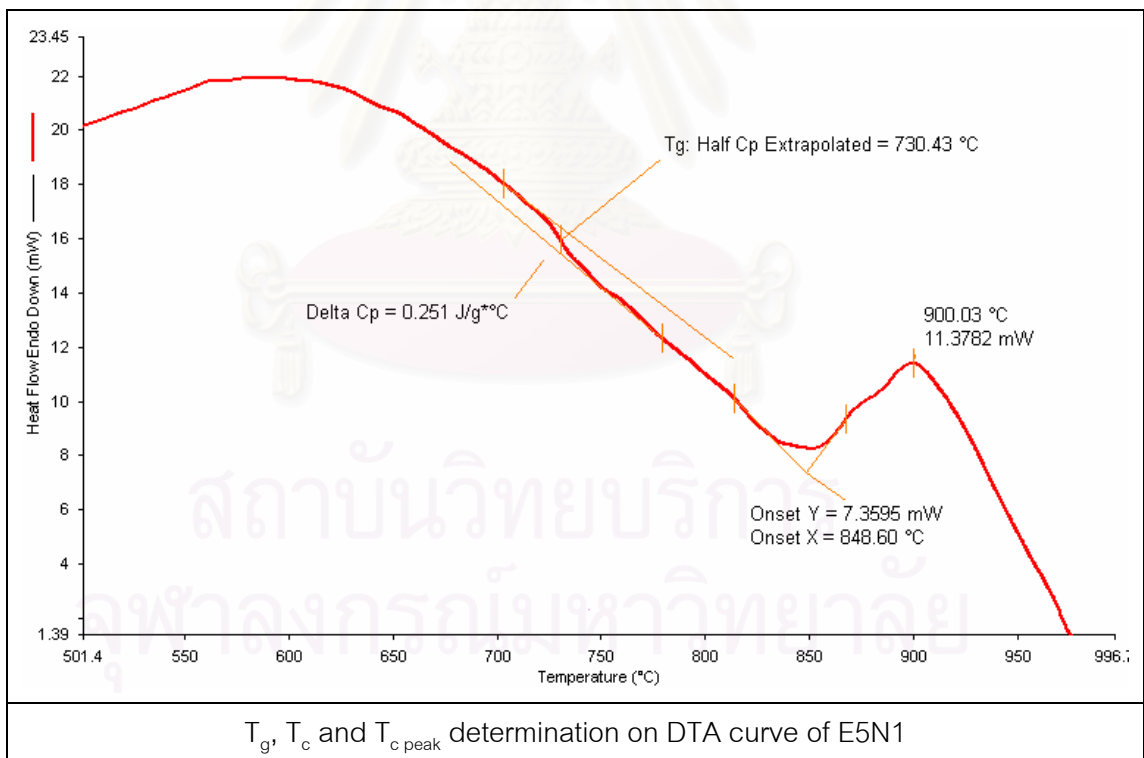
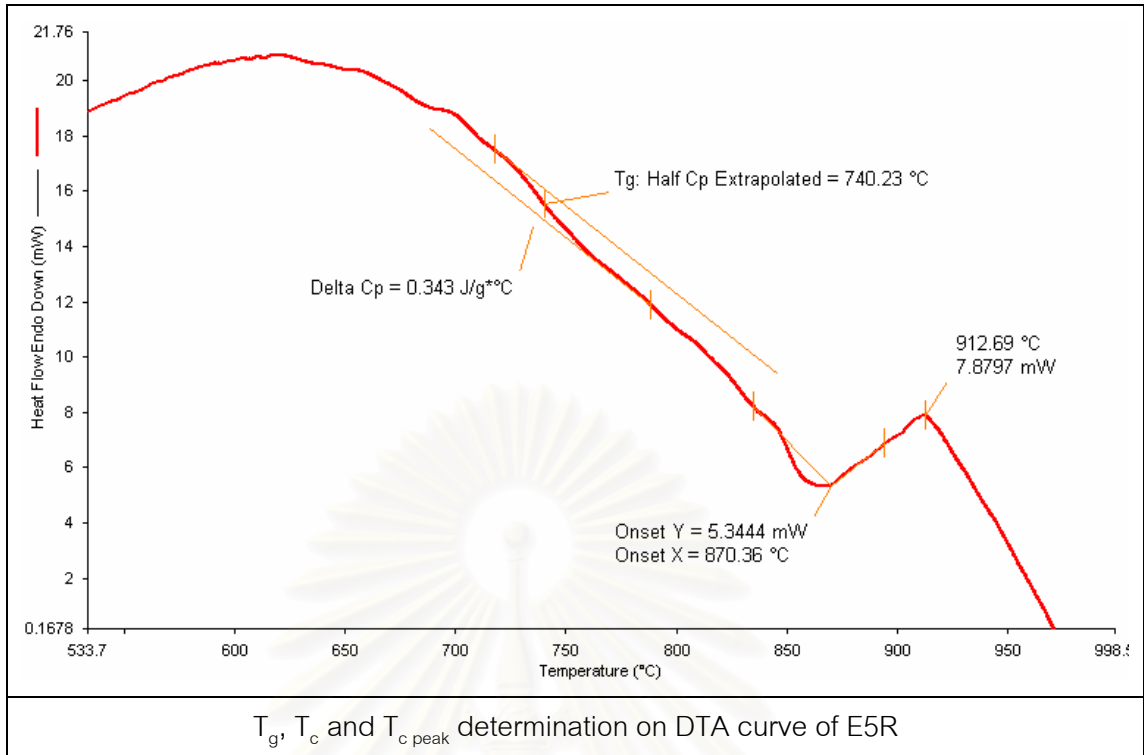




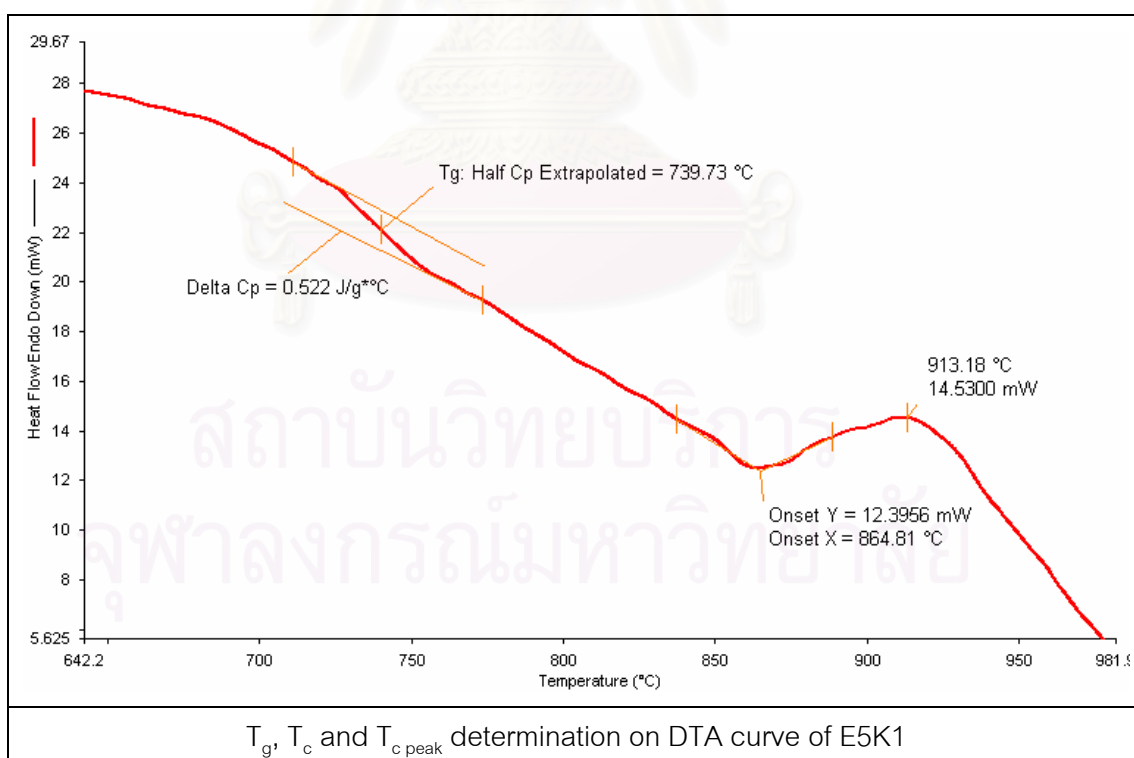
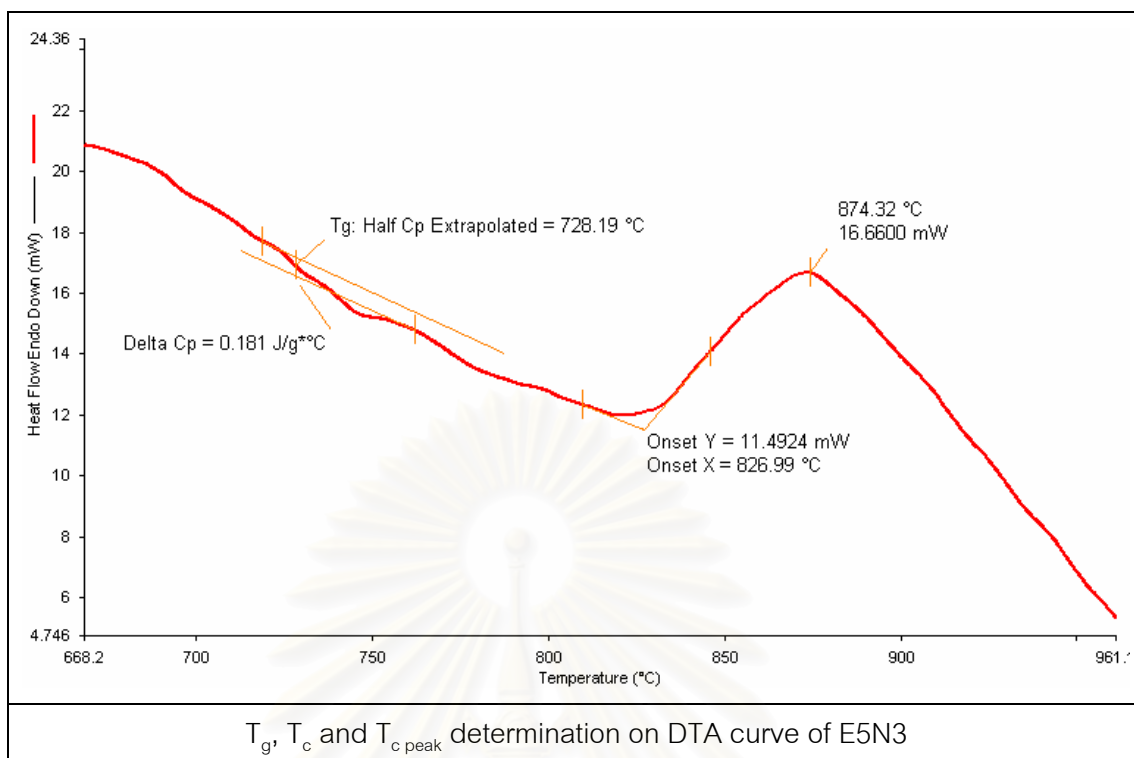


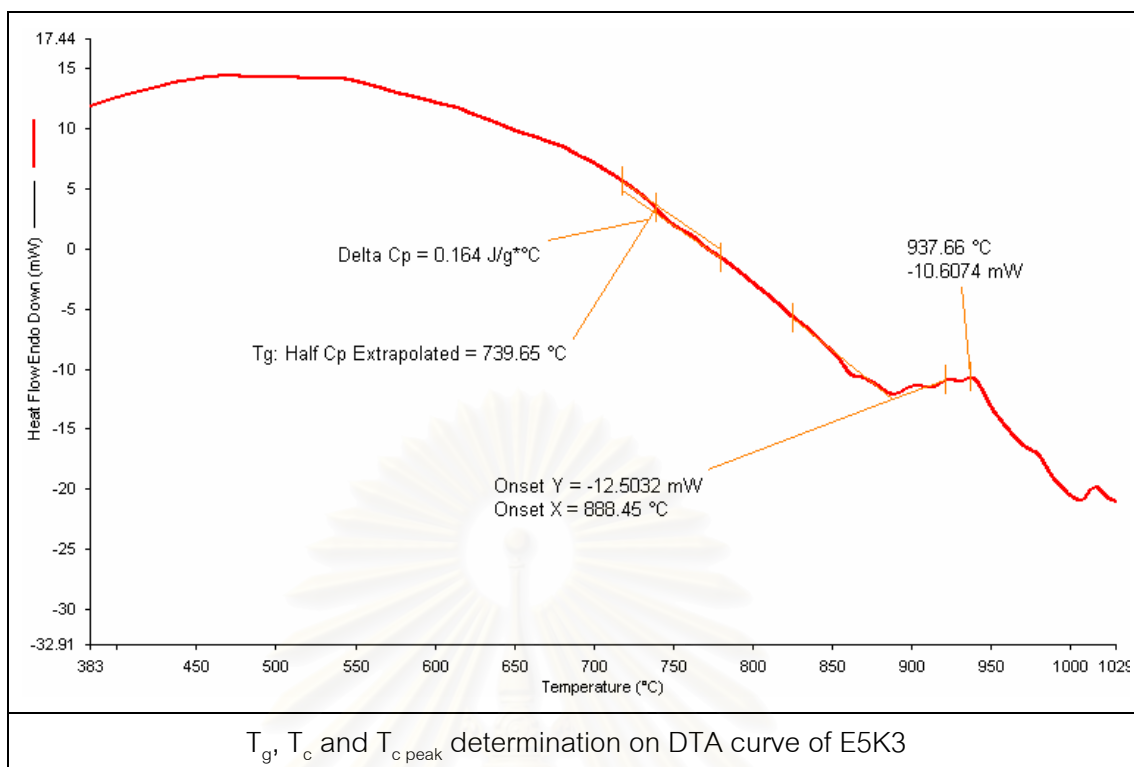







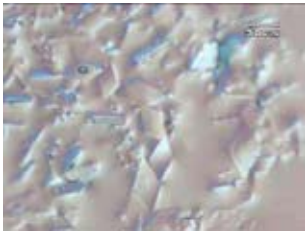

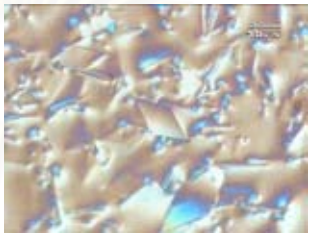
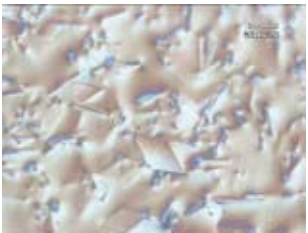


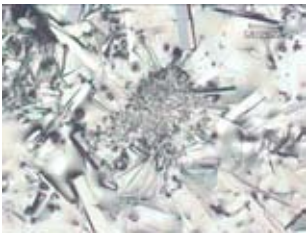











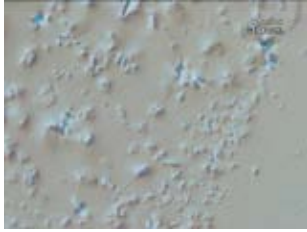

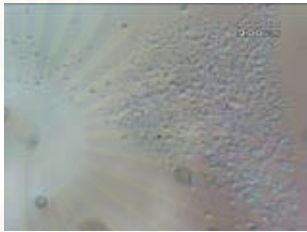
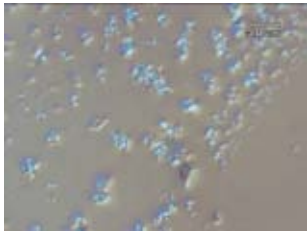
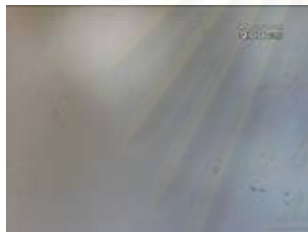
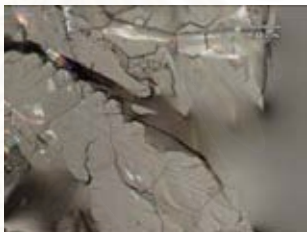
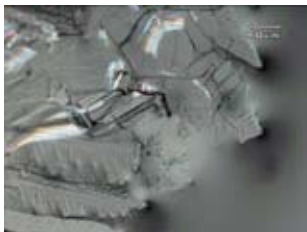
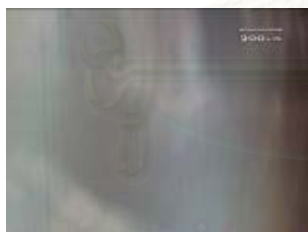







สถาบันวิทยบริการ  
จุฬาลงกรณ์มหาวิทยาลัย



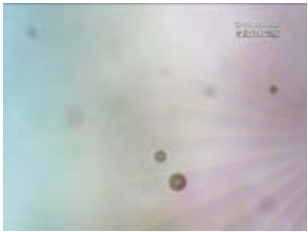
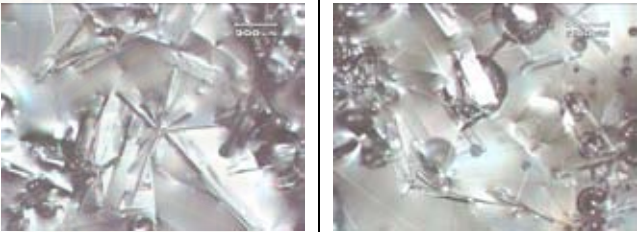

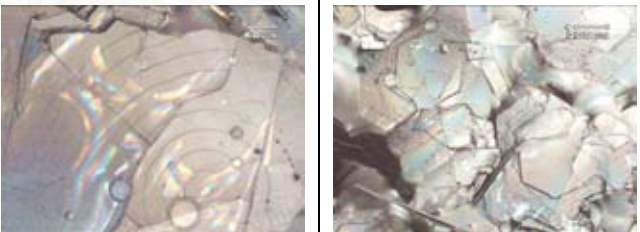



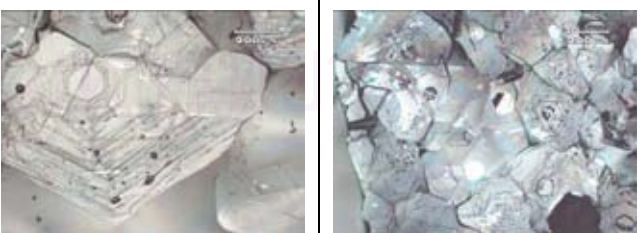
## APPENDIX G

| Sample | $T_2$   | $T_1$  |   |
|--------|---|--|---|
| E1R    |    |    |   |
|        | 1170°C  | 1160°C   |   |
| E1N1   |    |    |    |
|        | 1150°C  | 1140°C   |   |
| E1N3   |   |   |   |
|        | 1140°C  | 1130°C   |   |
| E1K1   |  |  |  |
|        | 1160°C  | 1150°C   | 1140°C  |
| E1K3   |  |  |  |
|        | 1130°C  | 1120°C   |   |




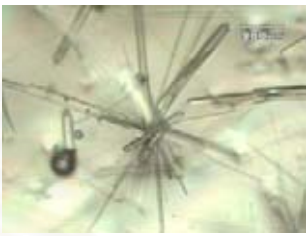
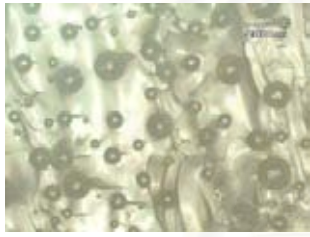
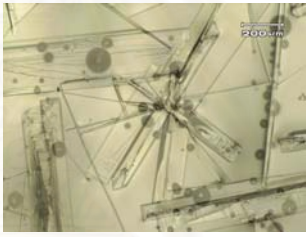
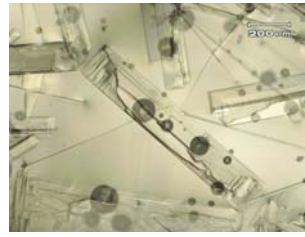




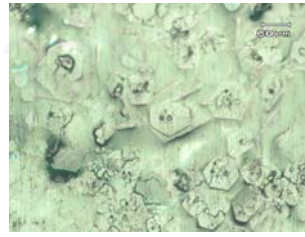
Visual observation of heat-treated E1 group for 24 h

| Sample | $T_2$   | $T_1$  |   |
|--------|---|--|---|
| E2R    |    |    |   |
|        | 1160°C  | 1150°C   |   |
| E2N1   |    |    |    |
|        | 1140°C  | 1130°C   |   |
| E2N3   |   |   |   |
|        | 1170°C  | 1160°C   |   |
| E2K1   |  |  |  |
|        | 1160°C  | 1150°C   | 1140°C  |
| E2K3   |  |  |  |
|        | 1190°C  | 1180°C   |   |





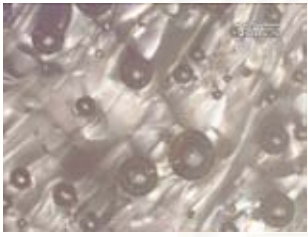


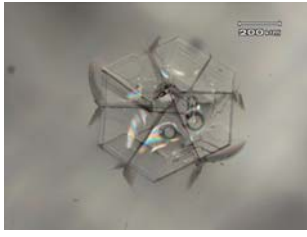


Visual observation of heat-treated E2 group for 24 h

| Sample | $T_2$   | $T_1$  |
|--------|---|--|
| E3R    |    |    |
|        | 1130°C  | 1120°C   |
| E3N1   |    |    |
|        | 1130°C  | 1120°C   |
| E3N3   |   |   |
|        | 1170°C  | 1160°C   |
| E3K1   |  |  |
|        | 1140°C  | 1130°C   |
| E3K3   |  |  |
|        | 1190°C  | 1180°C   |

Visual observation of heat-treated E3 group for 24 h

| Sample | $T_2$   | $T_1$  |   |
|--------|---|--|---|
| E4R    |    |    |   |
|        | 1210°C  | 1200°C   |   |
| E4N1   |    |    |   |
|        | 1200°C  | 1190°C   |   |
| E4N3   |   |   |   |
|        | 1230°C  | 1220°C   |   |
| E4K1   |  |  |   |
|        | 1220°C  | 1210°C   |   |
| E4K3   |  |  |  |
|        | 1260°C  | 1240°C   | 1250°C  |

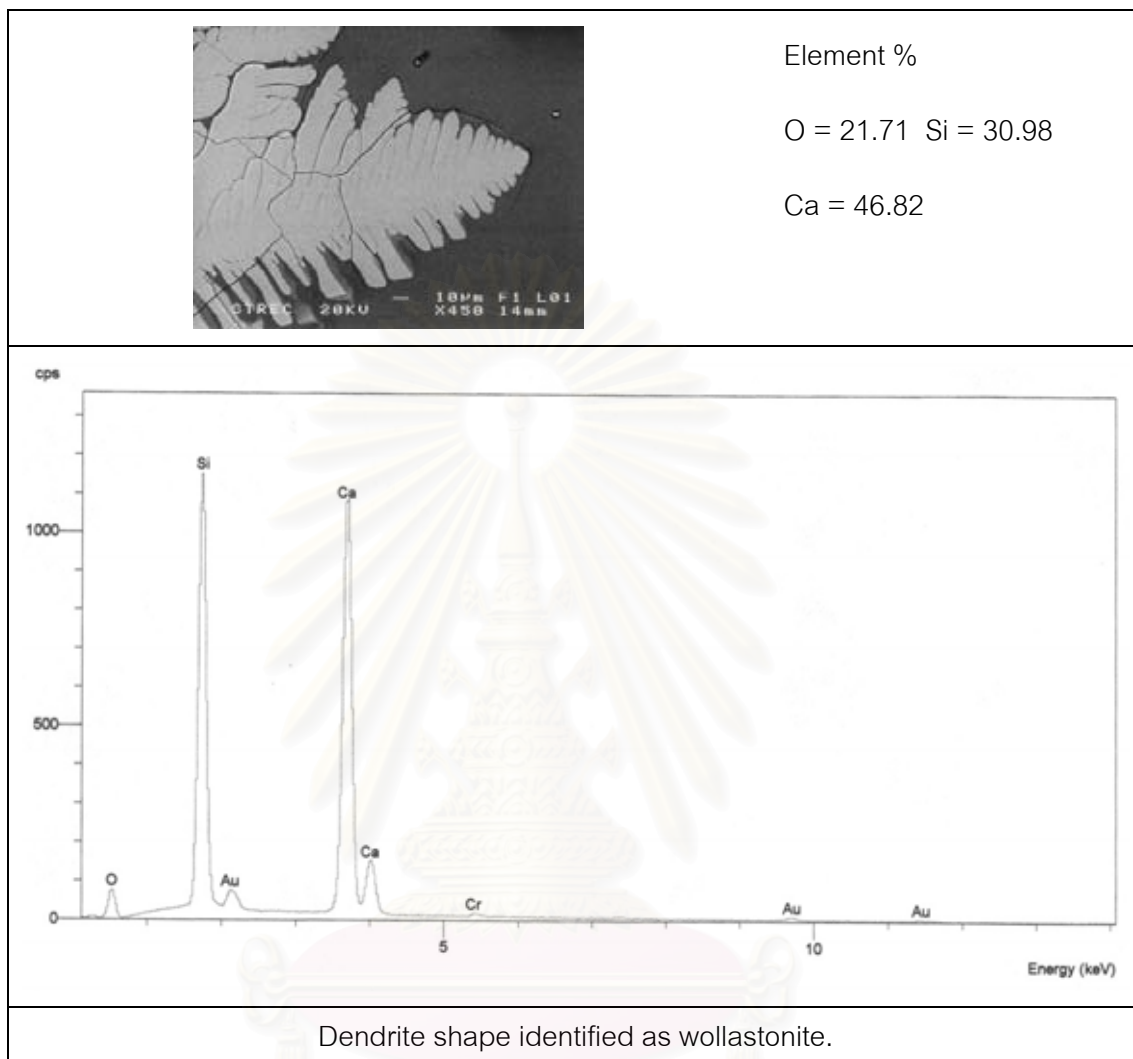
Visual observation of heat-treated E4 group for 24 h

| Sample | $T_2$   | $T_1$  |   |
|--------|---|--|---|
| E5R    |    |    |   |
|        | 1220°C  | 1210°C   |   |
| E5N1   |    |    |   |
|        | 1240°C  | 1230°C   |   |
| E5N3   |   |   |   |
|        | 1280°C  | 1270°C   |   |
| E5K1   |  |  |  |
|        | 1250°C  | 1240°C   |   |
| E5K3   |  |  |  |
|        | 1310°C  | 1300°C   | 1290°C  |

Visual observation of heat-treated E5 group for 24 h

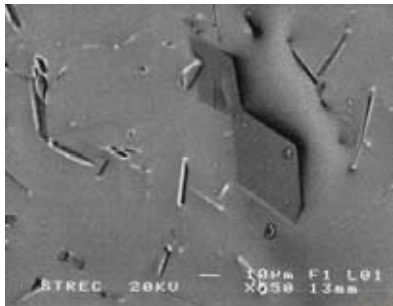
## APPENDIX H

SEM/EDX to aid crystalline phases identification.



สถาบันวิทยบริการ  
จุฬาลงกรณ์มหาวิทยาลัย

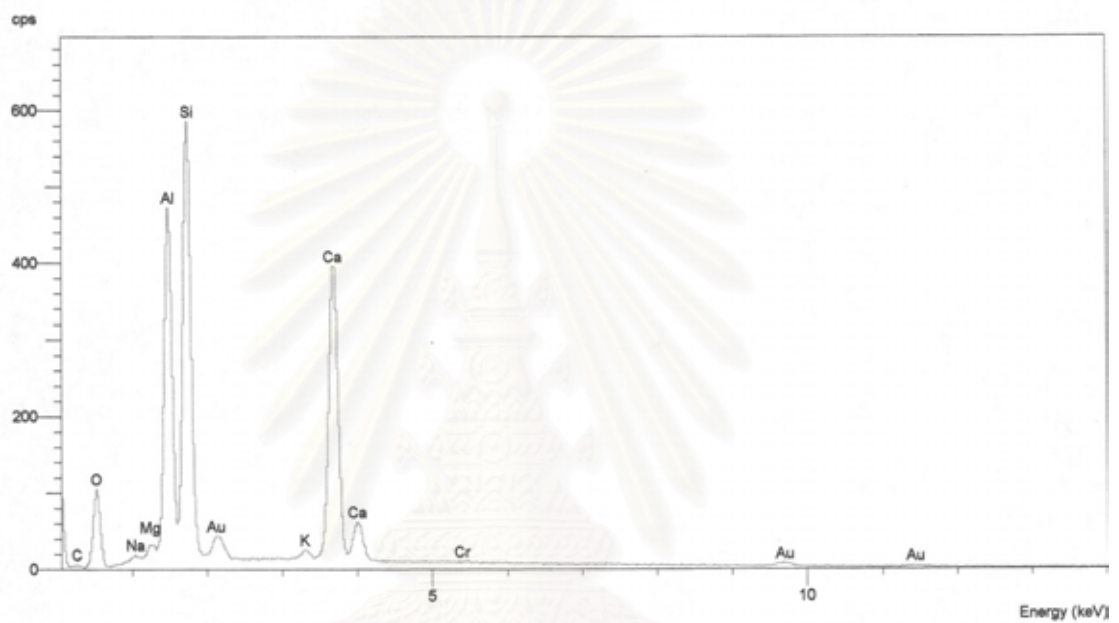




Element %

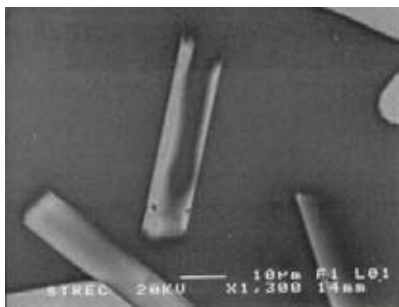
O = 39.04 Al = 18.73

Si = 24.45 Ca = 17.77



Diamond shape identified as anorthite.

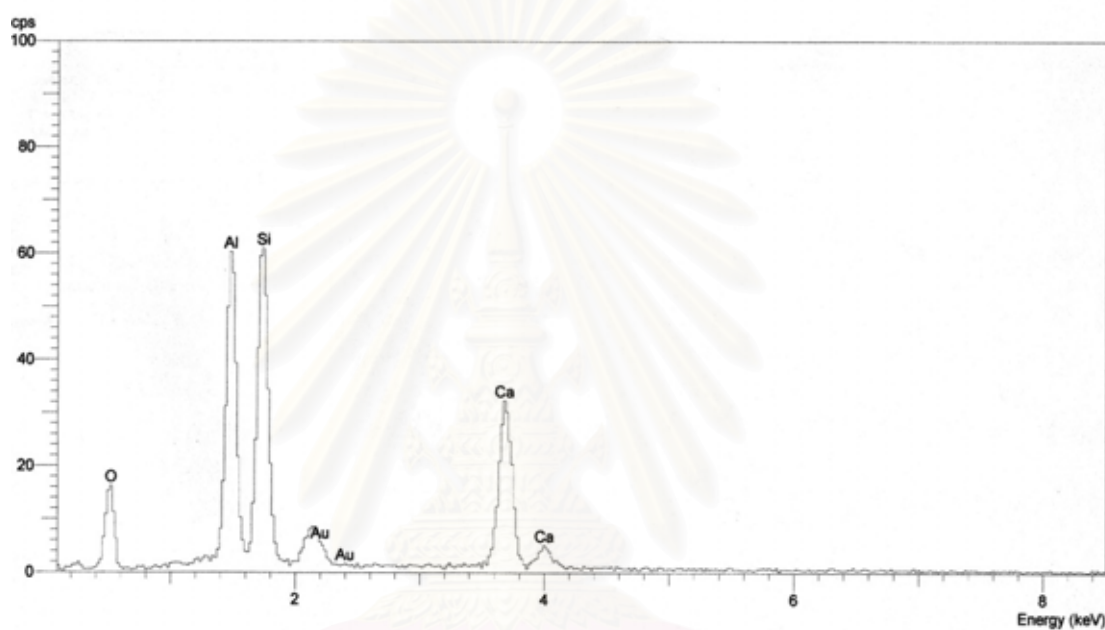
สถาบันวิทยบริการ  
จุฬาลงกรณ์มหาวิทยาลัย



Element %

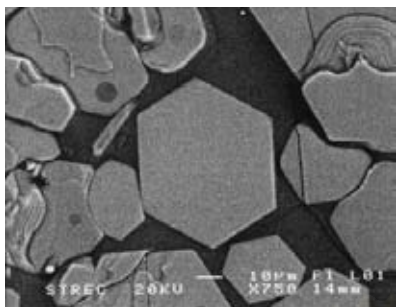
O = 37.22 Al = 20.10

Si = 26.59 Ca = 16.09



Rod shape identified as anorthite.

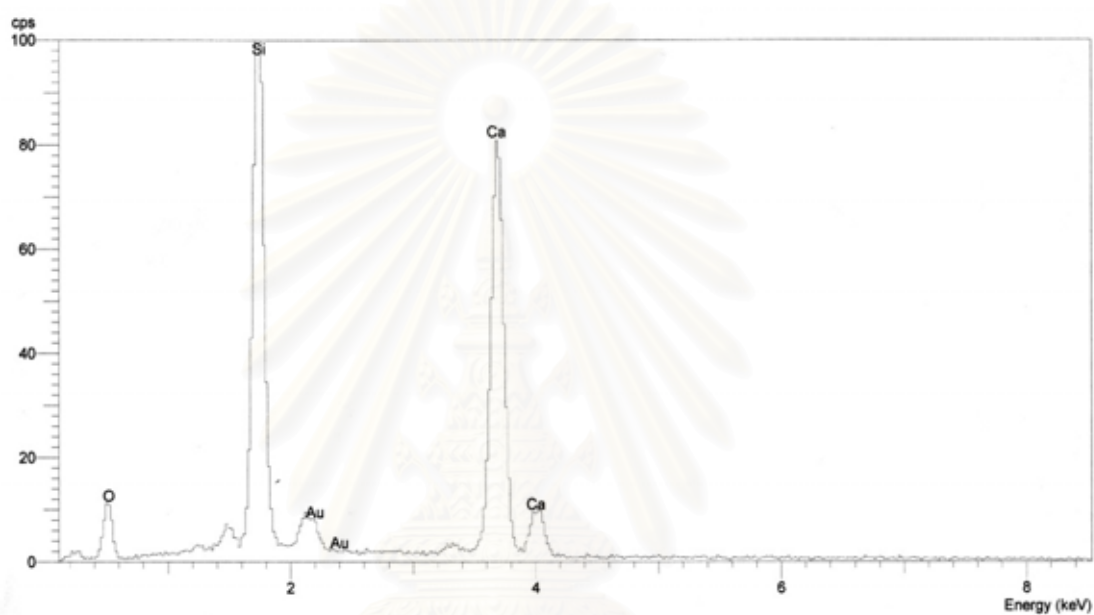
สถาบันวิทยบริการ  
จุฬาลงกรณ์มหาวิทยาลัย



Element %

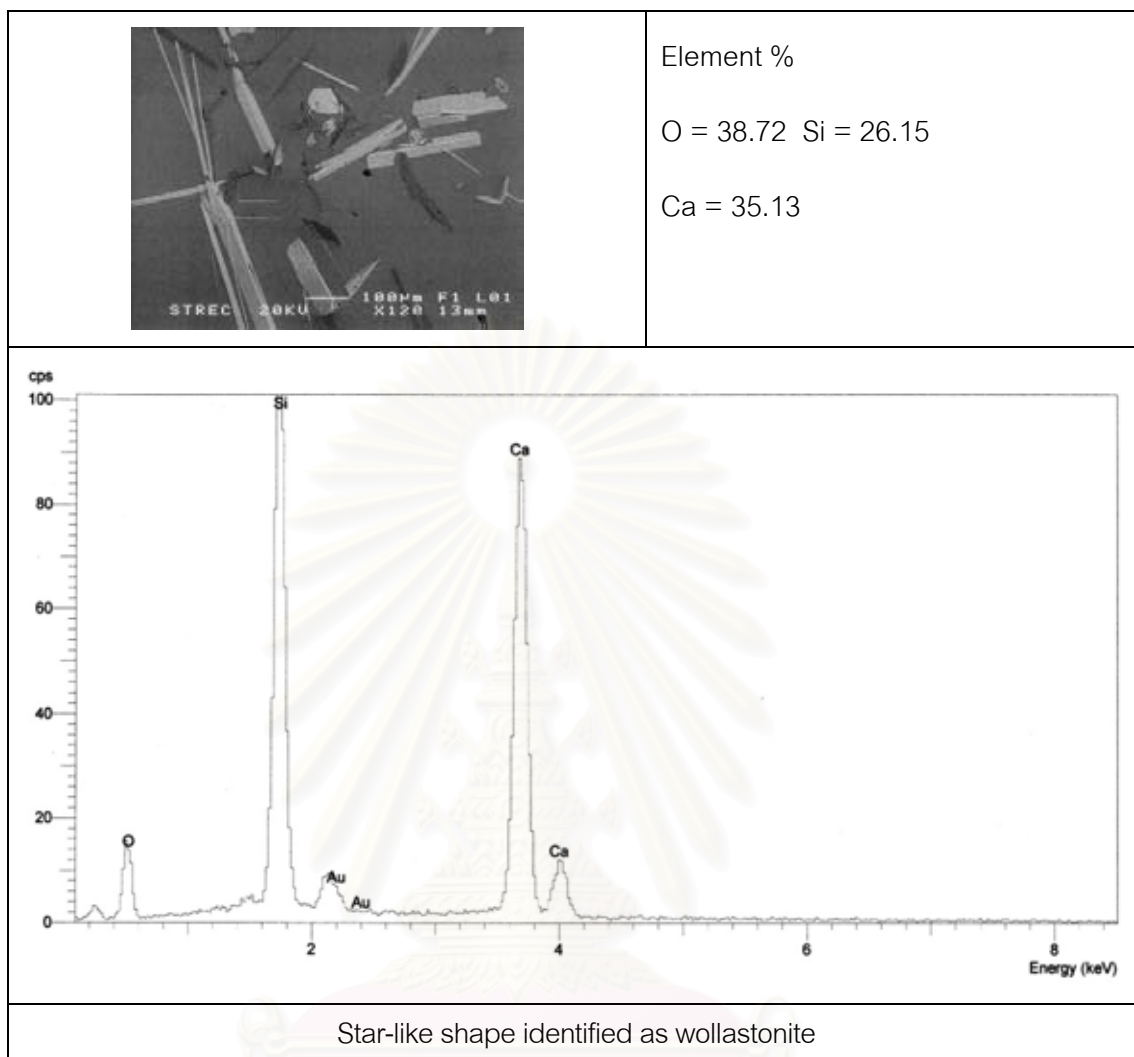
O = 34.83 Si = 28.85

Ca = 36.32



Hexagonal shape identified as wollastonite.

สถาบันวิทยบริการ  
จุฬาลงกรณ์มหาวิทยาลัย



สถาบันวิทยบริการ  
จุฬาลงกรณ์มหาวิทยาลัย

## APPENDIX I

First order coefficients calculation of liquidus temperature

|       |       |     |      |       |     |   |   |
|-------|-------|-----|------|-------|-----|---|---|
| 55    | 15    | 6   | 1    | 23    | 0   | 0 | 0 |
| 54.8  | 14.8  | 5.8 | 0.8  | 22.8  | 0   | 1 | 0 |
| 54.4  | 14.4  | 5.4 | 0.4  | 22.4  | 0   | 3 | 0 |
| 54.8  | 14.8  | 5.8 | 0.8  | 22.8  | 0   | 0 | 1 |
| 54.4  | 14.4  | 5.4 | 0.4  | 22.4  | 0   | 0 | 3 |
| 56    | 13    | 5   | 3    | 23    | 0   | 0 | 0 |
| 55.8  | 12.8  | 4.8 | 2.8  | 22.8  | 0   | 1 | 0 |
| 55.4  | 12.4  | 4.4 | 2.4  | 22.4  | 0   | 3 | 0 |
| 55.8  | 12.8  | 4.8 | 2.8  | 22.8  | 0   | 0 | 1 |
| 55.4  | 12.4  | 4.4 | 2.4  | 22.4  | 0   | 0 | 3 |
| 60    | 13    | 0   | 4    | 23    | 0   | 0 | 0 |
| 59.75 | 12.75 | 0   | 3.75 | 22.75 | 0   | 1 | 0 |
| 59.25 | 12.25 | 0   | 3.25 | 22.25 | 0   | 3 | 0 |
| 59.75 | 12.75 | 0   | 3.75 | 22.75 | 0   | 0 | 1 |
| 59.25 | 12.25 | 0   | 3.25 | 22.25 | 0   | 0 | 3 |
| 62    | 10    | 0   | 2    | 23    | 3   | 0 | 0 |
| 61.8  | 9.8   | 0   | 1.8  | 22.8  | 2.8 | 1 | 0 |
| 61.4  | 9.4   | 0   | 1.4  | 22.4  | 2.4 | 3 | 0 |
| 61.8  | 9.8   | 0   | 1.8  | 22.8  | 2.8 | 0 | 1 |
| 61.4  | 9.4   | 0   | 1.4  | 22.4  | 2.4 | 0 | 3 |

x = glass composition (wt%)

$$Z = X^T$$

|     |       |       |       |       |    |      |      |      |      |     |
|-----|-------|-------|-------|-------|----|------|------|------|------|-----|
| 55  | 54.8  | 54.4  | 54.8  | 54.4  | 56 | 55.8 | 55.4 | 56   | 55.4 |     |
| 15  | 14.8  | 14.4  | 14.8  | 14.4  | 13 | 12.8 | 12.4 | 13   | 12.4 |     |
| 6   | 5.8   | 5.4   | 5.8   | 5.4   | 5  | 4.8  | 4.4  | 5    | 4.4  |     |
| 1   | 0.8   | 0.4   | 0.8   | 0.4   | 3  | 2.8  | 2.4  | 3    | 2.4  |     |
| 23  | 22.8  | 22.4  | 22.8  | 22.4  | 23 | 22.8 | 22.4 | 23   | 22.4 |     |
| 0   | 0     | 0     | 0     | 0     | 0  | 0    | 0    | 0    | 0    |     |
| 0   | 1     | 3     | 0     | 0     | 0  | 1    | 3    | 0    | 0    |     |
| 0   | 0     | 0     | 1     | 3     | 0  | 0    | 0    | 1    | 3    | ... |
| 60  | 59.75 | 59.25 | 59.75 | 59.25 | 62 | 61.8 | 61.4 | 61.8 | 61.4 |     |
| 13  | 12.75 | 12.25 | 12.75 | 12.25 | 10 | 9.8  | 9.4  | 9.8  | 9.4  |     |
| 0   | 0     | 0     | 0     | 0     | 0  | 0    | 0    | 0    | 0    |     |
| 4   | 3.75  | 3.25  | 3.75  | 3.25  | 2  | 1.8  | 1.4  | 1.8  | 1.4  |     |
| 23  | 22.75 | 22.25 | 22.75 | 22.25 | 23 | 22.8 | 22.4 | 22.8 | 22.4 |     |
| 0   | 0     | 0     | 0     | 0     | 3  | 2.8  | 2.4  | 2.8  | 2.4  |     |
| 0   | 1     | 3     | 0     | 0     | 0  | 1    | 3    | 0    | 0    |     |
| ... | 0     | 0     | 0     | 1     | 3  | 0    | 0    | 1    | 3    |     |

$$ZX = Z * X$$

|        |        |        |        |        |       |       |       |
|--------|--------|--------|--------|--------|-------|-------|-------|
| 67235  | 14285  | 2856.4 | 2524.2 | 26245  | 826.8 | 923.5 | 923.5 |
| 14285  | 3145.1 | 714.2  | 529.25 | 5625.5 | 130   | 195.5 | 195.5 |
| 2856.4 | 714.2  | 271.4  | 82.6   | 1175.4 | 0     | 40    | 40    |
| 2524.2 | 529.25 | 82.6   | 118.45 | 979.65 | 22.8  | 31.5  | 31.5  |
| 26245  | 5625.5 | 1175.4 | 979.65 | 10271  | 304.2 | 359.5 | 359.5 |
| 826.8  | 130    | 0      | 22.8   | 304.2  | 36.2  | 10    | 10    |
| 923.5  | 195.5  | 40     | 31.5   | 359.5  | 10    | 40    | 0     |
| 923.5  | 195.5  | 40     | 31.5   | 359.5  | 10    | 0     | 40    |

$$izx = \text{inverse } zx = zx^{-1}$$

|       |          |         |         |         |          |         |          |           |
|-------|----------|---------|---------|---------|----------|---------|----------|-----------|
| izx = | 3.6572   | 2.8138  | 3.7567  | 2.8433  | -11.665  | 2.5954  | 0.005379 | 0.0053789 |
|       | 2.8138   | 3.8801  | 3.2365  | 4.0468  | -10.274  | 5.207   | 0.68266  | 0.68266   |
|       | 3.7567   | 3.2365  | 3.9665  | 3.3601  | -12.258  | 3.3776  | 0.16023  | 0.16023   |
|       | 2.8433   | 4.0468  | 3.3601  | 4.3801  | -10.505  | 5.6168  | 0.77885  | 0.77885   |
|       | -11.665  | -10.274 | -12.258 | -10.505 | 38.196   | -10.735 | -0.54086 | -0.54086  |
|       | 2.5954   | 5.207   | 3.3776  | 5.6168  | -10.735  | 7.9971  | 1.3075   | 1.3075    |
|       | 0.005379 | 0.68266 | 0.16023 | 0.77885 | -0.54086 | 1.3075  | 0.32485  | 0.29985   |
|       | 0.005379 | 0.68266 | 0.16023 | 0.77885 | -0.54086 | 1.3075  | 0.29985  | 0.32485   |

$$zy = z * y$$

|      |         |          |
|------|---------|----------|
| y =  | zy =    | b =      |
| 1145 | 1386451 | 22.397   |
| 1135 | 295181  | - 20.154 |
| 1165 | 59645   | - 3.5775 |
| 1145 | 51736   | - 36.141 |
| 1185 | 541456  | 11.255   |
| 1205 | 16781   | - 52.883 |
| 1195 | 19210   | 5.7698   |
| 1235 | 19540   | 14.02    |
| 1215 |         |          |
| 1255 |         |          |
| 1215 |         |          |
| 1235 |         |          |
| 1275 |         |          |
| 1245 |         |          |
| 1305 |         |          |

## BIOGRAPHY

Mr Apirat Theerapapvisetpong was born in Nan on May 4<sup>th</sup>, 1978. In 2001, he finished his Bachelor's Degree in Materials Science from the Department of Physics, Faculty of Science, Chiang Mai University. In the same year, he started working as a scientist at the Department of Mineral Resources and the Department of Primary Industries and Mines. In 2003, he left to study for Master's Degree in the field of Ceramic Technology at Chulalongkorn University and graduated in 2006.



สถาบันวิทยบริการ  
จุฬาลงกรณ์มหาวิทยาลัย